DOKUZ EYLUL UNIVERSITY
GRADUATE SCHOOL OF NATURAL AND APPLIED
SCIENCES

SYNTHESIS, CHARACTERIZATION AND APPLICATIONS OF POLYPHENOL-Fe(III) COMPLEXES AND TANNIC ACID RESIN

by
Pelin ERDEM

March, 2013
İZMİR

SYNTHESIS, CHARACTERIZATION AND APPLICATIONS OF POLYPHENOL-Fe(III) COMPLEXES AND TANNIC ACID RESIN

A Thesis Submitted to the
Graduate School of Natural and Applied Sciences of Dokuz Eylul University
In Partial Fulfillment of the Requirements for the Degree of Doctor of
Philosophy in Chemistry, Chemistry Program

by
Pelin ERDEM

March, 2013
İZMİR

Ph. D. THESIS EXAMINATION RESULT FORM

We have read the thesis entitled "**SYNTHESIS, CHARACTERIZATION AND APPLICATIONS OF POLYPHENOL-Fe(III) COMPLEXES AND TANNIC ACID RESIN**" completed by **Pelin ERDEM** under supervision of **Prof. Dr. Mürüvvet YURDAKOÇ** and we certify that in our opinion it is fully adequate, in scope and in quality, as a thesis for the degree of Doctor of Philosophy.

Prof. Dr. Mürüvvet YURDAKOÇ

Supervisor

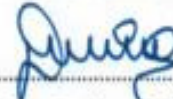Prof. Dr. Melek MERDİVAN

Thesis Committee Member

Assist. Prof. Dr. Z.Aylin ALBAYRAK

Thesis Committee Member

Prof. Dr. Sevil İRİŞLİ

Examining Committee Member

Prof. Dr. Perihan GÜRKAN

Examining Committee Member

Prof. Dr. Ayşe OKUR

Director

Graduate School of Natural and Applied Sciences

ACKNOWLEDGMENTS

SYNTHESIS, CHARACTERIZATION
AND APPLICATIONS OF POLYPHENOL-Fe(III) COMPLEXES AND
TANNIC ACID RESIN

ABSTRACT

Valonia tannin extract (Valex) is a kind of typical hydrolysable tannin which is naturally and widely grown in the western Anatolian region in Turkey especially in Salihli. In the first part of the study, Fe(III)-Valex and Fe(III)-Tannic acid complexes were synthesized and used for comparison purposes. Also, complexes were characterized by using: Magnetic susceptibility, Fourier transform infrared spectroscopy (FTIR), Thermogravimetric analysis (TGA), X-ray diffraction analysis (XRD), Electron spin resonance (ESR), Matrix-assisted laser desorption/ionization-time-of-flight mass spectroscopy (MALDI-TOF MS), X-ray photoelectron spectroscopy (XPS) and Proton nuclear magnetic resonance spectroscopy (^{1}H-NMR) analysis methods.

Stability constants and Stoichiometries of complexes were determined at pH=2.4, 4.4, 6.4 and 8.4 by using Slope and Mole Ratio methods. Antioxidant and antimicrobial activity of complexes have been made for the application. Their antioxidant activities were determined based on the *in vitro* radical scavenging activity of 2,2-Diphenyl-1-picrylhydrazyl. The antimicrobial activitity of complexes were also determined by the *in vitro* disc diffusion method. Complexes were found to have antioxidant activity but did not show any antimicrobial activity.

In the second part of the study, TA resin was synthesized and characterized. Application of TR was done with removal of boron by the boron adsorption as a function of contact time, temperature, initial boron concentration, pH and adsorbent dosage. TR was characterized by using FTIR, TGA, SEM (Scanning electron microscopy) and B.E.T. surface area analysis. The optimum adsorption conditions were found as 24 h, 308 K, 4 mgL^{-1} boron, pH=7.0 and 0.1g TR. The adsorption data

was well suited to Langmuir equation. Monolayer adsorption capacity was calculated as 2.56 mgg^{-1}.

The pseudo-second-order equation which indicated chemical adsorption provided the best correlation for the adsorption process. Thermodynamic parameters, standard free energy (ΔG^o), enthalpy change (ΔH^o) and entropy change (ΔS^o) were calculated. ΔG^o was turned out to be negative whereas ΔH^o was positive. Percent of adsorption yield and desorption yield with 0.01M HCl was calculated as 88 and 81, respectively.

Keywords: Polyphenol, tannin, metal complexes, valex, tannic acid, resin, boron, adsorption, adsorption kinetics, adsorption isotherms.

POLİFENOL-Fe(III) KOMPLEKSLERİNİN VE TANNİK ASİT REÇİNESİNİN SENTEZİ, KARAKTERİZASYONU VE UYGULAMALARI

ÖZ

Meşe palamudu ekstraktı olan Valeks, Türkiyede Ege bölgesinde özellikle Salihli'de yaygın olarak yetişen meşe ağaçlarının palamutlarından hidrolize edilen tanen çeşididir. Çalışmanın birinci bölümünde Fe(III)-Valeks ve karşılaştırma amacıyla kullanılan Fe(III)-Tannik asit kompleksleri sentezlenmiştir. Ayrıca, Manyetik özellikleri, Fourier dönüşümlü kızılötesi spektroskopisi (FTIR), Termogravimetrik analizi (TGA), X-ışınları kırınım analizi (XRD), Elektron spin rezonansı (ESR), Matriks yardımlı lazer desorpsiyon/iyonizasyon kütle spektrometresi (MALDI-TOF MS), X-ışını fotoelektron spektroskopisi (XPS) ve Proton nükleer manyetik rezonans spektroskopisi (^{1}H-NMR) kullanılarak karakterizasyonları yapılmıştır.

Fe(III)-Valeks ve Fe(III)-TA komplekslerinin pH=2,4, 4,4, 6,4 ve 8,4 'te kararlılık sabitleri ve Eğim ve Mol Oranları metodlarıyla stokiyometrileri belirlenmiştir. Uygulama amacıyla komplekslerin antioksidan ve antimikrobiyal aktiviteleri incelenmiştir. Komplekslerin antioksidan aktiviteleri *in vitro* olarak 2,2-difenil-1-pikrilhidrazil radikalinin söndürme aktivitesi esas alınarak belirlenmiştir. Antimikrobiyal aktiviteler *in vitro* koşullarda disk difüzyon duyarlılık testlerine göre yapılmıştır. Sonuç olarak komplekslerin antioksidan aktiviteye sahip olduğu ancak herhangi bir antimikrobiyal aktivite göstermedikleri bulunmuştur.

Çalışmanın ikinci bölümünde tannik asit reçine sentezlenerek karakterize edilmiştir. Çalışmanın uygulaması, sulu çözeltiden bor'un uzaklaştırılması için bor adsorpsiyonu yapılarak gerçekleştirilmiştir. Adsorpsiyona denge zamanının, sıcaklığın, başlangıç bor derişiminin, pH ve adsorban miktarının etkisi araştırılmıştır. Reçine, FTIR, TGA, SEM (Taramalı elektron mikroskopisi) ve B.E.T. yüzey alanı analizi kullanılarak karakterize edilmiştir. Optimum adsorpsiyon şartları; 24 saat, 308 K, 4 mgL^{-1} bor, pH=7,0 ve 0,1 g TR olarak belirlenmiştir. Adsorpsiyon verileri

adsorpsiyonun, Langmuir eşitliğine uyum sağladığını göstermiştir. Tek tabakalı adsorpsiyon kapasitesi 2,56 mgg^{-1} olarak hesaplanmıştır.

Adsorpsiyon kinetiğinin yalancı ikinci mertebeden tepkime kinetiğine uyduğu ve sorpsiyon işleminin kimyasal adsorpsiyon ile gerçekleştiği belirlenmiştir. Termodinamik parametreler, Standart serbest enerji (ΔG^o), entalpi değişimi (ΔH^o) ve entropi değişimi (ΔS^o) hesaplanmıştır. ΔG^o' nin negatif, ΔH^o'ın ise pozitif olduğu belirlenmiştir. Adsorpsiyon ve 0.01M HCl ile desorpsiyon verimleri sırasıyla yüzde 88 ve 81 olarak bulunmuştur.

Anahtar sözcükler: Polifenol, tanen, metal kompleksleri, valeks, tannik asit, reçine, bor, adsorpsiyon, adsorpsiyon kinetiği, adsorpsiyon izotermleri.

CONTENTS

Page

LIST OF FIGURES

Page

LIST OF TABLES

CHAPTER ONE

INTRODUCTION

1.1 Polyphenol

The "poly-" name is used as a prefix often meaning "many or much" in chemistry. It derives from the ancient Greek word "polus". Polyphenol word means a chemical structure formed by fastening to a phenol (Figure 1.1) groups and hydroxyl (-OH) groups.
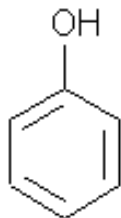
Figure 1.1 Phenol molecule structure

Using the term polyphenol does not mean that this class of larger phenols is a type of polymer. Despite the ordered or random repeating monomeric structures is found in polymers, this requirement is generally not seen in polyphenols. Polyphenols are forming a structural class of generally natural, but also synthetic or semisynthetic, organic chemicals (Nonaka, 1989).

Polyphenols are chemicals naturally found in plants and they are secondary metabolites which are broadly distributed in the plant kingdom. They contain two or more phenolic groups. They includes, ellagic acid and polygalloyl glucoses, which are lower molecular weight compounds and higher molecular weight compounds respectively. The higher molecular weight plant polyphenols are called tannins (Haslam, 1989).

1.1.1 Phenolic Acid

Plant phenolics include phenolic acids and they are deemed to be the most basic class of polyphenols. They are only contain one phenyl ring (Bagchi & Preuss, 2007). Phenolic acids could be classified into derivatives of hydroxybenzoic acid such as gallic acid (Figure 1.2 (a)) and hydroxycinnamic acids (Figure 1.2 (b)) such as sinapic acid (R_1, R_2= OCH_3), caffeic acid (R_2= OH) and ferulic acid (R_2= OCH_3) (Manach, Scalbert, Morand, Rémésy & Jiménez, 2004) as a function of the degree of hydroxylation and methylation of the phenol ring (Bagchi & Preuss, 2007).
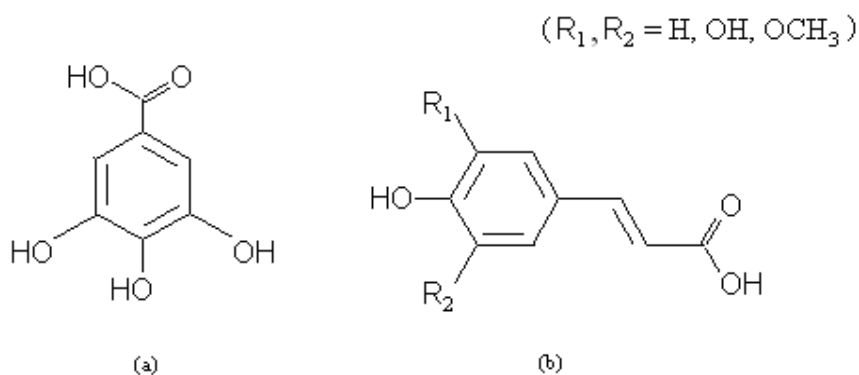
Figure 1.2 Chemical structure of (a) gallic acid and (b) Hydroxycinnamic acid

Hydroxybenzoic acids are less common found in the dietary than hydroxycinnamic acids. But these phenolic acids can be exist in a free or esterified form (Manach *et al.*, 2004).

1.1.1.1 Gallic Acid

Gallic acid, also known as 3,4,5-trihydroxybenzoic acid is a phenolic acid and it occurs as a free molecule or as part of tannin molecules (Figure1.3(a)). It found in gallnuts, grapes, tea leaves, hops, oak bark and some other plants (Abbasi, Daneshfar, Hamdghadareh & Farmany, 2011). Gallic acid contains two functional groups; hydroxyl groups and carboxylic acid group. If gallic acid lose carbondioxide, pyrogallol (Figure 1.3(b)) is formed. It can yield numerous esters and salts

2

containing digallic acid by the reaction of two moles of gallic acid with one to another, digalloly structure is occurred (Fig.1.3 (c,d)).

(a) gallic acid

(b) pyrogallol

(c) digalloyl (para-depside bond)

(d) digalloyl (meta-depside bond)
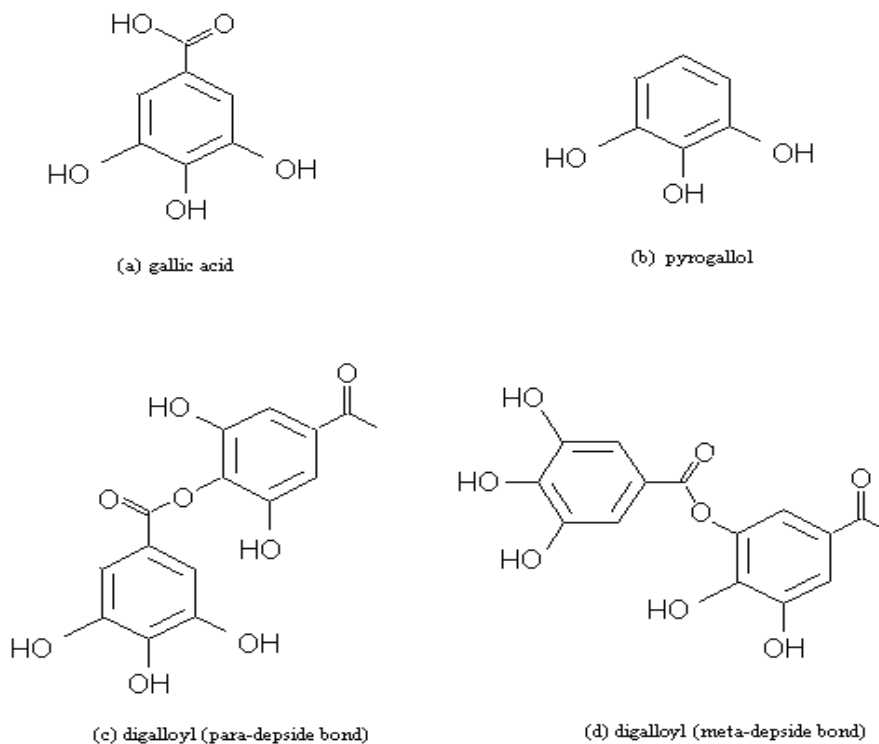
Figure 1.3 Molecule structure of gallic acid (a), pyrogallol (b), digalloyl para (c) and meta (d) depside bond (Hagerman, 2002).

Gallic acid and digalloly represent the polyphenolic part in the molecules of tannins as a result of their hydrolysis and condensation in the presence of acid and enzyme.

1.1.2 Tannin

Our diets, tannins are another mixtures of biodegradable polyphenolic compounds. Tannins are a large part of the plant kingdom, contains the natural products. The word 'tannin' is comes from the French 'tanin' (tanning substance) and it is used for natural polyphenols. Tannins are widely distributed in many

different families of the higher plants such as in chestnut, valonia oak, gall, acorn, sumac, etc, in nature. (Khanbabaee & van Ree, 2001).

Tannins are reported as oligomeric compounds with multiple structure units including free phenolic groups. In terms of structure, physicochemical and biological properties, tannins are constituted a very diversified group of plant secondary metabolites. Soluble in water with the exception of some high molecular weight structures (Rahim & Kassim, 2008). Tannins are generally classified into two main groups; the hydrolysable and condensed tannins (Okuda, 2005).

1.1.2.1 Hydrolysable Tannin

The hydrolysable tannins contain a polyol core (usually D-glucose and 6 to 9 galloyl groups) in which the OH groups of the core glucose are esterified either partially or wholly by gallic acid (Figure 1.4). The ester bond can be hydrolyzed by mild acids and bases or by the enzyme tannase to yield phenolic acids and carbohydrates (Nakamura, Tsuji & Tonogai, 2003).
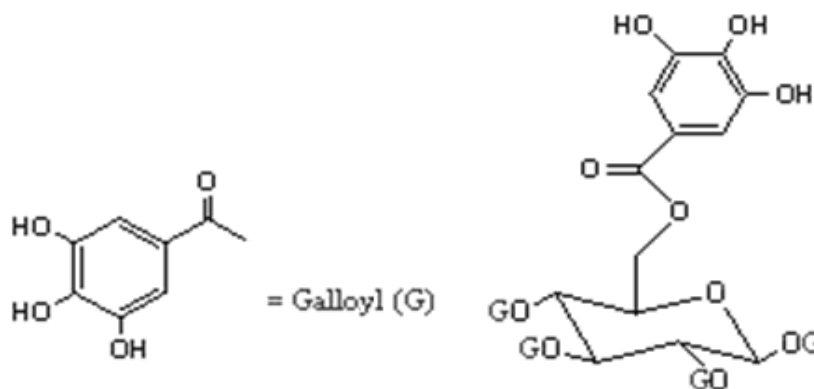
Figure 1.4 Hydrolysable tannins structure. (Niemetz & Gross, 2005)

Hydrolysable tannins are high molecular weight glucose esters of phenolic acids structurally related to gallic acid, ellagic acid and pyrogallol. Thus, they may be used as a model for the study of the inhibiting behavior of hydrolysable tannins (Jaén, González, Vargas & Olave, 2003).

In many different plant species, hydrolyzable tannins are present. But they are found in particularly high concentrations in nutgalls growing on *Rhus semialata* (Chinese and Korean gallotannins) and *Quercus infectoria* (Aleppo or Turkish gallotannins), the seedpods of *Caesalpinia spinosa* (Tara tannins) and the fruits of *Terminalia chebula* (Mussche, 1989). The hydrolyzable tannins are readily hydrolyzed by acids (or enzymes) into a sugar or a related polyhydric alcohol and a phenolic carboxylic acid (Garro-Galvez, Riedl & Conner, 1997).

1.1.2.1.1 Gallotannin. Gallotannins are hydrolysable tannins in which galloyl units or their *meta*depsidic derivatives are bound to diverse polyol-, catechin-, or triterpenoid units (Khanbabaee & van Ree, 2001). Gallotannins are formed from the reaction of glucose with dimers or higher oligomers of gallic acid in Figure 1.5 below;
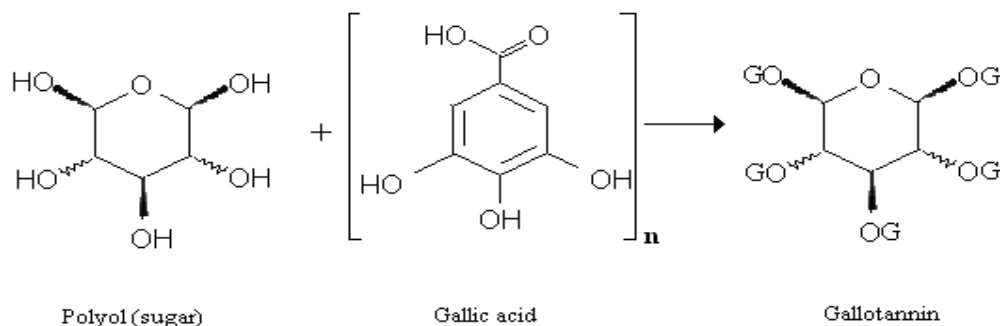
Figure 1.5 Reaction of glucose with gallic acid to form gallotannin

Due to their complex structure, gallotannins have many isomers. The beta anomer is the most common in nature (ex: 1,2,3,4,6-pentagalloly-β-D-glucose). These isomers have the same molecular mass, but chemical properties such as susceptibility to hydrolysis and chromatographic behaviour are structure dependent. Ellagitannins are produced by the oxidative coupling of galloyl groups in gallotannins. The most famous source of gallotannin is tannic acid obtained from the various plants (Hagerman, 2002).

5

1.1.2.1.2 Tannic Acid. Tannic acid (TA), a natural phenolic compound and its structure consisting of a central glucose ring and 10 galloyl groups is shown in Figure1.6. Tannic acid is a product found in most plants. Resources includes the bark of oak, hemlock, chestnut, and mangrove; the leaves of certain sumacs; and fruits of many plants. Tannic acid is amorphous powder with a yellow to light brown coloured with strong astringent taste and it has high molecular weight. Tannic acid solution is obtained by extracted with hot water from natural resources.
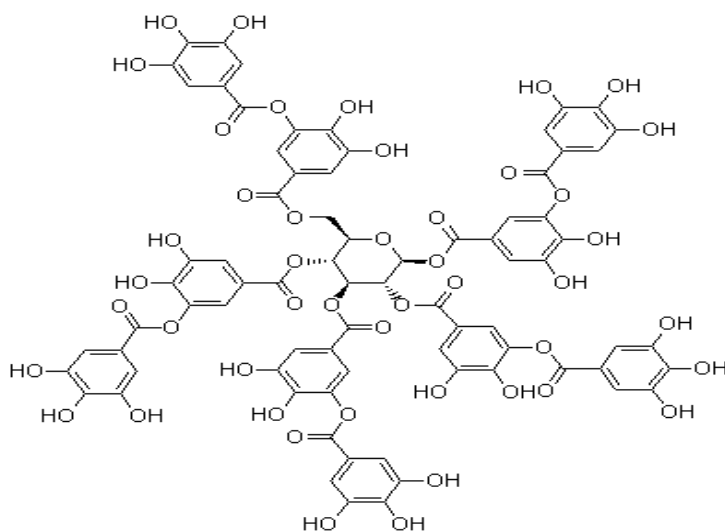
Figure 1.6 Schematic representation of Tannic Acid (ß-1,2,3,4,6-digalloyl-O-D-glucose) (Lopes, Schulman & Hermes-Lima, 1999)

The approximate empirical formula for commercial tannic acid is often given as $C_{76}H_{52}O_{46}$. Each of the five hydroxyl groups of the glucose molecule is esterified with a molecule of digallic acid and they are formed tannic acid structure.

The decomposition point of Tannic acid is in the range of 210–215 °C. It is soluble in water (1gram tannic acid dissolves in 0.35 mL of water), alcohols, acetone and warm gylcerin. But it is not soluble in ether and chloroform (Kiel, Thomas & Mani, 2004; Leflein & D'Addio, 2003).

Tannic acid is widely used in chemical industry, food, medicine and leather. Industrial wastewater from the factories, tannic acid may interact with metal in these

environmental water to form tannic acid–metal complexes/combination. Tannic acid may also interact with toxicants in aquatic ecosystems and may change their toxicity (Xie & Cui, 2003).

1.1.2.1.3 Ellagitannin. The ellagitannins are kind of gallotannin formed primarily from the oxidative linkage of galloyl groups in 1,2,3,4,6-Pentagalloyl glucose and diverse class of hydrolyzable tannins (Sepulveda et al., 2011). In ellagitannins, at least two galloyl units are C-C coupled to each other, and do not contain a glycosidically linked catechin unit (Khanbabaee & van Ree, 2001). Also tannins having the hexahydroxydiphenoyl (HHDP) group have been named ellagitannins as they produce ellagic acid upon hydrolysis and those having only the galloyl groups are called gallotannin. Ellagitannins contain various numbers of HHDP units, as well as galloyl units and/or sanguisorboyl units bounded to sugar moiety. In Figure 1.7 formation reaction of ellagic acid and ellagitannin was shown. Hexahydroxydiphenic acid, created after hydrolysis, spontaneously lactonized to ellagic acid (Yoshida, Hatano, Ito, Okuda & Quideau, 2009).
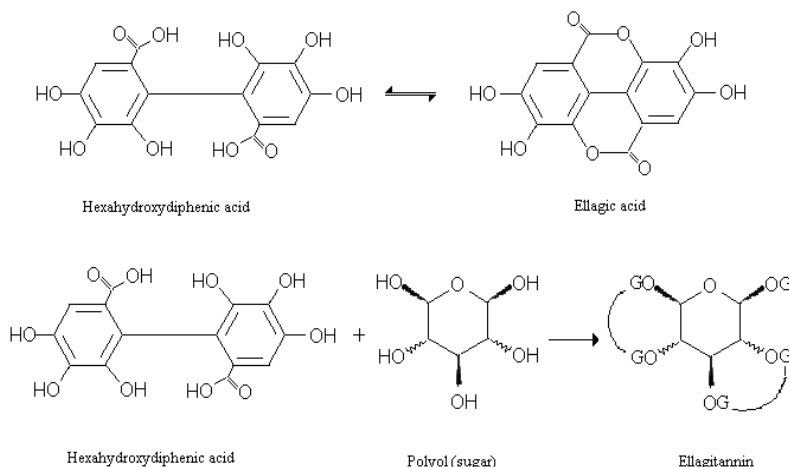
Figure 1.7 Formation reaction of Ellagic acid and Ellagitannin (Hagerman, 2002).

7

1.1.2.2 Condensed Tannin

Condensed tannins (polyflavonoid tannins, non-hydrolyzable tannins or flavolans) are polymers and they obtained by the condensation of flavans (Cammack et al., 2006). Different types of condensed tannins exist such as the proanthocyanidins. The basic structure of the proanthocyanidins are flavonoids and they include the flavones, flavonols, flavanones, catechins or epicatechin, anthocyanidins and isoflavones (Ross & Kasum, 2002). In general, condensed tannins important commercial sources are the quebracho tannins, catechu tannins, mimosa and mangrove tannins. Schematic representation of main monomer of condensed tannins; epicatechin and catechin was shown in Figure1.8 and they are then expanded, by the sequentially addition of similar phenol units to produce condensed tannin (Figure 1.9).
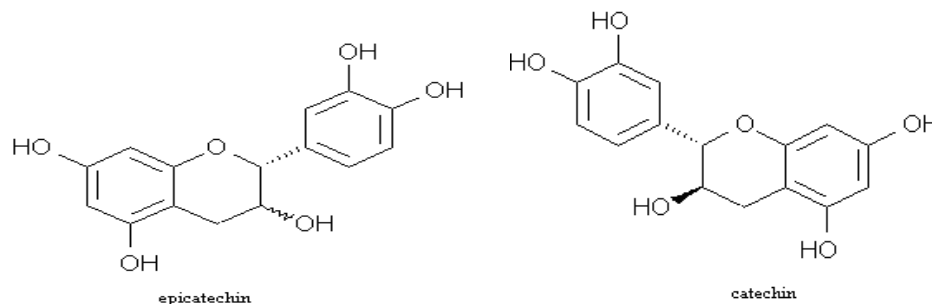
Figure 1.8 Schematic representation of epicatechin and catechin (Hagerman, 2002).

Condensed tannins are all oligomeric and polymeric proanthocyanidins formed by linkage of C-4 of one catechin with C-8 or C-6 of the next monomeric catechin (Khanbabaee & van Ree, 2001).

8
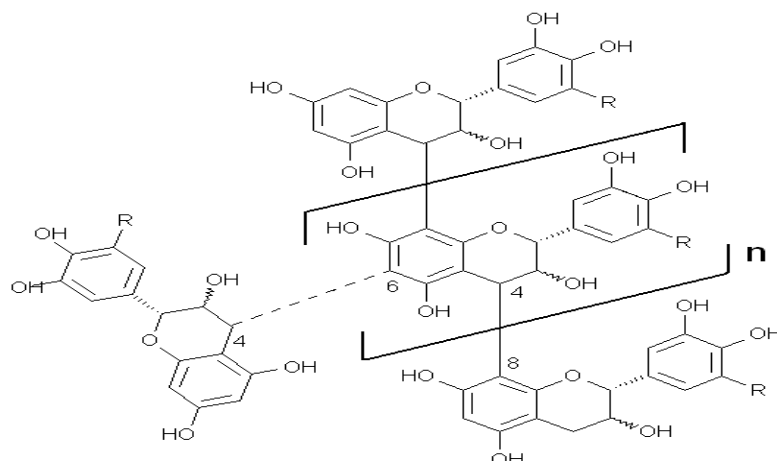
Figure 1.9 Schematic representation of condensed tannin (Schofield, Mbugua & Pell, 2001)

1.2 Applications of Tannin

Tannins are natural compounds and they uses in many areas. Figure 1.10 are summaries of the general usage areas of the tannins.

TANNIN

Figure 1.10 Examples of tannin uses in many areas

- Phenolics are contribution to the taste, colour and nutritional properties of fruit. So they are important component of fruit quality (Cheynier, 2005). Polyphenols are known to influence the pharmacological activities of plants. For instance,

prevention of lung cancers (Stoner & Morse, 1997) and the protection of the body tissues against oxidative stress (Salah et al., 1995) have been attributed to plant polyphenols.

- For many years, tannins are used in textile field. Natural tannins the earliest textile applications with the dyeing of cotton and silk with dye woods, where in the tannin was used to 'fix' the metal salt (e.g. $CuSO_4$) that was employed as a mordant for the dye (Burkinshaw & Bahojb-Allafan, 2003).

- Tannins are used for produce of inks, as a mordant in dyeing. According to the type of tannin different colors of ink are manufacturing with ferric chloride (either blue, blue black, or green to greenish black) (Bele, Jadhav & Kadam, 2010).

- Coffee, beer, tea, red wine, etc. beverages contain large amounts of flavonoids (Sungur & Uzar, 2008). Tannins have positive impact on the quality of the wine and acts as a preservative and mellow, helping the wine to grow into its complexity and become truly exceptional. Tannic acid is used as aroma ingredient in alcoholic drinks, soft drinks or juices.

- Flavonoids shows important role for biological and pharmacological activities as antioxidant, anti-inflammatory, antimicrobial, anticancer, cardiovascular protection, etc (De Souza & De Giovani, 2005). It can be used in medicine as an astringent and for treatment of burns or may be employed medicinally in antidiarrheal, hemostatic, and antihemorrhoidal compounds (Di Carlo, Mascolo, Izzo & Capasso, 1999).

- Oak bark has traditionally been the primary source of tannery tannin. Tannin is used in the leather industry as a filler material. It transforms certain proteins of animal tissue into compounds that resist decomposition.

- Tannins were continued researches as corrosion inhibitors in aqueous media.

• They are also referred to as condensed tannins because they possess the ability to precipitate proteins from aqueous solution (Bagchi & Preuss, 2007). More precisely, proanthocyanidins form complexes with salivary protein which then account for the astringent taste of chocolate and certain fruits (grapes, peaches, kakis, apples, pears, berries) and beverages (Manach *et al.*, 2004).

• Local applications of tannic acid are often made to inflamed mucous membranes, especially in pharyngitis. Tannic acid has astringent action. However, often causes nausea and vomiting, and hence some one of the protein combinations is better for action on the intestine.

• Tannins can also be effective in protecting the kidneys. Tannins have shown potential antiviral (Lu, Liu, Jiang & Wu, 2004), antibacterial (Akiyama, Fujii, Yamasaki, Oono & Iwatsuki, 2001) and antiparasitic effects (Kolodziej & Kiderlen, 2005).

• Tannins remedial values of include application on burns to heal the injury and on cuts to stop bleeding. On the exposed tissues, tannins are form a strong 'leather' resistance to helps protecting the wound. While it stops infection from above, internally tannin continues to heal the wound (Pasumarthi, Chimata, Chetty & Challa, 2011).

1.2.1 *Tannin as Metal Ion Chelators*

Tannins are often bound to basic compounds, proteins, other high molecular mass compounds and metallic ions. Tannins can also bind with metal ions to form polyphenol-metal complexes, which are probably soluble or precipitated, depending on the type of their plants (Quideau, 2009).

Most tannins are cyclic structures and they have multiple adjacent phenolic hydroxyl groups (-OH); exhibit specific chelating capability to metal ions such as thorium (IV) (Liao, Li & Shi, 2004), uranium (Liao, Ma, Wang & Shi, B., 2004),

hexavalent chromium (Nakano, Takeshita, Tsutsumi, 2001), cadmium, mercury (Vazquez, Gonzalez-Alvarez, Freire, Lopez-Lorenzo & Antorrena, 2002), copper (Karamać, 2009; Liao, Lu, Zhang, Liu & Shi, 2004; Şengil & Özacar 2009), gold (Parajuli, Kawakita, Inoue, Ohto & Kajiyama, 2007), silver, palladium (Kim & Nakano, 2005), lead (Özacar, Şengil & Türkmenler, 2008; Zhan & Zhao, 2003) and vanadium(III) (Fatima & Maqsood, 2005). Furthermore, condensed tannins multicatecholate nature is allows reticulation. This situation favors the formation of metal-tannin precipitates (Haslam et al., 1992; McDonald, Mila & Scalbert, 1996; South & Miller, 1998).

Metal complexation by polyphenols is a phenomenon with many biological implications. Formation of stable H_2O-soluble polyphenol complexes with Al^{+3} may, e.g., contribute to general mechanisms of Al^{+3} uptake in plants and Al^{+3} toxicity in humans in relation to neurological and bone disorders (Deng et al., 2000). Al^{+3} complexation by polyphenols may also inhibit the antioxidant activity of dietary polyphenols circulating in plasma (Yoshino, Ito, Haneda, Tsubouchi & Murakami, 1999) and participate in colour expression in plants (Takeda, Yamashita, Takahashi & Timberlake, 1990).

Tannins also have been referred as rust converters since their presence converts active rust into non-reactive protecting oxides. Protection properties result from the reactions of polyphenolic parts of the tannin molecule with ferric ions thereby forming a highly cross-linked network of ferric-tannates (Yahya, Mohamad-Shah & Rahim, 2008).

The formed tannin complexes are often coloured, and it has been suggested that characteristic colours can be used to identify specific arreangements of the phenolic groups in tannins. Metal ion chelation can alter the redox potential of the metal, or prevent its partecipation in redox reactions (e.g. oxidation leading to cancer).

Al(III) and Zn(II) metal complexes syntheses and structural investigations with condensed tannin (quercetin, rutin and galangin) have been reported by De Souza

and De Giovani (2005). Electrospray mass spectrometry have used to investigate metal ion interactions with six flavonoids by Fernandez, Mira, Florencio & Jennings (2002). Complexes of flavonoids (rutin, taxifolin, epicatechin, luteolin) with transition metals have investigated by Kostyuk, Potapovich, Strigunova, T.V. Kostyuk & Afanas'ev (2004). Brown, Khodr, Hider & Rice-Evans (1998) have examined the ability of some flavonoids (quercetin, rutin, luteolin, kaempferol) to interact with Cu^{2+} ions. Spectrophotometrically the interactions of flavonoids with metal ions have demonstrated Mira et al. (2000). Bai et al. (2004) have investigated the structure and fragmentation mechanism of transition metal–rutin complexes by electrospray ionization tandem mass spectrometry (Sungur & Uzar, 2008).

Burkinshaw & Bahojb-Allafan (2003) has been developed a one-bath, two-stage, tannic acid based after treatment for nylon 6,6 dyed with acid dyes, in which an enzyme was used to complex tannic acid. Electrospray mass spectrometry was used to characterize metal-complexing ligands derived from tannic acid, a component of natural dissolved organic matter (Ross, Ikonomou & Orians, 2000). A complete physico-chemical study of the chelation of iron(III) by catechin, an abundant polyphenol in green tea have been reported by Elhabiri, Carrer, Marmolle & Traboulsi (2007). Investigate the effect of increasing Cu concentrations on Cu speciation in aqueous solution with tannic acid and to quantify labile soluble Cu species from ISE (pHoenix Electrode Corporation, Houston, USA) and DGT (Diffusive gradients in thin-films) measurements were the objectives of Kraal, Jansen, Nierop & Verstraten (2006) study.

Interactions between tannic acid and heavy metal ions by several voltammetric techniques as a model for the metal binding of tannin substances have been studied by Cruz, Diaz-Cruz, Arino & Estaban (2000). Also they evaluate the possible effects of such compounds on the voltammetric analysis of natural samples.

Cheng & Crisosto (1997) investigate the formation of metallic complexes in acetate buffer solutions at physiological pH, and then to assess the role of copigmentation, iron-phenolic complex formation and cellular iron chelators in

peach and nectarine skin discoloration. Kinetics and mechanisms of the complex formation and antioxidant behaviour of the polyphenols EGCg and ECG with iron(III) have been studied by Ryan & Hynes (2007).

Chemical properties of complexes of tannic acid and myricetin from flavonoids with Fe(III) have investigated by Sungur & Uzar (2008). For the Fe(III), flavonoids are effective metal ions chelators and strong chelating agents. The chelation of metal ions (especially iron) by flavonoids may render those ions inactive in generating radicals or, alternatively, the generated radicals will be intercepted by the flavonoids themselves. Therefore, it is expected that in metal overload diseases such as β-thalassemia, flavonoids may play an important role.

1.2.2 Tannin Resin

During the last years, the interest on biomaterials and specifically in tannins was growing (McDougall, Martinussenb & Stewart, 2008). Tannins are naturally occurring phenolic compounds, which have been a subject of extensive research leading to development of a wide range of industrial applications. Tannins can probably be used as alternative, effective and efficient adsorbents for the recovery of metal ions because of natural biomass containing multiple adjacent hydroxyl groups and exhibiting specific affinity to metal ions (Şengil, 2009).

Tannins had showed high performance in removing heavy metal ions such as cobalt, chromium and uranium due to the present of many adjacent phenolic hydroxyl groups in their structure. Tannins in nature are able to react with heavy metal ions in aqueous solution; however, their application as adsorbent is restricted because of their solubility in water. Tannins are water soluble compounds, so in order to use tannins as adsorbents; they need to be modified to insoluble tannin gels. This could be done either through the reaction between gallic acid units of gallotannins and formaldehyde due to the strong nucleophilicity of their rings or immobilization of the tannins onto various water-insoluble matrices (Sudrajat, Bang & Trung, 2008).

Its volume is easy to be reduced by drying and incinerating, because of insoluble tannin gel consists of only carbon, hydrogen and oxygen. So it is considered highly applicable. In general, the residue after incineration will be the oxide of the adsorbed metals (Sudrajat, Bang & Trung, 2008).

In the literature, some researchers synthesized sorbents from commercial condensed tannin extracts and applied them in removal of heavy metals such as uranium, americium, copper, chromium, cadmium, vanadium and lead (Özacar, Şengil & Türkmenler, 2008).

Another study to overcome this disadvantage, attempts have been made to immobilize tannins onto various water-insoluble matrices (Arts & Hollman, 2005).

Zeng et al, was prepared a novel adsorbent, collagen immobilized tannin adsorbent (CITA) and its adsorption behaviors to Th(IV) were investigated. The fundamental adsorption behaviors of CITA to thorium(IV), including adsorption capacity, effects of pH and ionic strength on adsorption, adsorption kinetics, adsorption isotherms and the adsorption-desorption properties on column, were investigated (Zeng, Liao, He & Shi, 2009).

Yurtsever & Şengil (2009)were investigated the effect of temperature, pH and initial metal concentration on Pb(II) biosorption on modified quebracho tannin resin (QTR). Also, Şengil et al were studied the biosorption of Cu(II) from aqueous solutions by valonia tannin resin as a function of particle size, initial pH, contact time and initial metal ion concentration (Şengil, Özacar & Türkmenler, 2009).

The sorption of lead(II) and mercury(II) ions from aqueous solutions by moss peat (from Poiana Stampei, Romania) was studied in a batch system by Bulgariu, Rătoi, Bulgari & Macoveanu, (2008). The data obtained from experiments of a single-component sorption were analyzed using Langmuir and Freundlich isotherm models.

The removal of poisonous Pb (II) from wastewater by different low-cost abundant adsorbents was investigated by Abdel-Ghani, Hefny & El-Chaghaby, (2007). Rice husks, maize cobs and sawdust, were used at different adsorbent/metal ion ratios. The influence of pH, contact time, metal concentration, adsorbent concentration on the selectivity and sensitivity of the removal process was investigated.

Sudrajat et al were extracted tannins from mangrove bark of *Bruguiera sexangula Poir* species, which is a by-product of charcoal industry in Vietnam. The extracted tannins then immobilized by polymerization using formaldehyde as a cross-linking agent to produce tannin-based adsorbent. The optimum adsorption and desorption pH and adsorption isotherms of this tanin-based adsorbent towards Cd^{2+} were characterized and evaluated (Sudrajat, Bang & Trung, 2008).

Recently, a novel adsorbent prepared from condensed tannin molecules by cross-linking with formaldehyde which had a significant ability to adsorb toxic metal ions (Nakano et al., 2001; Zhan et al., 2001; Kim et al., 2007a) and precious metal ions (Kim et al., 2007b, 2008). Moreover, it has been succeeded in enhancing the adsorbability for precious metal ions by the amine modification of these tannin gels (Kim, 2009; Morisada, 2011). The application of such tannin-based materials has been also investigated actively by other research groups (Pizzi, 1982, 2009; Thevenon, 2009; Sanchez-Martin, 2010).

1.3 Boron and Methods of Boron Removal

Boron is a relatively rare element in the earth's crust and it is representing with only 0.001%. Boron does not appear in nature in elemental form. It always occurs in nature bound to oxygen in the form of borates. So boron is found combined in borax, boric acid, colemanite, kernite, ulexite and borates minerals (Parks & Edwards, 2005).

Boron is widely distributed in surface and ground waters, occurring naturally or from anthropogenic contamination, mainly in the form of boric acid or borate salts (Sabarudin, Oshita, Oshima & Motomizu, 2005).

When the acid dissociation constant of boric acid (5.81×10^{-10} at 25 ^{o}C; $pK_a=9.24$) is considered, it can be predicted that H_3BO_3 is the predominant form at neutral and low pH values whereas $B(OH_4)^-$ is expected to be present at high pH. Both forms may exist in equilibrium (1.1) at a pH range of 7.0-11.5 (Darbouret & Kano, 2000).

$$H_3BO_3 + H_2O \leftrightarrow B(OH)_4^- + H^+ \tag{1.1}$$

Turkey has the largest boron reserve. It is approximately 90 million tons in the world. It was estimated that Turkey has about 70% of the known reserves of the world. There is a variety of application including various boron fertilizers, insecticides, corrosion inhibitors in anti-freeze formulations for motor vehicle and other cooling system, buffers in pharmaceutical and dye stuff production. The use of boron compounds for moderator in nuclear reactor, where anthropogenic water-soluble boron compounds are discharged to aqueous environment (Yılmaz, Boncukcuoglu & Kocakerim, 2007). Many industries use boron compounds as their raw materials. The principal industrial uses of this element and its compounds are in the production of fiberglass insulation, borosilicate glass, and detergents. Other uses are in fertilizers, nuclear shielding and metallurgy.

Boron is important as a micronutrient for living creatures. Recently it has come into focus of researchers because of its unique characteristics. Its range between deficiency and toxicity is very narrow. Although not confirmed, but it was claimed that over intake of boron may cause acute boron toxicity with nausea, headache, diarrhea, kidney damage, and death from circulatory collapse (Moore, 1997; Korkmaz, 2007).

In soil and irrigation waters boron is normally in very low amounts. But it accumulates very fast in soils irrigated with boron-containing wastewaters because of difficulty of washing it. Boron compounds passing to soil, surface waters and ground waters form many complexes with heavy metals such as Pb, Cd, Cu, Ni, etc. and these complexes are more toxic than heavy metals forming them.

Although little amount of boron is a nutrient for some plants, its excessive amount affects badly the growth of many agricultural products. Also, the maximum boron level in drinking water for human health is given as 0.5 mg/L in WHO standards and is 0.75 mg/L for irrigation water (Rowe, 1995; Yılmaz, 2005).

The increasing use of boron in industries and consequently its discharge to the environment as industrial wastes has become a serious threat to human, plants, animals and ecological systems. Boron removal will be necessary in the near future since the fresh water in the world is decreasing. Removal of boron from seawater, which has become of interest as a drinking water supply, would be essential. There is no simple technique for removal of boron in aqueous solutions.

Studies have been conducted to remove boron from water and wastewater in order to decrease boron concentration to a certain range demanded by different standards. Removal of boron from aquatic media is still a great environmental problem. Technologies for boron removal have been reviewed and reported (Yonglan & Jiang, 2008).

There are several physicochemical treatment processes typically used to remove boron from water and wastewater such as adsorption onto clays and clay minerals (Goldberg, 1996; Karahan, 2006; Öztürk, 2004), ion exchange (Hanay, 2003; Kabay, 2004, 2006; Simonnot, 2000; Xiao, 2003), solvent extraction (Bicak, 2003; Özay, 2006; Yurdakoc, 1999), polymer-supported resins (Bicak, 1998; Senkal, 2003), polymer-assisted ultrafiltration (Dilek, 2002; Smith, 1995), electrocoagulation (Bektas, 2004; Jiang, 2006), N-methyl-D-glucamine functionalized silica–polyallylamine composites (Li et al., 2011) and reverse osmosis (Bouguerra, 2008;

Koseoglu, 2008). However, the interaction between boron and polyhydroxy compounds has been well known because of the affinity of boron towards adjacent hydroxyl groups of polyhydroxy compounds such as diols and aromatic o-hydroxymethylphenolic compounds (Bursali, 2011; Özay, 2006; Yurdakoc, 1999).

The investigations have indicated that the only method adapted for potable water is ion exchange using selective resins, in spite of their high costs. It also has been shown that chelating resins containing functional groups in the 1-2 or 1-3 positions of phenyl ring have higher selectivity for boron removal. The trend is toward operating cost reduction which is an issue to deal with when using ion Exchange resins. For boron removal process, not only the effectiveness of removal process, but also the availability and the cost efficiency should be considered as the most important characteristics for this process. The removal efficiency for reverse osmosis was about 40-80% and in alkaline solutions with higher pH (10-11) over 90%. But RO process is not effective because of the membrane cost, scaling, and stability.

Another method for removal of boron was co-precipitation through which dilute boron solutions (1.6-0.16 mg/L) could be treated by 90% efficiency using aluminum sulfate and calcium hydroxide. However, the sludge was being produced at the end of this process made it an expensive process. Electrodialysis was another boron removal method. The boron removal efficiency in this process was about 40-75% that was not enough.

Adsorption is a cost effective process too. Some adsorbents have been used by researchers were amorphous aluminum and iron oxides, kaolinite, allophone (Su & Suarez, 1995) acid soils (Data & Bahadoria, 1999), pyrohyllite (Keren et al., 1994), hydrous ferric oxide (Peak et al., 2003), chitosan resin (Matsumoto et al., 1999), activated carbon (Ristic & Rajakovic, 1996), fly ash (Sütçü, 2005), and clays and soils (Goldberg et al., 1996). Although ion exchangers seem not to be cost-effective considering their regeneration processes, they offer high removal efficiencies up to 99%. Not to mention that we can reduce the cost via producing new resins by local materials.

Adsorption can be used for advanced treatment of boron. Adsorption is a comparatively more useful and economical technique at low pollutant concentrations. The most widely used adsorbent for wastewater treatment is currently activated carbon, but recognizing its high cost, many investigators have studied the feasibility of cheaper and commercially available materials as its possible replacements (Kavak, 2009).

1.4 Objectives and Scope of the Study

Polyphenols are a group of chemicals found in many fruits, vegetables and other plants, such as berries, walnuts, olives, tea leaves and grapes. The higher molecular weight plant polyphenols are called tannin. Tannins are complex mixtures of polyphenolic compounds and they were extracted from chestnut, valonia oak, gall, acorn, sumac, etc. plants. Tannins are obtained from the plants with appropriate chemical methods, shows special interests against metal ions. Also many biological activities, antioxidant and antimicrobial activities have been reported for plant tannins (Igbinosa, O.O., Igbinosa, E.O. & Aiyegoro, 2009; Nohynek et al., 2006) and recent articles about tannins are still being published. 2,2-Diphenyl-1-picrylhydrazyl (DPPH) radical scavenging activity is a rapid, simple and inexpensive method for determining antioxidant activity indirectly. It has also been used to quantify antioxidants in complex biological systems in recent years (Blois, 1958; Esmaeili & Sonboli, 2010).

Valonia oak (Quercus Ithaburensis sp. Macrolepis) fruit of Valonia which is naturally and widely grown in the western Anatolian region in Turkey (especially in Salihli), is rich in tannin. They include hydrolyzable tannins used in many areas called Valex.

In this thesis, two different studies have been conducted on tannin. In the first study tannin-Fe (III) complex formation and characterization of the complex was investigated. The synthesis complex is intended for use with "electrostatic spray painting technique" in the paint industry. And also an antioxidant and antimicrobial

properties of the complexes were investigated and the changes in antioxidant and antimicrobial activities of Valex and TA were investigated in the case of iron binding.

The antioxidant activity of Fe(III)-Valex, Fe(III)-TA complexes were assayed with DPPH radical scavenging activity (Chu, Lim, Radhakrishnan & Lim, 2010) and BHA, BHT were used as positive controls. The antimicrobial activity of Fe(III)-Valex, Fe(III)-TA complexes were determined *in vitro* conditions by the disc diffusion test of National Committee for Clinical Laboratory Standards (NCCLS) rules for five different bacterial cultures and one fungus (Clark, Jacobs & Appelbaum, 1998).

Then the stoichiometric composition and K values were determined at optimum pH. The Slope and Mole Ratio method were used for the spectrophotometric determination of the complex stoichiometries in pH range from 2.4 to 8.4.

The characterization of Fe(III)-Valex, Fe(III)-TA complexes were realized by Magnetic Susceptibility, FTIR, TGA, XRD, ESR, MALDI-TOF MS, XPS and H-NMR analysis methods.

In the second study "Synthesis, characterization and applications of tannic acid resin", we have synthesized by chemical activation with formaldehyde in aqueous ammonia and characterized a tannic acid resin (TR) by using Fourier transform infrared spectroscopy (FTIR), scanning electron microscopy (SEM), thermogravimetric analysis (TGA) and BET surface area analysis.

Then its adsorption behavior of boron from aqueous solution was investigated. The effect of pH on the boron adsorption has been examined to elucidate the boron adsorption mechanism onto the TR. Using theoretical kinetic models, the adsorption kinetics of TR have been analyzed.

Lastly, the adsorption isotherms and thermodynamic parameters (such as standard free energy (ΔG^o), enthalpy change (ΔH^o) and entropy change (ΔS^o)) of boron adsorption have been investigated and then compared with those of other boron adsorbents. were calculated. Finally, boron desorption study was investigated 0.01M HCl.

CHAPTER TWO

MATERIALS AND METHOD

2.1 Materials and Apparatus

For the "Synthesis, characterization and applications of polyphenol-Fe(III) complexes" study, Valex was obtained from Balaban Company from Salihli/Manisa. Valex was extracted with hot water from valonia tannin in the factory and no further purification was made before use. For the experiments the valex determined by the filder method and its content was: tannins, 68-70%; non-tannins, 25%; undissolved materials, 1.10-1.15%; moisture: 4.05-5.50% (Anonymous, 1984; Dıgrak, Ilçım, Alma & Sen, 1999)

Iron(III) chloride hexahydrate (Merck 103943) was used for the preparation of Fe(III)-Valex and Fe(III)-TA (Riedel-de Haën 1401-55-4, powder) complexes in buffer solutions.

The optimum pH were investigated in the range of 2.4-8.4 for the complex experiments. For pH=2.4 formate buffer (0.025M formic acid (Merck 822254) / 0.025M sodium hydroxide(1064981000)), for pH=4.4 acetate buffer (0.2M acetic acid (Merck 100063) / 0.2M sodium acetate trihydrate (Merck 106265), for pH=6.4 citrate buffer (2M citric acid (Merck 1.00242) / 2M sodium hydroxide) and for pH=8.4 Tris/HCl buffer (0.1M tris-(hydroxymethyl)amino-methane (Merck 1.08387.0500) / 0.1M hydrochloric acid (Riedel-de Haën 07102)) were used.

All other chemicals were used analytical grade. Working solutions were also freshly prepared from the stock solutions. All spectrophotometric measurements were performed with Shimadzu 1601 UV-Vis. spectrophotometer. The pH was measured with a Denver 215 model pH meter and a Heidolph MR standard magnetic stirrer was used during the experiments.

For the "Synthesis, characterization and applications of tannic acid resin" study, TA powder (Riedel-de Haën 1401-55-4), ammonium hydroxide solution (Riedel-de Haën 05003), formaldehyde (Fluka 47630), nitric acid (Fluka 17078), boric acid (H_3BO_3) (Merck 1.00160), citric acid monohydrate (Merck 1.00242), L(+)-ascorbic acid (Merck 5.00074), tri-sodium citrate dihydrate (Fluka 71406) and azomethine-H sodium salts (Fluka 11637) of analytical grade reagents were used without any further purification. Stock solution of boron (100 mgL^{-1}) was prepared by dissolving boric acid in ultra pure water. Working solutions were freshly prepared from the stock solutions.

A Denver 215 model pH meter, a Heidolph MR standard magnetic stirrer, a Polyscience 9006 model refrigerating-heating circulator, a GFL 1086 model shaking water bath and Nüve NF 1215 model centrifuge were used during the experiments.

Boron concentrations in aqueous solutions were determined spectrophotometrically by azomethine-H method (Yurdakoc, 1999; Rump, 1992) with Shimadzu 1601 UV-Vis. spectrophotometer.

Unless otherwise stated, all experiments were carried out by using ultra pure water. The specification of the ultra pure water is the followings. Resistivity of ultra pure water is 18.2 MΩcm (25°C). TOC and pyrogen levels of ultra pure water are 1-5 ppb and <0.001 Eu/mL, respectively. Bacteria and particulates are <1 cfu.mL^{-1} and <1 P.mL^{-1}, respectively.

2.2 Synthesis, Characterization and Application of Polyphenol-Fe(III) Complexes

2.2.1 Preparation of Fe(III)-Valex and Fe(III)-TA Complexes

Complex formation was carried out at pH range from 2.4 to 8.4. After determining the optimum pH value all the characterization experiments will take place in this pH value. For the synthesis of Fe(III)-Valex and Fe(III)-TA complexes, 10^{-4}M ligand (Valex or TA) and 10^{-3}M Fe(III) solutions were mixed with the ratio of 1:1 (v/v) and diluted to 10 mL with decided buffer solutions. The mixture was stirred mechanically to complete the reaction at room temperature for one day (Jaén & Navarro, 2009). Eventually precipitate was formed and separated from the supernatant phase. The precipitate was washed with distilled water, dried under vacuum and recrystalized from acetone before characterization. Absorption spectra of the ligands and their complexes were recorded between 200-800 nm to determine the λ_{max}.

Absorption spectroscopy to organic compounds most applications are based upon transitions for n or π electrons to the π* excited state. For the various types of molecular orbitals the energies are very different. Normally, the energy level of a nonbonding electron lies between the bonding and the antibonding π and σ orbitals.

The n$\rightarrow\sigma$ * transitions are produced in saturated compounds containing atoms with unshared electron pairs. These transitions require less energy than $\sigma\rightarrow\sigma$ * transition and are normally produced in the region between 150 and 250nm. The n$\rightarrow\pi$ * and $\pi\rightarrow\pi$ * transitions are the most important transitions for the absorption spectroscopy for organic compounds, because these transitions are in a convenient spectral region between 200 and 700nm (Bermejo-Barrera & Cocho de Juan, 2006).

Aromatic hydrocarbons UV spectra are characterized by three sets of bands E1, E2 and B bands. B bands (Benzenoid bands) that originate from $\pi\rightarrow\pi$ * transitions in aromatic or heteroaromatic compounds. E bands, similar to B bands, these are

characteristic of aromatic and heteroaromatic compounds and originate from $\pi \rightarrow \pi *$ transitions of the ethylenic bonds present in the aromatic ring. E bands which appears at a shorter wavelength and is usually more intense is called E1 band. The low intensity band of the same compound appearing at a longer wavelength is called E2 band. Generally the E2 and B bands are of most interest to chromatographers.

Auxochromes are a functional group that does not itself absorb in the UV region but have the effect of shifting chromophore peaks to longer wavelengths and increasing their intensity. The –OH and –NH_2 groups have an auxochromic effect on benzene chromophore. These substituents have at least one pair of n electrons capable of interacting with π electrons of the ring. This stabilizes the π^* state and lowers its energy. The phenolate anion auxochromic effect is more pronounced than for phenol because the anion has an additional pair of unshared electrons (Skoog, Holler & Nieman, 1998).

2.2.2 Stoichiometry and Stability Constant of Complexes

The Slope and Mole Ratio method were used for the spectrophotometric determination of the complex stoichiometries in pH range from 2.4 to 8.4 with the appropriate buffers. Primarily λ_{max} values of complexes were determined with the using buffers for the both methods.

In the slope ratio method, two series of solutions mixtures were prepared. In the first serie, ligand (Valex or TA) concentration was kept constant $(2 \times 10^{-3} M)$ while the Fe(III) concentration was increased $(0.6 \times 10^{-4}, 1.2 \times 10^{-4}, 1.8 \times 10^{-4}, 2.4 \times 10^{-4}, 3.0 \times 10^{-4} M)$ in a regular way. In the second serie, Fe(III) concentration was kept constant $(2 \times 10^{-3} M)$ while the ligand concentration was increased $(0.6 \times 10^{-4}, 1.2 \times 10^{-4}, 1.8 \times 10^{-4}, 2.4 \times 10^{-4}, 3.0 \times 10^{-4} M)$ in a regular way, as well.

The absorbances of the solutions were plotted against the concentration of the metal or ligand component. The obtained lines had different slope values. The first and second series slope values were equal to molar absorptivity constants of metal

(ε_M) and ligand (ε_L) respectively. The ratio of the Fe(III) to ligand (Metal/Ligand) was calculated from the ratio of the molar absorptivity constants ($\varepsilon_M/\varepsilon_L$) (Skoog & Leary, 1992).

In the Mole ratio method; 5×10^{-4}M ligand (TA or Valex) and 5×10^{-4}M Fe(III) were prepared in buffer solution. In this method, two sets solution mixtures were used. In the first case, metal (5×10^{-4}M) was kept constant with the increase of ligand concentration. Then the absorbances were noted at the λ_{max} of the complex. The absorbance values were then plotted against L/M ratio. In the second set, ligand was kept fixed while metal was gradually increased. The absorbance was noted at the λ_{max} of the complex. Then the absorbance was plotted versus M/L ratio.

The stability constants were provided the information required to calculate the concentration of the complexes in solution. The formation of the equilibrium expressions between metal (M) and ligand (L) were represented as equilibrium (2.1):

$$M + 2L \leftrightarrow ML_2 \tag{2.1}$$

M, L and ML_2 were showed, the metal ion, the ligand and the complex respectively. When the M/L ratio is very large, the equilibrium was shifted completely to the right and the concentration of complex was determined by the following equation (2.2):

$$[ML_2] \approx C_M = A/\varepsilon b \tag{2.2}$$

Where A is the absorbance, ε is the molar absorptivity constant, b is the light path length in centimeters and C_M is the analytical concentrations of metal.

Fe(III) [10^{-2}M] and ligand [(2×10^{-5}M, 4×10^{-5}M, 6×10^{-5}M, 8×10^{-5}M, 10×10^{-5}M)] mixtures observed absorbance values and molar absorptivity constant were used for the determination of complex concentration. The following equations (Eq. 2.3-2.5)

can be written for the calculation of the stability constant (K) of the complex. If one or more than one ligand was bound to one metal ion:

$$M + L \rightarrow ML \qquad K_1 = [ML]/[M][L] \qquad (2.3)$$

$$ML + L \rightarrow ML_2 \qquad K_2 = [ML_2]/[ML][L]^2 \qquad (2.4)$$

$$: \quad : \quad : \qquad :$$
$$: \quad : \quad : \qquad :$$

$$ML_{n-1} + L \rightarrow ML_n \qquad K_n = [ML_n]/[ML_{n-1}][L]^n \qquad (2.5)$$
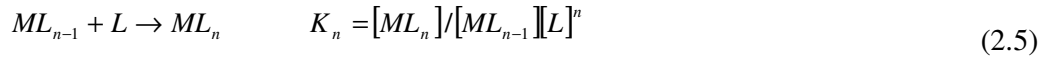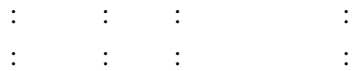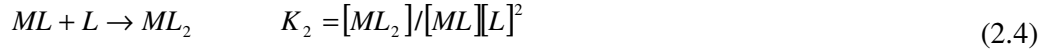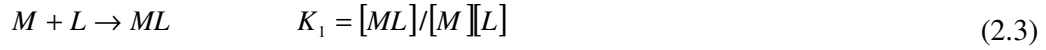
If one ligand was bound to one or more than one metal ion were described by Eq. (2.6-2.8):

$$M + L \rightarrow ML \qquad K_1 = [ML]/[M][L] \qquad (2.6)$$

$$2M + L \rightarrow M_2L \qquad K_2 = [M_2L]/[M]^2[L] \qquad (2.7)$$

$$: \quad : \quad : \qquad :$$
$$: \quad : \quad : \qquad :$$

$$nM + L \rightarrow M_nL \qquad K_n = [M_nL]/[M]^n[L] \qquad (2.8)$$
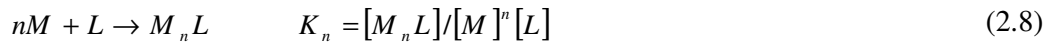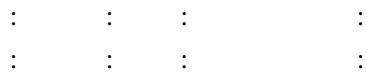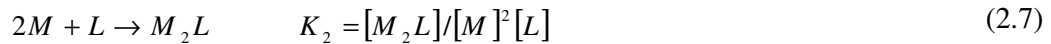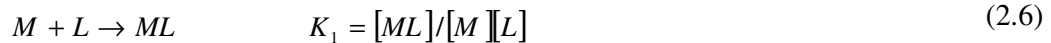
The appropriate equations given above (Eq.2.3-2.8) were used for the calculating the stability constants of the complexes (Sungur & Uzar, 2008). The characterization of complexes were performed after the determination of the stoichiometry and stability constants of Fe(III)-Valex and Fe(III)-TA complexes.

2.2.3 Characterization Techniques of Complexes

2.2.3.1 FTIR Analysis

An infrared spectrum shows a fingerprint of a sample with absorption peaks which correspond to the frequencies of vibrations between the bonds of the atoms forming the molecule. Because each different molecule is a unique combination of atoms, no two compounds produce the exact same infrared spectrum. Therefore, every different kind of material can result in a positive identification (qualitative analysis) of by the infrared spectroscopy (Sinha, et.al, 2011).

FTIR analyses of Valex, Fe(III)-Valex complex, TA, Fe(III)-TA complex were conducted with Perkin–Elmer Spectrum BX-II Model FTIR spectrophotometer. All samples were dried to a constant weight in an air oven at 80 ºC for 2h before use. FTIR spectra of the samples as KBr pellets were recorded in the range of 4000 and 400 cm^{-1}, at a resolution of 4 cm^{-1} and averages of 50 scans.

2.2.3.2 Thermal Analysis

Thermogravimetric Analysis (TGA) measures the rate and amount of change in the weight of a sample as a function of time or temperature in a controlled gas atmosphere. Measurements are given primarily to determine the composition of samples and to predict their thermal stability at temperatures up to 1000°C. The technique can also be used to characterize samples that exhibit weight loss or gain due to decomposition, oxidation, or dehydration.

Thermogravimetric analyses (TGA) of the Valex, Fe(III)-Valex complex, TA, Fe(III)-TA complex were carried out with Perkin Elmer Diamond TG/DTA Analyzer. The analyses were made in platinum pans under a dynamic nitrogen atmosphere in temperature range of 50-1000°C at a heating rate of 10°C/min.

The Fe(III)-Valex and Fe(III)-TA complexes melting point was measured by using a digital melting point apparatus BI 9100 Barnstead/Electrothermal.

2.2.3.3 XRD Analysis

The powder diffraction method is thus ideally suited for the identification and characterization of samples. The X-ray diffraction patterns (XRD) of the Fe(III)-Valex and Fe(III)-TA complexes were recorded with oriented mounts, in a Philips X'Pert Pro X-Ray diffractometer using Cu K_α radiation at 45 kV and 40 mA in the 2θ range of 2-60°.

2.2.3.4 ESR and Magnetic Susceptibility Analyses

The Electron Spin Resonance (ESR) spectra was measured using a Bruker ELEXSYS E580 model spectrometer for the Fe(III)-Valex and Fe(III)-TA complexes under the conditions of microwave frequency, 9.86 GHz; field amplitude, 100 mT; modulation frequency of 100kHz, microwave power 5mW, and the time constant, 0.01 s.

ESR studies are based upon the measurement of the interaction between an external magnetic field and the magnetic moment of an unpaired (free radical) electron. Unpaired electron energy E, can be described by the equation (2.9):

$$E = g \; \beta HMz \hspace{5cm} (2.9)$$

Where g is the spectroscopic splitting factor (or so-called ''g-value''), β is the Bohr magneton, H represents the external magnetic field, and Mz represents the two orientations of the electron spin (+1/2 or -1/2).

Measurement of the samples' response to the external magnetic field can thus yield information about the number of unpaired electrons, in spins per gram of sample (Chen, Gu, LeBoeuf, Pan & Dai, 2002).

On the otherhand Gouy method was used to measure magnetic susceptibility of the complexes with Balance Sherwood Scientific. Due to the application of a magnetic field, the apparent change in the weight of the sample is measured by a

sensitive balance. This weight change is directly proportional to the magnetic susceptibility. Substances are classified in to two groups as paramagnetic or diamagnetic, based upon the sign and magnitude of the susceptibilities. The physical effect of paramagnetism and diamagnetism is an attraction to the source of magnetism (increase in weight when measured by Gouy balance) and a repulsion from the source of magnetic field (decrease in weight when measured by a Gouy balance) respectively.

A small amount of solid has been placed into the weighted sample tube. The homogeneous packing is essential to making accurate measurements. Following are used for the susceptibility calculation, where C is the calibration constant for the balance (1.086), l is the length of the sample in centimeters (2.5cm), R is the reading on the balance with the sample in the tube R_0 is the reading the value of an empty tube in the balance. Weigh the filled sample tube and then calculate the mass of the sample m in grams ($m = m_2 - m_1$ where m_1 is the empty tube mass, m_2 is the mass of sample with the tube). Note the sign, a negative reading represent that the sample is diamagnetic.

Magnetic susceptibility per gram is called the mass magnetic susceptibility, X_g and it was calculated following equation (2.10):

$$X_g = \left[C \cdot \ell \cdot (R - R_0) \right] \Big/ 10^9 . m \qquad (2.10)$$

The molar magnetic susceptibility X_m, is obtained from the mass magnetic susceptibility by multiplying by the molecular weight (M_a) of the sample in units of g/mol (Eq.2.11);

$$X_m = X_g . M_a \qquad (2.11)$$

The magnetic susceptibility measurements of complexes were carried out at 293K and the value of the effective magnetic moment, μ_{eff}, can be determined by the following Eq. (2.12).

$$\mu_{eff} = 2.84\big(X_M \times T\big)^{1/2} \tag{2.12}$$

Where X_M is the molar susceptibility of complex and T is the absolute temperature (Kelvin).

2.2.3.5 MALDI-TOF MS Analysis

Generally, polymers mass determination is performed using gel permeation chromatography. However, this method only gives relative values compared to the most often used polystyrene standard and therefore carries a high risk of inaccurate values. Besides this, MALDI TOF mass spectrometry offers the possibility to measure absolute mass values for narrow distributed polymers. MALDI-TOF MS produces only a singly charged molecular ion for each parent molecule and allows detection of high mass with precision (Montaudo, G., Montaudo, M.S. & Samperi, F., 2002).

In MALDI-TOF MS, the ions generated in the ion source are accelerated through a known potential and travel through a flight tube to reach the ion detector. At the detector ion arrival time is measured and it is directly related to the m/z values of ions. For heavy ions it takes a longer time to reach the detector, but light ions arrive at the detector earlier (Chen, Zhang & Pramanik, 2006).

Determination of molecular weights and fragmentation patterns with the mass spectrometry is a widely used method of identifying plant polyphenols (Salminen, Ossipov, Loponen, Haukioja & Pihlaja, 1999; Self et al., 1986) MALDI-TOF MS of Fe(III)-Valex and Fe(III)-TA complexes were performed using Bruker Daltonics Microflex Mass Spectrometer. Positive reflectron mode was used for the samples.

2.2.3.6 XPS Analysis

XPS is also known as ESCA (Electron Spectroscopy for Chemical Analysis). The technique is widely used because it is very simple to use and the data is easily analyzed. XPS works by irradiating atoms of a surface of any solid material with X-Ray photons, causing the ejection of electrons.

X-ray photoelectron spectroscopy (XPS) analysis methods was performed by using non-monochromated Thermo Scientific K-ALPHA radiation and they were acquired with analyser pass energy of 150 eV.

2.2.3.7 ^{1}H-NMR Analysis

Proton NMR (also Hydrogen-1 NMR, or ^{1}H NMR) is the application of nuclear magnetic resonance in NMR spectroscopy with respect to hydrogen-1 nuclei within the molecules of a substance, in order to determine the structure of its molecules (Silverstein, Bassler & Morrill, 1991).

^{1}H NMR spectra of samples were recorded on Varian AS 400 Mercury instrument at 300°C. Simple NMR spectra are recorded in solution, and solvent protons must not be allowed to interfere. Deuterated dimethyl sulfoxide (DMSO-d_6) and deuterated methanol (CD$_3$OD) (3:1) solvent mixture was employed.

2.2.4 Complex Percent Yield Calculation

The theoretical yield (m_1) of a reaction is the calculated quantity of product that one expects from given quantities of reactants. The quantity of product that is actually produced is called actual yield (m_2). The percent yield is defined as in equation (2.13):

$$\text{Yield}\% = \left[\, m_2 \, / \, m_1 \, \right] x100 \qquad\qquad (2.13)$$

In many reactions the actual yield almost exactly equals the theoretical yield, and the reactions are said to be quantitative. We can use such reactions in performing quantitative chemical analyses, for example. On the other hand, in some reactions the actual yield is less than the theoretical yield, and the percent yield is less than 100%.

The yield may be less than 100% for many reasons. The product of a reaction rarely appears in apure form, and in the necessary purification steps some product may be lost through handling. This reduces the yield (Petrucci & Harwood, 1997).

Percent yield of complex was performed with the pure TA. 2.126g $(1.25 \times 10^{-3}$ mol) TA and 0.676g $FeCl_3.6H_2O$ $(2.5 \times 10^{-3}$ mol) solutions were used for the preparation of complex as described in section 2.2.1. After the purification of the synthesized complex with the acetone, it was weighed for the calculation of efficiency.

2.2.5 In vitro Antioxidant Activities of Complexes

Tannins have accepted considerable attention in the fields of nutrition, health and medicine, largely due to their physiological activity, such as antioxidant activity (Lim & Murtijaya, 2007), anti-microbial effects (Sisti et al., 2008), and antiinflammatory properties (Santos-Buelga & Scalbert, 2000). They are a group of antioxidants often characterised by the presence of several hydroxyl groups on an aromatic ring.

Tannins are OH radical scavengers because phenolic groups are excellent nucleophile. Their importance stems from their abundance in the diet, their antioxidant properties and ability to regulate various biological/biochemical processes (Manach *et al.*, 2004).

The antioxidant properties of the Fe(III)-Valex and Fe(III)-TA complexes were investigated and compared with Valex and TA. The free radical scavenging activities of samples were determined by using 2,2-Diphenyl-1-picrylhydrazyl (DPPH; Aldrich

D9132) method (Chu et al., 2010). Buthylated hydroxyanisole (BHA; Sigma B1253) and buthylated hydroxytoluene (BHT; Sigma B1378) were used as controls. All samples were reacted directly and quenched with DPPH radicals to different degrees with increased activities in a concentration-dependent manner. In the DPPH assay 50μL samples (5-50 µg/mL) were mixed with 50μL of 500 μM DPPH in ethanol (Sigma-Aldrich 32221) and kept in the dark for 40 min. The absorbances of the mixtures were measured at 492 nm.

The DPPH radical scavenging activity was determined based on percentage inhibition of absorbance, which was calculated using the following Eq.(2.14):

$$\text{DPPH radical scavenging activity } (\%) = [(A_0 - A_1/A_0) \times 100] \tag{2.14}$$

Where A_0 is the absorbance of the control reaction and A_1 is the absorbance in the presence of the samples.

2.2.6 Antimicrobial and Antifungal Activities of Complexes

2.2.6.1 Test Microorganisms

The *in vitro* antimicrobial activities of synthesized complexes were tested against laboratory control strains belonging to the American Type Culture Collection (Maryland, USA): *Escherichia coli* [ATCC 25922], *Staphylococcus aureus* [ATCC 25923], *Streptecocus pyogenes* [ATCC 19615], *Pseudomonas aeruginosa* [ATCC 27853], *Bacillus subtilis* [ATCC 11774] used as microorganisms and *Candida albicans* [ATCC 10231] used as a fungi.

2.2.6.2 Evaluation of Antimicrobial Activity

Antimicrobial activity tests were assayed by the disc diffusion susceptibility test according to the recommendation of the National Committee for Clinical Laboratory

Standards (NCCLS) (Clark, Jacobs & Appelbaum, 1998). The disk diffusion tests were performed on Muller-Hinton agar plates.

Plates were dried at 35–36 ^{0}C for about 30 min in an incubator before inoculation. Bacterial strains were inoculated into 25 mL of Mullar–Hinton broth medium in a shaking water bath for 4–6 h until a turbidity of 0.5 McFarland ($1x10^8$ CFU/mL) was reached. At 625 nm absorbance was setting between 0.08 to 0.1. Candida albicans were inoculated into 25mL of Sabouraud dextrose broth in a shaking water bath for 8–10h until a turbidity of 0.5 McFarland was reached. The inoculum (50 mL) from the final inocula was applied to each agar plate and uniformly spread with a sterilized cotton spreader over the surface (Kızıl, 2002). Inhibition zone diameter (mm) surrounding each sample was measured after 24h incubation of samples discs (20 µL/9 mm) onto agar plates at 37 $^°$C. The diameters of the inhibition zones were measured in millimeters using an inhibition zone ruler.

Standard discs of amoxicillin/clavulanic acid (30µg/disc), ofloxacin (5µg/disc), netilmycin (30µg/disc), erythromycin (15µg/disc) and amphotericin B (30µg/disc) were individually used as positive controls.

2.2.7 Determination of Superoxide Anion Radical-Scavenging Activity

Superoxide anion-scavenging activities of complexes were determined. Superoxide radicals are generated in phenazine methosulphate (PMS)-nicotinamide adenine dinucleotide (NADH) systems by the oxidation of NADH and are assayed by the reduction of nitroblue tetrazolium (NBT) (Ozen, Demirtaş & Akşit, 2011). The percentage inhibition of superoxide anion generation was calculated using the following Eq.(2.15):

% Inhibition of superoxide anion generation = $[(A_0 - A_S) / A_0]$ x 100 (2.15)

A_0 is absorbans of the control and A_S is absorbans of the samples. Superoxide anion, that is derived from dissolved oxygen through the PMS/NADH coupling

36

reaction, reduces NBT and increases absorption at 560 nm in the superoxide anion-scavenging assay. At 560 nm absorption decreases in with antioxidants thus indicates the consumption of superoxide anion (Chen & Yen, 2007).

Superoxide anions indirectly initiated lipid oxidation as a result of superoxide and hydrogen peroxide serving as precursors of singlet oxygen and hydroxyl radicals. It is reported that, the antioxidant properties of flavonoids are effective mainly via the scavenging of superoxide anion (Gupta, Mazumdar, Gomathi & Kumar, 2004).

2.2.8 Determination of Deoxyribose Assay

The scavenging capacity of complexes for hydroxyl radical was measured according to the modified method of Halliwell, Gutteridge & Aruoma (1987). The absorbance was measured at 532 nm. DMSO (dimethyl sulfoxide) was used as a standard. The % inhibition of degradation of deoxyribose was calculated by equation (2.16):

$$\% \text{ Inhibition} = [(A_o - A_1/A_o) \times 100] \tag{2.16}$$

where A_o is the absorbance of the assay (without sample) and A_1 is the absorbance of the assay (with sample). The control contained DMSO: ethanol (v/v) instead of the samples. One of the most reactive free-radicals are hydroxyl radicals. They are generated in reaction of iron ions with hydrogen peroxide in biological systems (Gutteridge & Halliwell, 1988) and foods.

2.3 Synthesis, Characterization and Applications of Tannic Acid Resin

2.3.1 Synthesis of Tannic Acid Resin

Tannic acid resin (TR) was synthesized according to the procedure given in literature (Özacar, Soykan & Şengil, 2006). The procedure was shortly given below. TR was prepared from commercial TA by chemical activation with formaldehyde (cross-linking agent). TA was added to 50mL 13.3N ammonium hydroxide solution and stirred for 5 min. to dissolve. Then 65mL of 37% formaldehyde solution was added to this mixture and stirred for 35 min.

The formed suspension was filtered. A yellow precipitate thus obtained was added to 50 mL distilled water and heated at 343 K for 3h with stirring to remove free formaldehyde. The heated suspension was filtered again. Subsequently, the precipitate thus obtained was added to 100 mL 0.1M HNO_3, followed by stirring for 30 min. HNO_3 solution was used to make the precipitate insoluble in acidic and basic medium. After filtration, the precipitate was rinsed with distilled water followed by drying at 353 K to thereby obtain an insoluble TR. Samples with a particle size of 70 meshes was used in the adsorption experiments.

2.3.2 Adsorption Experiments

Batch technique was used for the adsorption of boron from aqueous solutions at different temperatures (288, 298 and 308 K). All the experiments were performed in polypropylene volumetric flasks. (0.1 g) of adsorbents were added to 25 mL boron solutions at different concentrations (1-15 mgL^{-1} boron at pH=7) in order to investigate the effect of initial boron concentration on boron adsorption. The suspensions were shaken at 150 rpm for 24 h.

After equilibrium was reached, samples were centrifuged and boron concentration in the supernatant was analyzed spectrophotometrically at wavelength of 412 nm. The effect of pH on the adsorption of boron was also analyzed. The pHs of the

solutions were adjusted to various pH values between 4 and 8 by using dilute HCl or NaOH solutions. The effect of the adsorbent dosage (0.1-0.5g of TR) on the amount of adsorbed boron was determined with 25 mL of the solution containing 4 mg L^{-1} boron at pH=7 and 308 K.

The Langmuir and Freundlich adsorption models were applied to the adsorption data to obtain adsorption capacity of TR. Finally, the adsorption experiment was carried out at the optimum values of pH, temperature, initial boron concentration and adsorbent dosage. Adsorption yields (R%) were calculated from the following equation (2.17).

$$R(\%) = \frac{(C_0 - C_e)}{C_0} \times 100 \tag{2.17}$$

where C_e is the equilibrium concentration of the boron solution (mgL^{-1}) at equilibrium and C_o is the initial boron concentration (mgL^{-1}).

Desorption of boron from the TR was studied with 0.01M HCl solutions. The loaded adsorbents were treated with 25mL of effluent for 24h. Then the suspensions were centrifuged and the liquid phase was analyzed. Desorption yields (D%) were calculated from equation (2.18);

$$D(\%) = \left(\frac{C_e}{C_s}\right) \times 100 \tag{2.18}$$

where C_e is the equilibrium concentration of the boron solution (mgL^{-1}) at desorption experiment and C_s is the equilibrium amount adsorbed at adsorption experiment (mgg^{-1}).

2.3.3 Characterization of Tannic Acid Resin

Fourier transform infrared spectroscopy analysis of TA, TR and TR-B (boron loaded TR) was conducted with Perkin–Elmer Spectrum BX-II Model FTIR spectrophotometer. FTIR spectra of the samples as KBr pellets were recorded in the range of 4000 and 400 cm^{-1}, at a resolution of 4 cm^{-1} and averages of 50 scans.

Morphological analysis of samples was performed with an emission scanning electronic microscope (SEM), JEOL JSM 6300F operated at an acceleration voltage of 3 kV.

Thermogravimetric analysis (TGA) of TR and TR-B was carried out with Perkin Elmer Diamond TG/DTA Analyzer. The analyses were made in ceramic pans under a dynamic nitrogen atmosphere in temperature range of 50-800°C at a heating rate of 10°Cmin.$^{-1}$

The specific surface area of TR was determined according to the B.E.T method after N$_2$ adsorption-desorption at 77 K by using Sorptomatic 1990. For porosity analysis, desorption data was evaluated by using the Dollimore–Heal method (Dollimore & Heal, 1964). Specific surface area of TR, its monolayer volume, pore specific volume, total adsorbed volume, pore volume maximum were calculated as 335 m^{2}g^{-1}, 77 cm^{3}g^{-1}, 0.22 cm^{3}g^{-1}, 142 cm^{3}g^{-1} and 0.158 cm^{3}g^{-1} respectively.

2.3.4 Kinetics Studies of Adsorption

Lagergren first-order equation is the most popular kinetics equation only for the rapid initial phases. This model was successfully applied to describe the kinetics of many adsorption systems (Şengil & Özacar, 2009; Ghaedi, 2012a, 2012b, 2012c). The pseudo-first-order equation was given by equation (2.19):

$$\log(q_1 - q_t) = \log q_1 - k_1 t / 2.303 \tag{2.19}$$

where t is time (min), q_t (mg g^{-1}) is the amount of adsorbed at time t, k_1 is rate constant and q_1(mg g^{-1}) is the experimental data of the amount of boron adsorbed at equilibrium.

The second-order kinetic model is more likely to predict the kinetic behavior of adsorption with chemical sorption being the rate controlling step (Yurtsever & Sengil, 2009). This relation was given by equation (2.20):

$$\frac{t}{q_t} = \frac{1}{k_2 q_2^2} + \frac{t}{q_2} \tag{2.20}$$

where k_2 (gmg^{-1}min^{-1}) is the rate constant of adsorption, q_2 is the amount of boron adsorbed at equilibrium (mgg^{-1}) (Ho & McKay, 1998). The values of k_1, q_1 and k_2, q_2 were obtained from the slopes and intercepts of plots of log (q$_1$−q$_t$) versus t and t/q$_t$ versus t at different temperatures, respectively.

2.3.5 Adsorption Isotherms

The distribution of molecules between the liquid phase and the adsorbent is a measure of the position of equilibrium in the adsorption process and can generally be expressed by one or more of a series of isotherm models (Üçer, Uyanık & Aygün, 2006). The amount of adsorption at equilibrium, C_s (mgg^{-1}), was computed as equation (2.21):

$$C_s = (C_o − C_e).\frac{V}{W} \tag{2.21}$$

where C_o and C_e are the initial and equilibrium concentrations (mgL^{-1}), respectively; V is the volume of the solution (L); and W is the amount of TR used (g).

The Langmuir model was described by equation (2.22) which may be written in linearized form as equation (2.23):

$$C_s = \frac{K_L C_e}{1 + a_L C_e} \qquad (2.22)$$

$$\frac{C_e}{C_s} = \frac{1}{K_L} + \frac{a_L}{K_L} C_e \qquad (2.23)$$

where C_s is the amount sorbed boron ($mg\,g^{-1}$), C_e is the equilibrium concentration of the adsorbate ($mg\,L^{-1}$). The empirical constants K_L and a_L for Langmuir model are related to the maximum capacity ($L\,g^{-1}$) and bonding strength ($L\,mg^{-1}$), respectively.

The monolayer adsorption capacity is Q_o and is numerically equal to K_L/a_L (Langmuir, 1918).

The Freundlich model can be described by the following equation (2.24):

$$C_s = K_f C_e^{n_f} \qquad (2.24)$$

where C_s is the amount of boron adsorbed per unit weight and C_e is the equilibrium concentration of boron. K_f ($mg\,g^{-1}$) and n_f are Freundlich constants related to adsorption capacity and intensity of adsorption, respectively. The linearized form of this equation (Freundlich, 1906) was expressed in equation (2.25):

$$\ln C_s = \ln K_f + n_f \ln C_e \qquad (2.25)$$

2.3.6 Thermodynamics of Adsorption

$\Delta G°$ was calculated from equation 2.26 and the values of ΔH^o and ΔS^o were determined from the slope and intercept of van't Hoff equation (Eq. 2.27), respectively (Özcan, A.S. & Özcan, A., 2004).

$$\Delta G^o = -RT \ln K_d \qquad (2.26)$$

$$\ln K_d = (\frac{\Delta S^o}{R}) - (\frac{\Delta H^o}{R})(\frac{1}{T}) \qquad (2.27)$$

where K_d is the equilibrium constant (unitless), R is the universal gas constant ($8.314 \text{ J mol}^{-1} \text{ K}^{-1}$) and T is the temperature (Kelvin).

RESULTS

3.1 Synthesis, Characterization and Applications of Polyphenol-Fe(III) Complexes

3.1.1 Preparation of Fe(III)-Valex and Fe(III)-TA Complexes

The Fe(III) ion is a hard acid and consequently is bound most strongly by hard bases. The most effective of these are oxyanions, such as hydroxide, phenoxide, carboxylate, hyroxamate and phosphonate. Fe binds to the adjacent hydroxyls on the galloyl group of Valex or TA.

Initially, the synthesis of Fe(III)-Valex and Fe(III)-TA complexes were investigated at pH range from 2.4 to 8.4 (Figure 3.1). Complexes that are created in different buffers was decided to use a dark violet-colored complex (pH=4.4) in the paint industry.
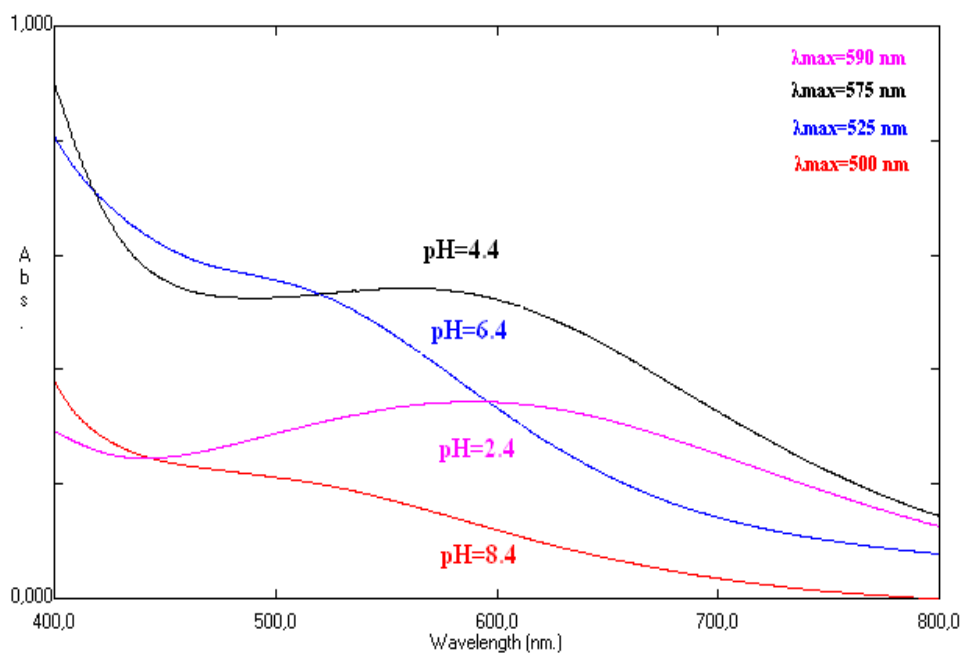
Figure 3.1 UV-Vis. Spectra of 5×10^{-4}M Fe(III)- 5×10^{-4}M Valex (1:1) at pH=2.4 (590nm), pH=4.4 (575nm) pH=6.4 (525nm) and pH=8.4 (500nm).

pH=4.4 was selected as the optimum pH because of its dark violet color in the pH range of 2.4, 4.4, 6.4 and 8.4 (Figure 3.1). The characterization, antioxidant and antimicrobial activity experiments were held at that pH.
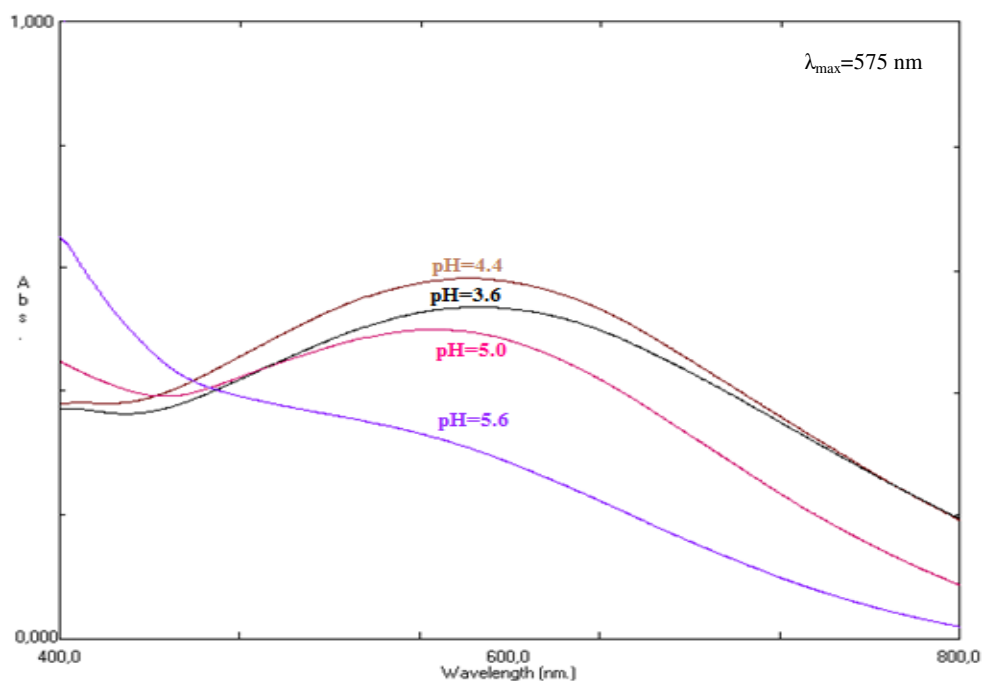
Figure 3.2 UV-Vis. Spectra of 10^{-3}M Fe(III)-10^{-4}M TA (1:1) at pHs

UV-Vis Spectra of 10^{-3}M Fe(III)-10^{-4}M TA (1:1) in the acetate buffer at different pH values was shown in Figure 3.2 at a constant wavelength (λ=575 nm). Eventually pH=4.4 was selected for the giving the appopriate and desired color.

The procedure for the preparation of complex as follows; ligand (Valex or TA) (10^{-4}M) and Fe(III) (10^{-3}M) solutions were mixed with the ratio of 1:1 (v/v) and diluted to 10 mL with pH=4.4 solutions. UV-Vis spectra of 10^{-4}M Valex, 10^{-3}M Fe(III) - 10^{-4}M Valex complex and 10^{-4}M TA, 10^{-3}M Fe(III)-10^{-4}M TA complex at pH=4.4 were shown in Figure 3.3 and Figure3.4 respectively.
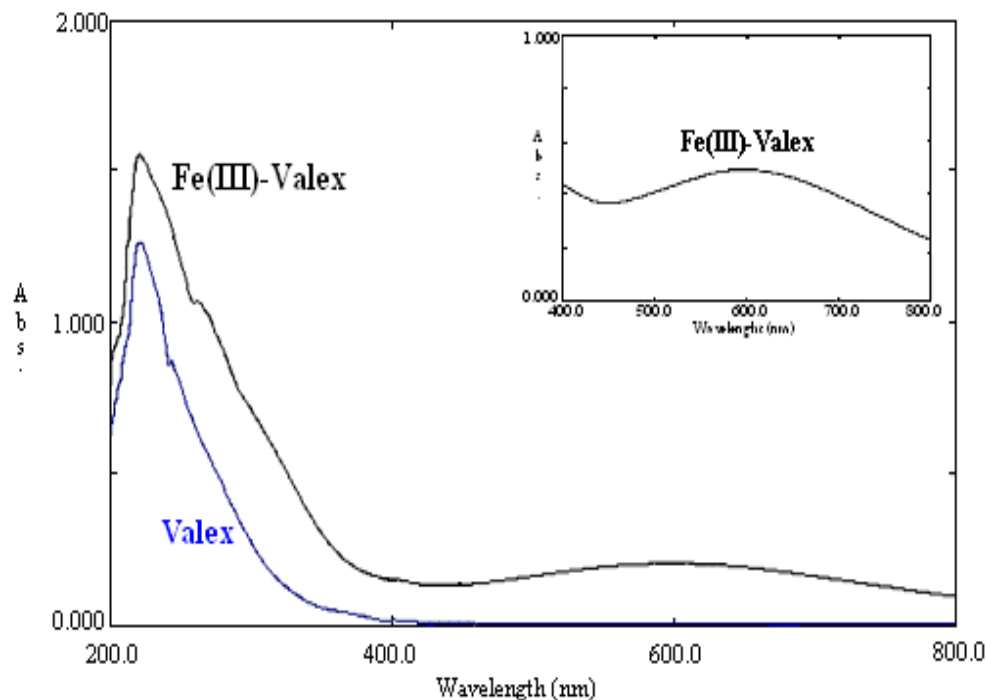
Figure 3.3 UV-Vis. Spectra of 10^{-4}M Valex and 10^{-3}M Fe(III)-10^{-4}M Valex (1:1)at pH=4.4

Absorption spectra of Valex were characterized by a peak at 221nm and a shoulder at 252 nm. These were assigned for $\pi \rightarrow \pi$ * transitions which was given by aromatic units and C=O groups in UV region (200-400 nm) (Balaban, Banciu & Pogany, 1983). At Fe(III)-Valex UV-Vis spectra, two absorbance peaks were observed at 221 and 575 nm. The shoulder of Valex at 252 nm under gone a batochromic shift to 273 nm due to the formation of Fe(III)-Valex complex. Mean while, a new absorbance peak was observed at 575 nm, which was assigned to the Fe(III)-Valex complex peak in the visible range (Brune, Hallberg & Skanberg, 1991). This may be assigned to the ligand-to-metal charge transfers (LMCT) between Fe(III) and Valex (Yang, Lu & Wang, 2005).

On the other hand two peaks at 219 and at 276nm were observed at the absorption spectra of TA. These peaks for TA were assigned for $\pi \rightarrow \pi$ * transitions as in the valex absorption spectra which was given by aromatic units and C=O groups in UV region (200-400 nm) (Balaban, Banciu & Pogany, 1983).

46
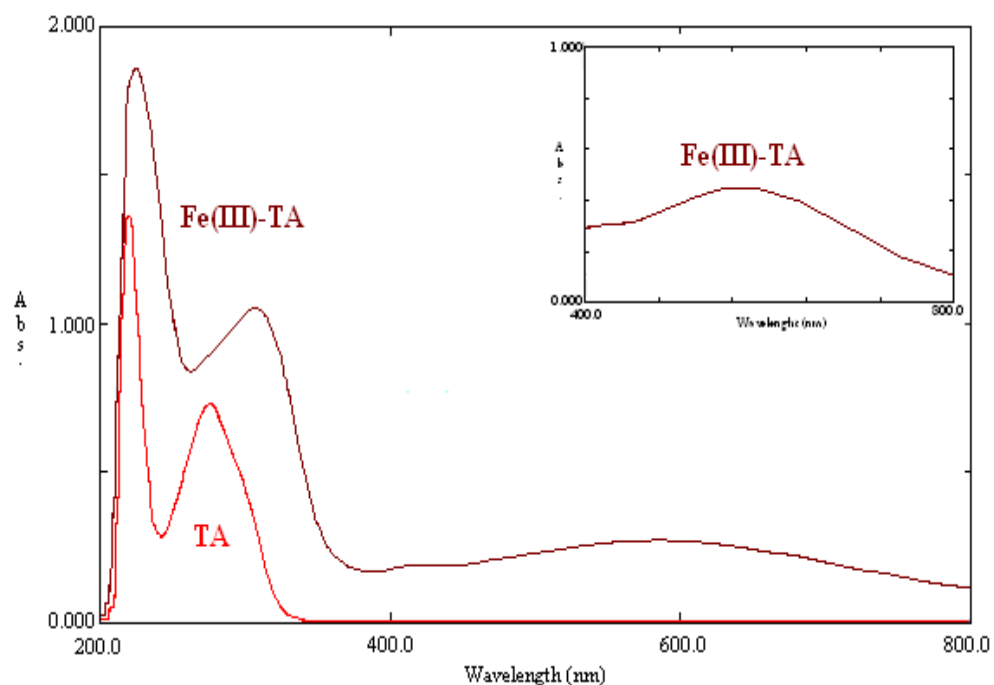
Figure 3.4 UV-Vis. Spectra of 10^{-4}M TA and 10^{-3}M Fe(III)-10^{-4}M TA (1:1) pH=4.4

The absorption spectra of Fe(III)-TA complex was obviously showed a blue shift compared to that of the TA. Also three absorbance peaks were observed at Fe(III)-TA absorption spectra at 221, 318, 575nm.

Absorption peaks of Fe(III)-Valex and Fe(III)-TA complexes at 575nm were attributed to charge transfers from the p_π orbitals of Valex and TA to the d_π and d_σ orbitals of Fe(III) (Elhabiri, Carrer, Marmolle & Traboulsi, 2007). At slightly acidic, iron is bound by ligands to metal ion, giving blue-purple Fe^{3+} complexes for their ligand-to-metal charge transfer energy (LMCT) bands (Perron & Brumaghim, 2009). So the Fe(III)-Valex and Fe(III)-TA complexes formed a dark violet color with an absorbance maximum at 575nm.

3.1.2 Stoichiometry and Stability Constant

The interaction between Ligand (Valex or TA) and Fe(III) is important to understand the metal-ligand behavior. M/L ratio or pH could significantly change the coordinated species in solution (Perron & Brumaghim, 2009; Perron, Hodges, Jenkins & Brumaghim, 2008; Binbuga, Chambers, Henry & Schultz, 2005). For the stoichiometries of Fe(III)-Valex and Fe(III)-TA complexes, the slope ratio method was determined for pH= 4.4, 8.4 and mole ratio method was determined for pH= 2.4, 6.4.

3.1.2.1 Fe(III)-Valex and Fe(III)-TA Complexes Stoichiometries at pH=2.4

Figures 3.5-3.8 showed the absorbance versus M/L values for Fe(III)-Valex and Fe(III)-TA complexes to the determine the stoichiometrie with the mole ratio method. Absorbance values of Valex complex and TA complex were noted at 590nm.

Figure 3.5 Absorbance vs M/L of Fe(III)-Valex ([M] constant) at pH=2.4

Figure 3.6 Absorbance vs M/L of Fe(III)-Valex ([L] constant) at pH=2.4
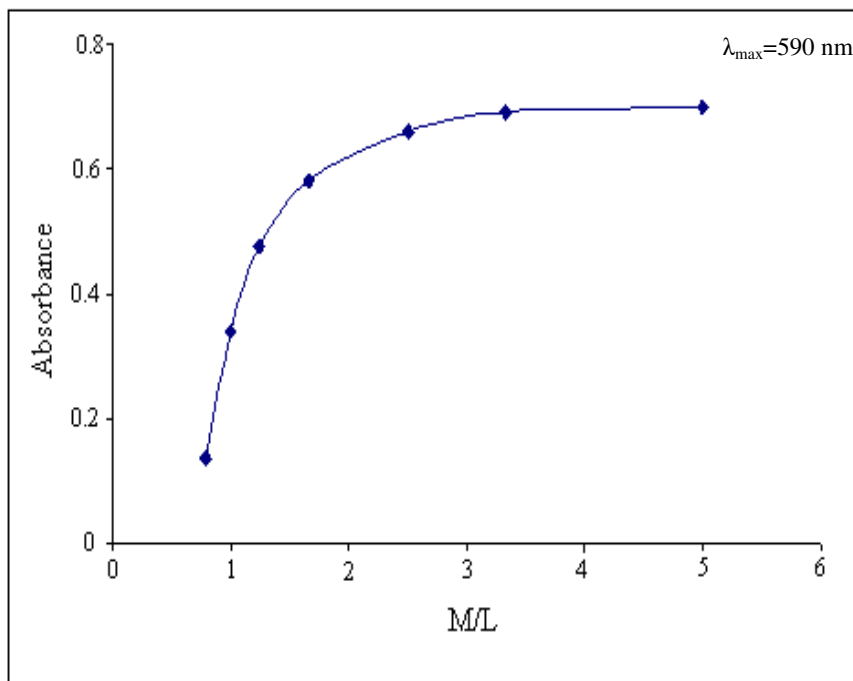
Figure 3.7 Absorbance vs M/L of Fe(III)-TA ([M] constant) at pH=2.4
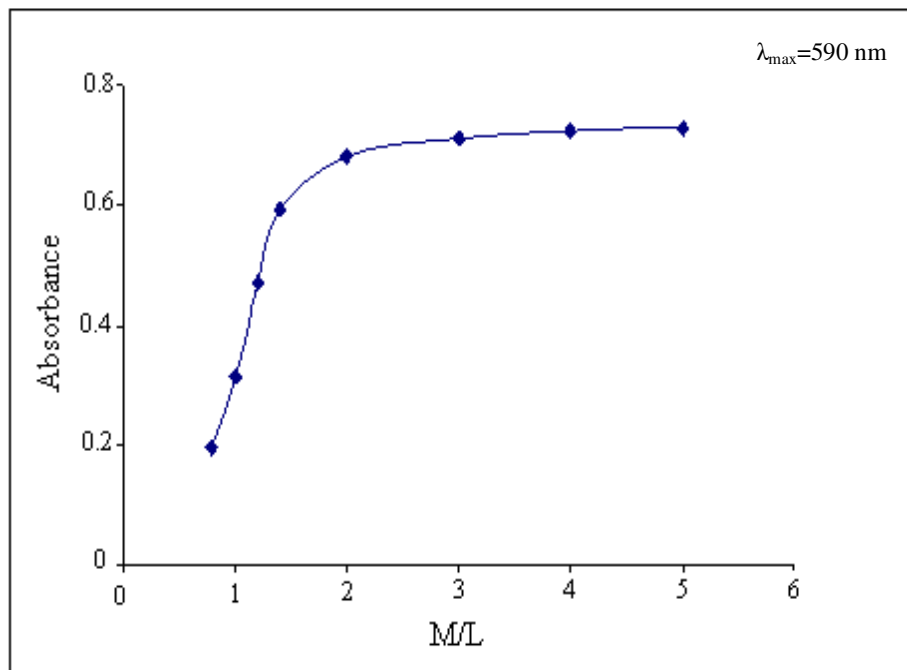
Figure 3.8 Absorbance vs M/L of Fe(III)-TA ([L] constant) at pH=2.4

The results obtained using mole ratio method were showed that the stoichiometry of Fe(III)-Valex and Fe(III)-TA complexes were 1:1 at pH=2.4.

3.1.2.2 Fe(III)-Valex and Fe(III)-TA Complexes Stoichiometries at pH= 4.4

For the slope ratio method, λ_{max} of Fe(III)-Valex and Fe(III)-TA complexes were found at 575nm for the pH=4.4. In the first series of both Valex and TA experiments, $2 \times 10^{-3}M$ Fe(III) was kept constant and $0.6 \times 10^{-4}M$ Valex or TA solutions were increased. The second series was performed in the opposite manner.

Molar absorptivity constants of Fe(III), Valex and TA obtained from the two series of experiments of slope ratio method at $\lambda_{max}= 575nm$ were shown in Figures 3.9-3.12.
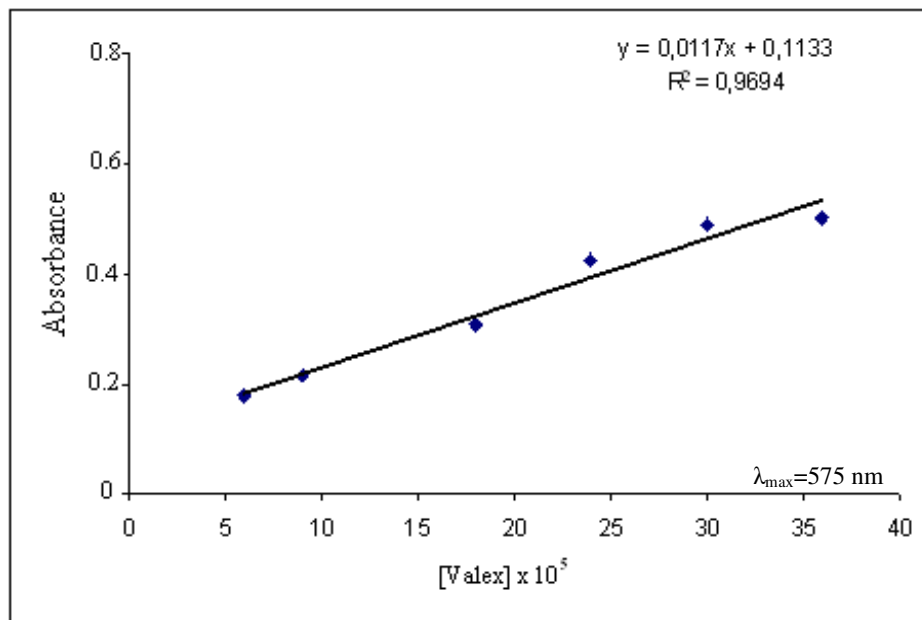
Figure 3.9 Calibration curve of Fe(III)-Valex ([M] constant) at pH=4.4
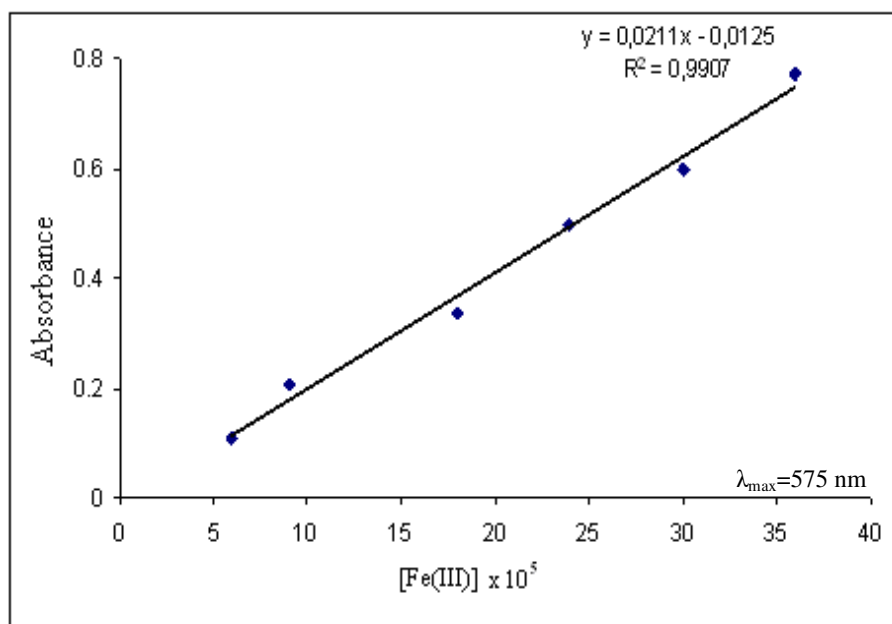
Figure 3.10 Calibration curve of Fe(III)-Valex ([L] constant) at pH=4.4

Molar absorptivity constants were obtained from the two series of experiments at λ_{max}= 575nm as Fe(III) (ε_M=2110) and Valex (ε_L=1170). As a result the ratio of the molar absorptivity constants of the Fe(III) and Valex was calculated as $\varepsilon_M/\varepsilon_L$=1.8 ($\approx$2).
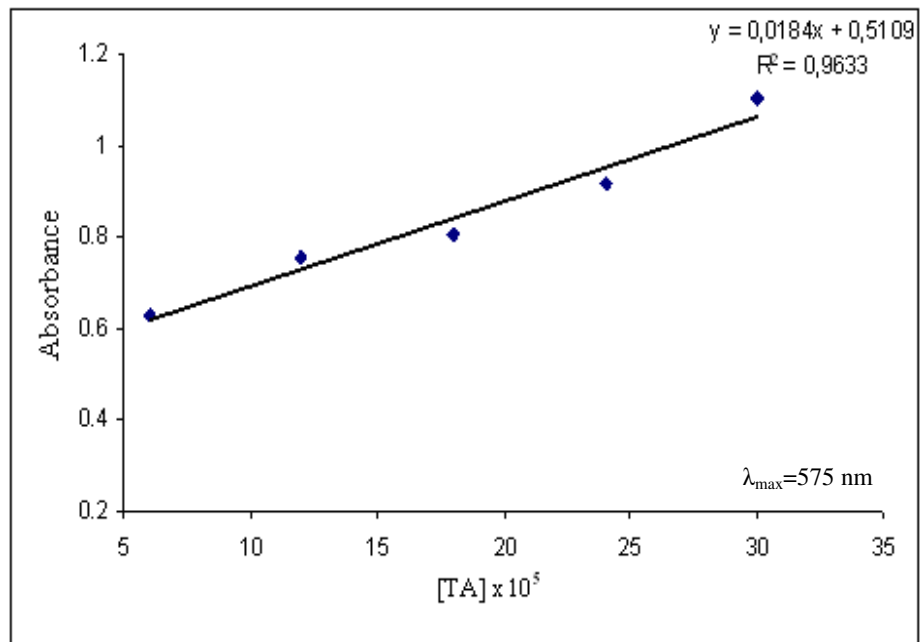
Figure 3.11 Calibration curve of Fe(III)-TA ([M] constant) at pH=4.4
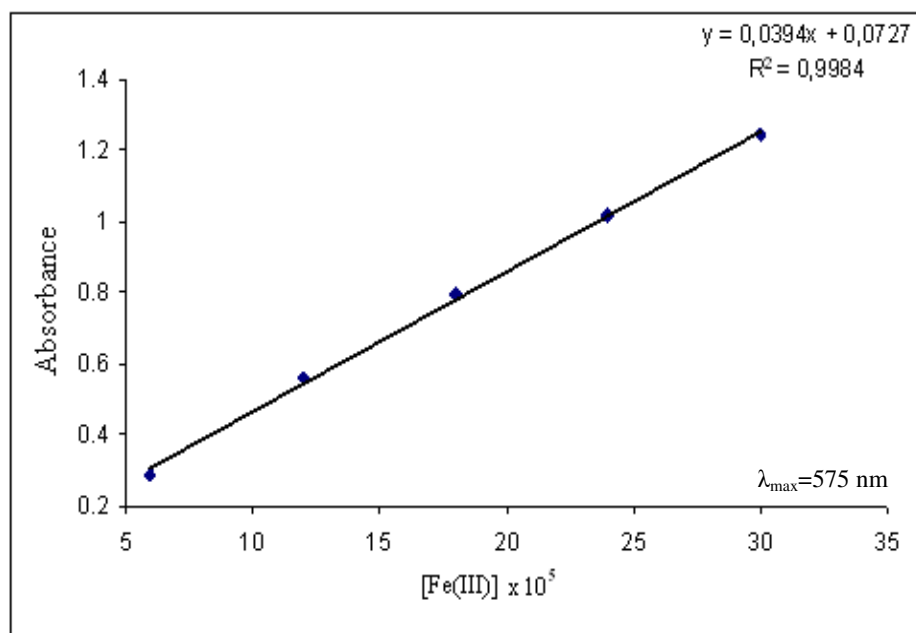
Figure 3.12 Calibration curve of Fe(III)-TA ([L] constant) at pH=4.4

Molar absorptivity constants were obtained from the two series of experiments at λ_{max}= 575nm as Fe(III) (ε_M=3940) and TA (ε_L=1840). As a result the ratio of the molar absorptivity constants of the Fe(III) and TA was calculated as $\varepsilon_M/\varepsilon_L$= 2.14.

The results obtained using slope ratio method showed that the stoichiometry of Fe(III)-Valex and Fe(III)-TA complexes were 2:1 at pH=4.4.

3.1.2.3 Fe(III)-Valex and Fe(III)-TA Complexes Stoichiometries at pH= 6.4

Figures 3.13-3.16 showed the Fe(III)-Valex and Fe(III)-TA complexes to determine of the stoichiometrie with the mole ratio method. λ_{max} value of Fe(III)-Valex and Fe(III)-TA complexes at pH=6.4 was found to be 525nm.
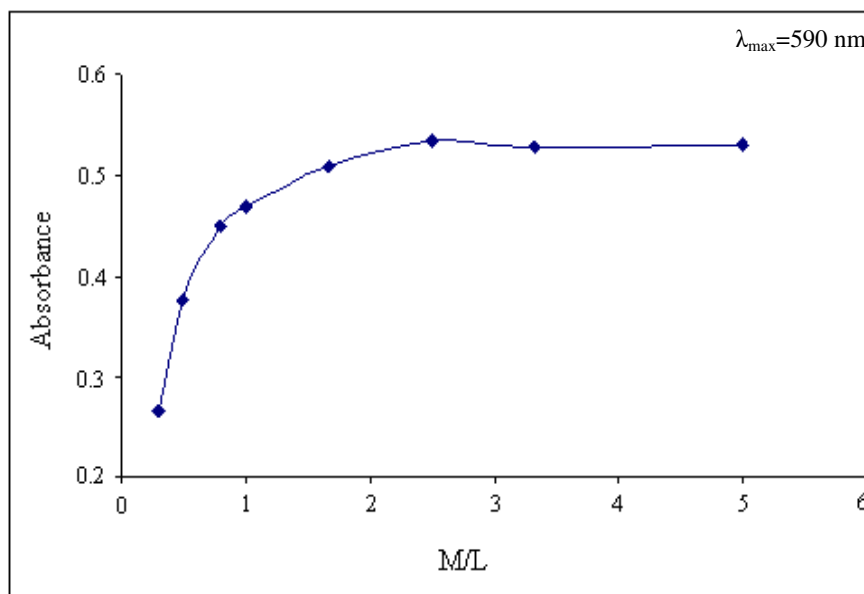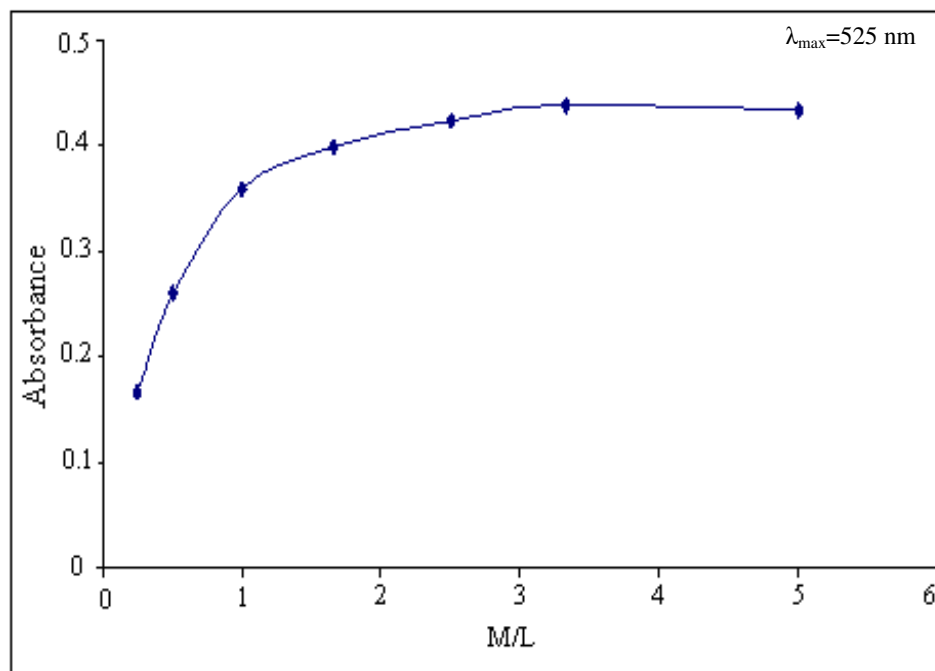

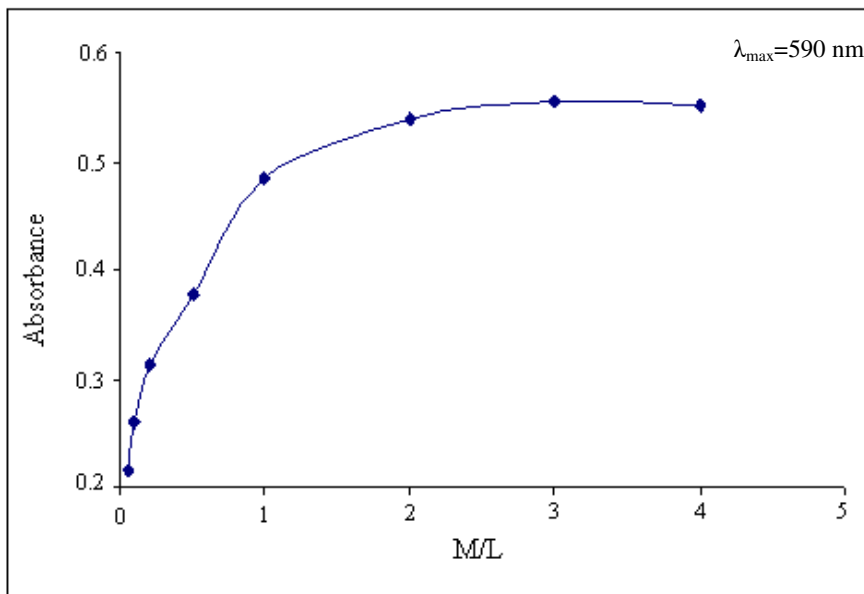Figure 3.13 Absorbance vs M/L of Fe(III)-Valex ([M] constant) at pH=6.4
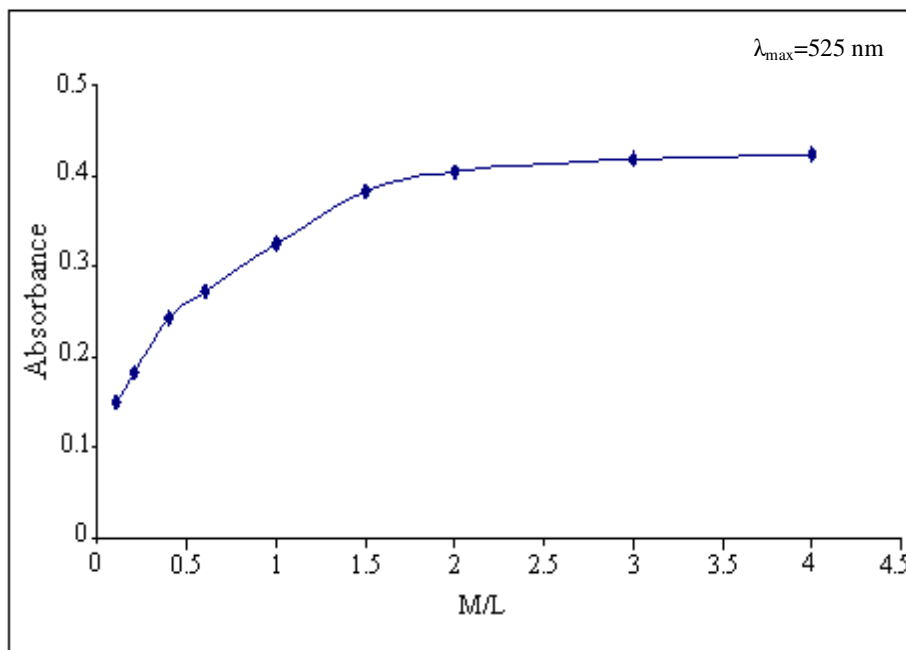
Figure 3.14 Absorbance vs M/L of Fe(III)-Valex ([L] constant) at pH=6.4
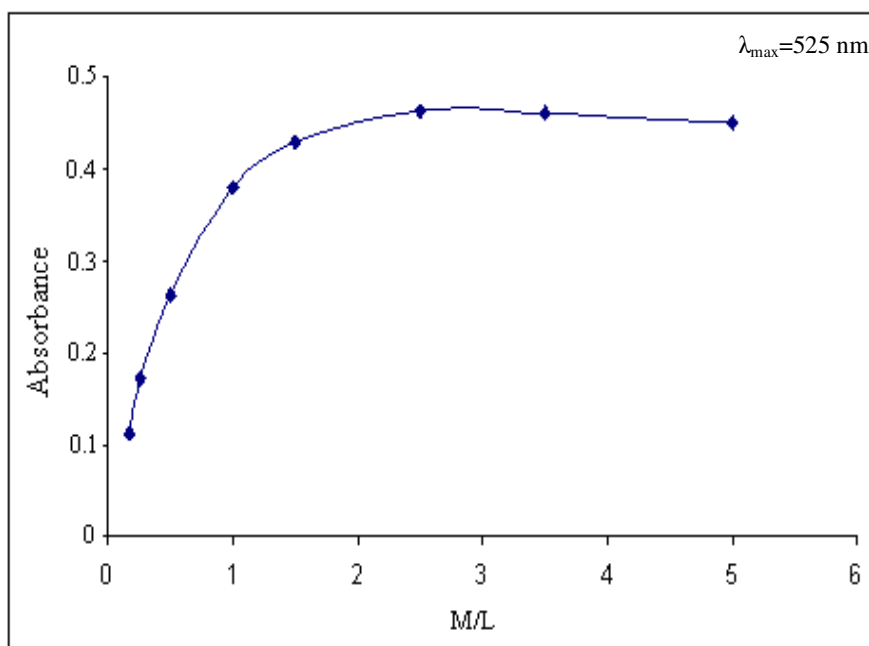
Figure 3.15 Absorbance vs M/L of Fe(III)-TA ([M] constant) at pH=6.4
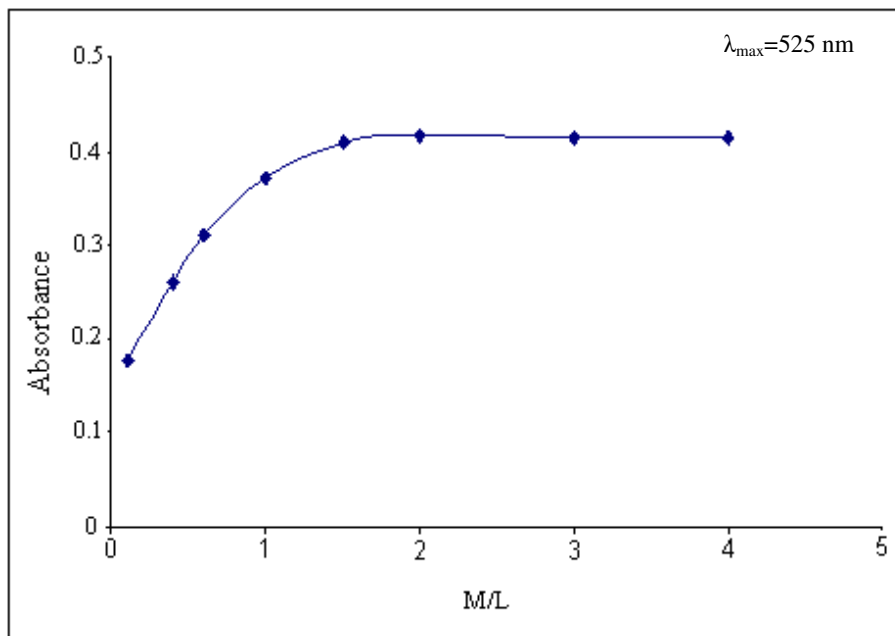
Figure 3.16 Absorbance vs M/L of Fe(III)-TA ([L] constant) at pH=6.4

The results obtained using mole ratio method showed that the stoichiometry of Fe(III)-Valex and Fe(III)-TA complexes was 2:1 at pH=6.4

3.1.2.4 Fe(III)-Valex and Fe(III)-TA Complexes Stoichiometries at pH= 8. 4

At this pH value λ_{max} of Fe(III)-Valex and Fe(III)-TA complexes were found as 500nm and two series of slope ratio method experiment were done at this λ_{max} value (Figures 3.17-3.20).
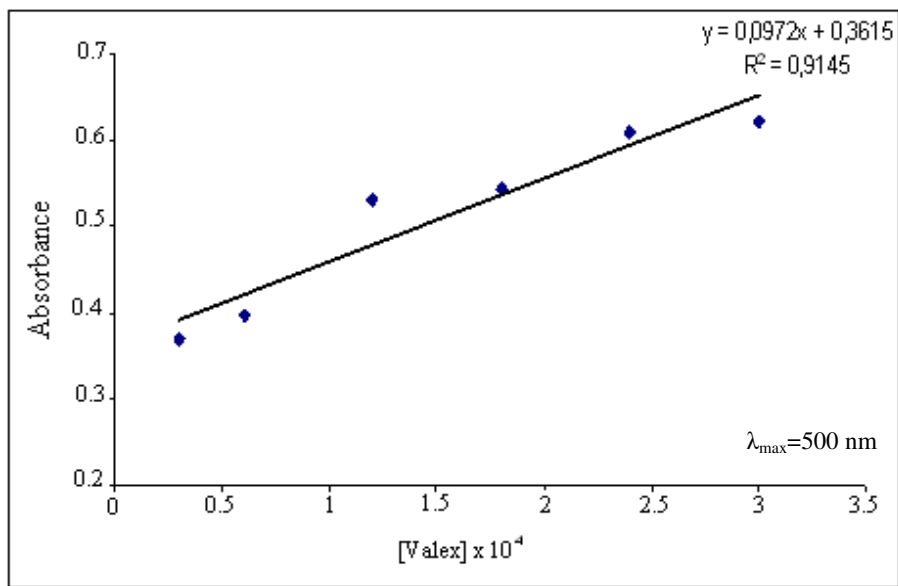
Figure 3.17 Calibration curve of Fe(III)-Valex ([M] constant) at pH=8.4
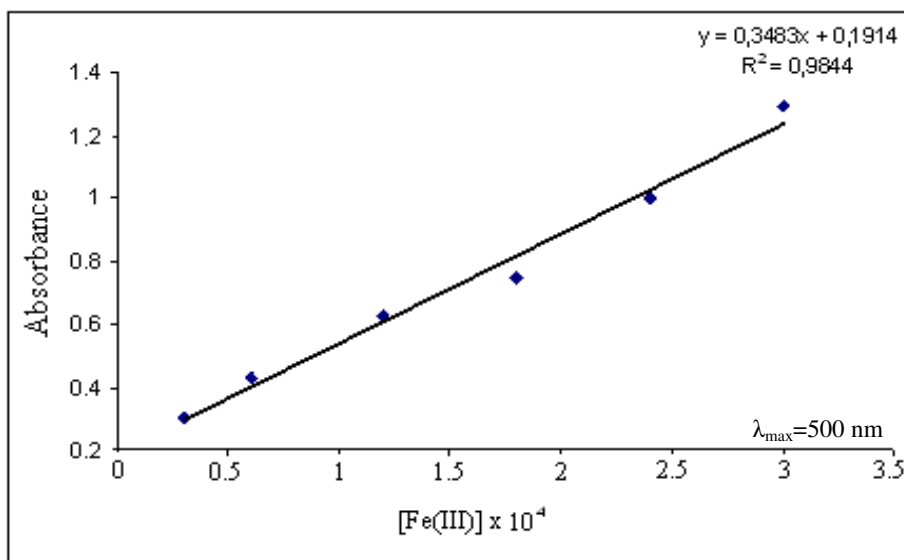
Figure 3.18 Calibration curve of Fe(III)-Valex ([L] constant) at pH=8.4

Molar absorptivity constants were obtained from the two series of experiments at λ_{max}= 500nm as Fe(III) (ε_M=3483) and Valex (ε_L=972). As a result the ratio of the molar absorptivity constants of the Fe(III) and Valex was calculated as $\varepsilon_M/\varepsilon_L$=3.6 ($\approx$4).
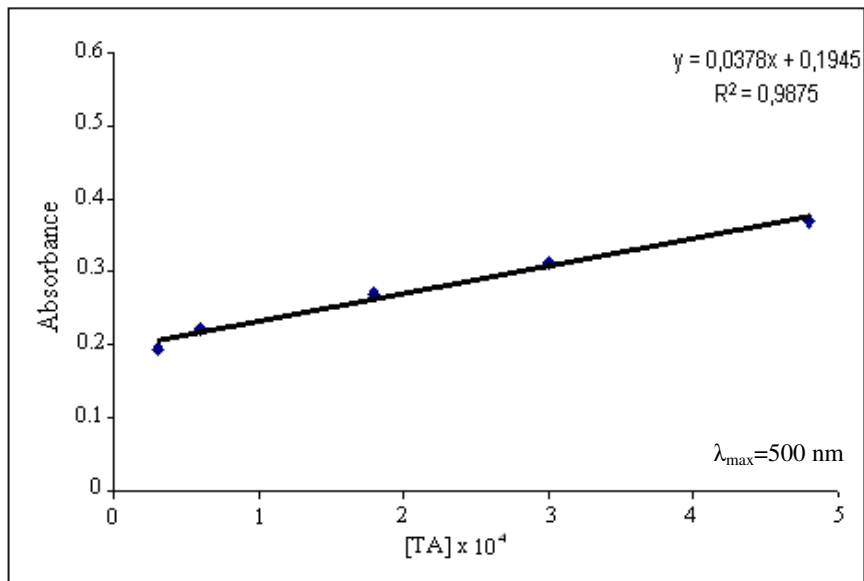
Figure 3.19 Calibration curve of Fe(III)-TA ([M] constant) at pH=8.4
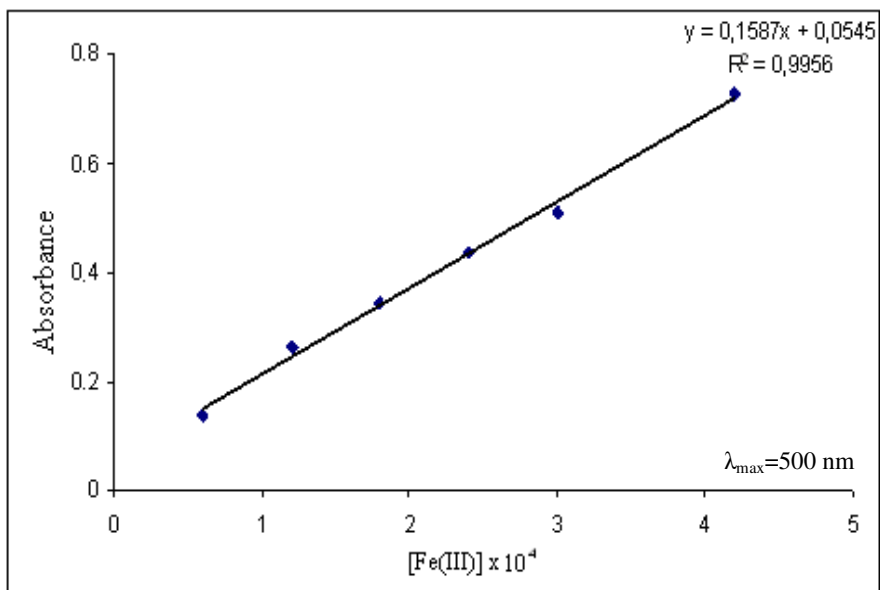
Figure 3.20 Calibration curve of Fe(III)-TA ([L] constant) at pH=8.4

Molar absorptivity constants were obtained from the two series of experiments at λ_{max}= 500nm as Fe(III) (ε_M=1587) and TA (ε_L=378). As a result the ratio of the molar absorptivity constants of the Fe(III) and TA was calculated as $\varepsilon_M/\varepsilon_L$= 4.2. Lines had different slope values and the ratio of the Fe(III) to ligand (M/L) was calculated from the ratio of these slopes of the lines. The results obtained using slope ratio method

showed that the stoichiometry of Fe(III)-Valex and Fe(III)-TA complexes were 4:1 at pH=8.4.

3.1.2.5 Stability Constants of the Complexes

The Fe(III)-Valex and Fe(III)-TA complex concentrations were determined by using Beer's law molar absorption coefficients and measured absorbances of the mixtures at pH= 2.4, 4.4, 6.4, 8.4. Stability constants (K) of Fe(III)-Valex and Fe(III)-TA complexes were calculated by using the equations (2.6-2.8) which were given in section "2.2.2" and results were given in Table 3.1 and 3.2.

Table 3.1 Stoichiometries and Stability constants of Fe(III)-Valex complexes at various pH

pH	Stoichiometry	K
2.4	ML	0.8×10^3
4.4	M_2L	1.5×10^8
6.4	M_2L	1.1×10^9
8.4	M_4L	3.9×10^{17}

Table 3.2 Stoichiometries and Stability constants of Fe(III)-TA complexes at various pH

pH	Stoichiometry	K
2.4	ML	1.1×10^3
4.4	M_2L	1.5×10^8
6.4	M_2L	2.0×10^9
8.4	M_4L	1.4×10^{17}

This stability constants values reflected that Valex and TA had affinity to the Fe(III), so they formed stable complexes. Several studies supported that the metals form complexes with the hydroxyl groups of tannins and the presence of a third

adjacent hydroxyl increases the stability of the complexes and they offer special opportunities for formation of metal complexes (Özacar, Şengil & Türkmenler, 2008). Although the stability constants of basic medium complexes are more stable, because of its dark violet color M_2L complex at pH=4.4 was chosen.

3.1.3 Characterization of Complexes

3.1.3.1 FTIR Analysis

The FTIR analysis of Valex, Fe(III)-Valex and TA, Fe(III)-TA complexes were shown in Figure 3.21 and 3.22 respectively.
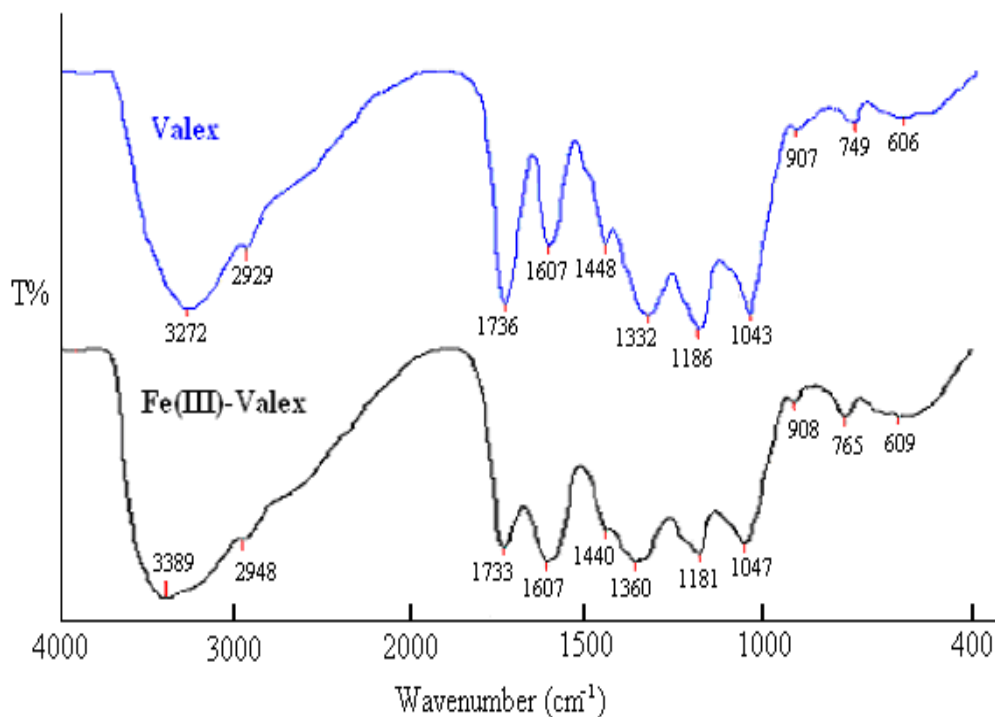
Figure 3.21 FTIR spectra of Valex and Fe(III)-Valex
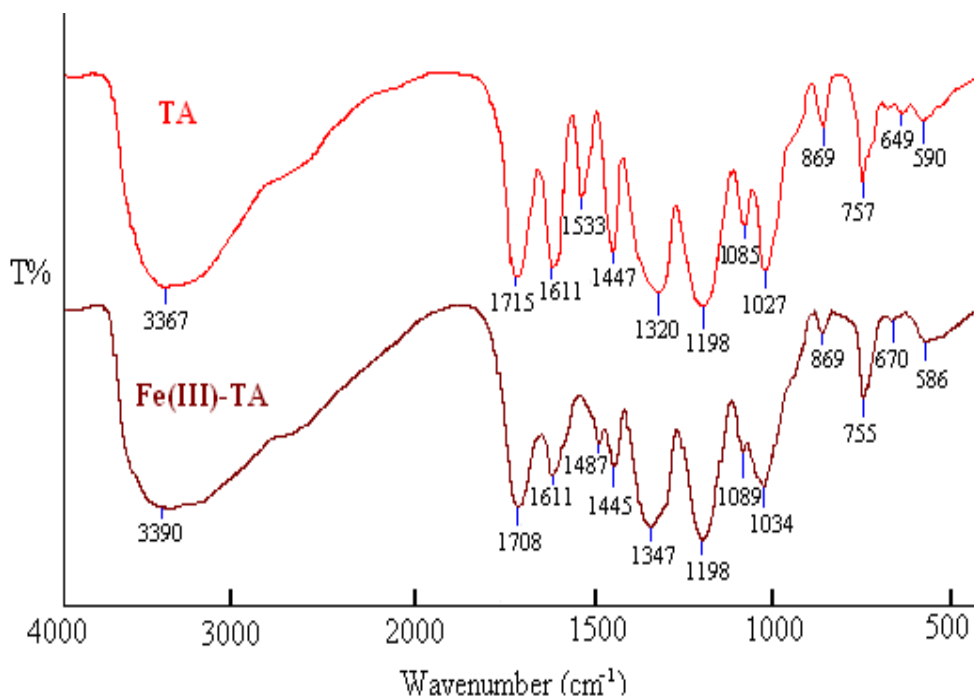
Figure 3.22 FTIR spectra of TA and Fe(III)-TA

In all spectra, the wide bands in the region of 3600–3000 cm^{-1} were due to -OH stretchings. The characteristic phenolic -OH groups were intensively presented within the nature of Valex and TA. A weak band was observed at the 2929 cm^{-1} due to aliphatic C-H stretching vibrations of Valex (Kim, S. & Kim, H.J., 2003).

The band at 1736 cm^{-1} in the spectrum of Valex and 1715 cm^{-1} in the spectra of TA was related to carboxyl–carbonyl groups. The absorption bands at 1607 cm^{-1} for Valex and 1611cm^{-1}, 1533cm^{-1} for TA were due to aromatic -C=C- bonds and the band at 1448 cm^{-1} for Valex and 1447cm^{-1} for TA were due to -C-C- deformation vibrations in the phenolic groups.

The band at 1332 cm^{-1} in the spectrum of Valex and 1320 cm^{-1} in the spectrum of TA were attributed to phenol groups. The aromatic C-H deformation bands were observed at 1186 cm^{-1} for Valex and 1198 cm^{-1} for TA. The band at 1043 cm^{-1} in valex spectrum and the bands at 1085 cm^{-1} and 1027 cm^{-1} for TA were related to the C-O stretching and C-H deformations.

60

The deformation vibrations of the C-H bonds in the benzene rings also gave weak absorption bands between the ranges of 900–550 cm^{-1}.

When the spectra of Valex and TA were compared with the spectra of their complexes some distinctive features were observed. Several bands were not only shifted slightly, but also reduced in intensity because of complex formation between metal ions and phenolic groups of Valex or TA (Özacar, Soykan & Şengil, 2006).

The broad band at 3272 cm^{-1} in Valex spectrum was shifted to 3389 cm^{-1} and the shape of this wide band was changed in the Fe(III)-Valex complex spectrum. The weak band at 2929 cm^{-1} was shifted to higher frequencies. The relative intensities of the bands of Fe(III)-Valex complex between 1750 and 1000 cm^{-1} region were shifted and remarkable changes were observed in the shapes of these bands.

The intensities of band at 1736 cm^{-1} and 1607 cm^{-1} which were related to carboxylic acid group (-C=O) and -C=C- vibrations were reduced and the band at 1736 cm^{-1} was shifted to 1733 cm^{-1}. The -C-C- deformation band at 1448 cm^{-1} became imperceptible in the Fe(III)-Valex complex spectrum.

The bands at 1332, 1186, 1043 cm^{-1} were shifted to 1360, 1181 and 1047 cm^{-1} and the intensities of these bands were reduced as compared to the Fe(III)-Valex complex spectrum. The Fe-O stretching vibrations were located in the region of 700-400 cm^{-1} (Predoi, 2007; Toderaş, Filip, Ardelean, 2006).

In the spectrum of Fe(III)-Valex, very broad band at 609 cm^{-1} and the band at 765 cm^{-1} may be attributed for Fe-O stretchning vibrations. However, significant changes in the band intensities were observed in the range of 1750 and 1000 cm^{-1} region on Fe(III)-Valex complex spectrum by the complexation of Fe(III) with the Valex.

Similiarly the intensities of band series between 1700 and 1000 cm^{-1} region were changed because of the complex formation between Fe(III) and phenolic groups of TA. When the spectrum of TA was compared to the spectrum of the Fe(III)-TA

complex, it was observed that the broad band at 3367 cm^{-1} was shifted to 3390 cm^{-1} and the shape of this wide band was little bit changed. The bands at around 1715 cm^{-1} and 1611 cm^{-1} belonging to –C=O and –C=C– vibrations were reduced and combined with each other.

When the Fe(III)-TA complex formed, the band at 1533 cm^{-1} was relatively reduced and appeared at 1487 cm^{-1}. The band at 1447 cm^{-1} and 1320cm^{-1} were shifted to 1445 cm^{-1} and 1347 cm^{-1} respectively. The bands at 1198 cm^{-1} and 869 cm^{-1} did not change in shape or intensity.

The bands at 1085 cm^{-1} and 1027 cm^{-1} were combined and appeared at 1089–1034 cm^{-1}. The bands at 757 cm^{-1}, 649 cm^{-1} and 590 cm^{-1} were shifted to 755 cm^{-1}, 670 cm^{-1} and 586 cm^{-1} respectively.

As mentioned before in the Fe(III)-Valex spectrum, the Fe-O stretching vibrations were located in the region of 700-400 cm^{-1}. Due to this reason, the change in the band intensity at 586cm^{-1} might argue that the Fe(III) and TA was complex.

3.1.3.2 Thermal Analysis

The thermal stabilities of Valex, Fe(III)-Valex complex and TA, Fe(III)-TA complex were investigated by thermogravimetric analysis and the results were presented in Figure 3.23-3.26 and Table 3.3.
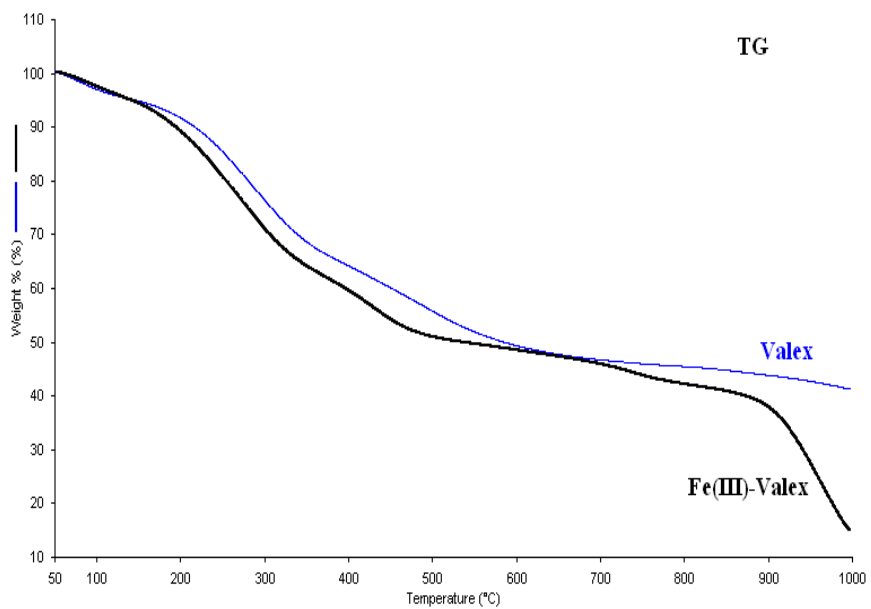
Figure 3.23 TG curves of Valex and Fe(III)-Valex.
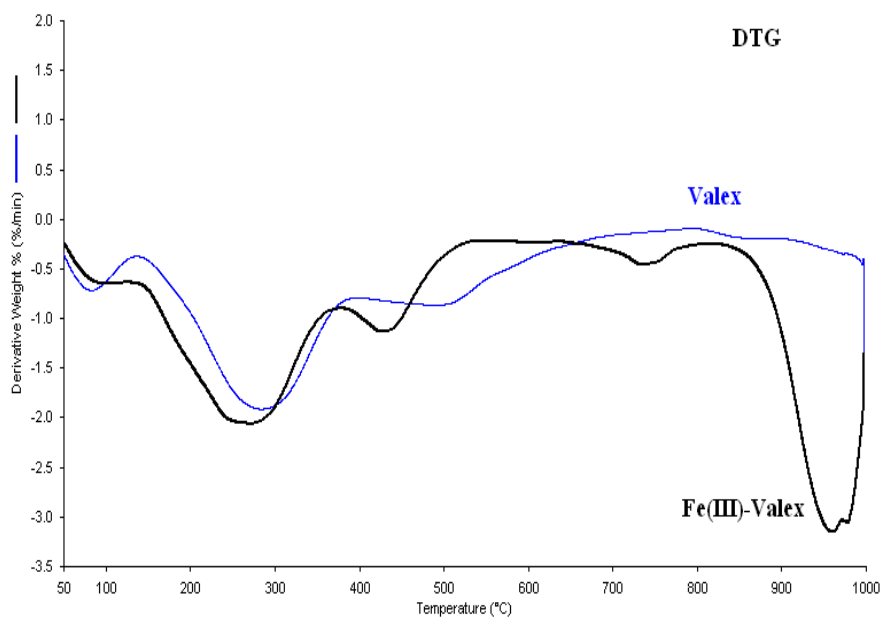
Figure 3.24 DTG curves of Valex and Fe(III)-Valex.
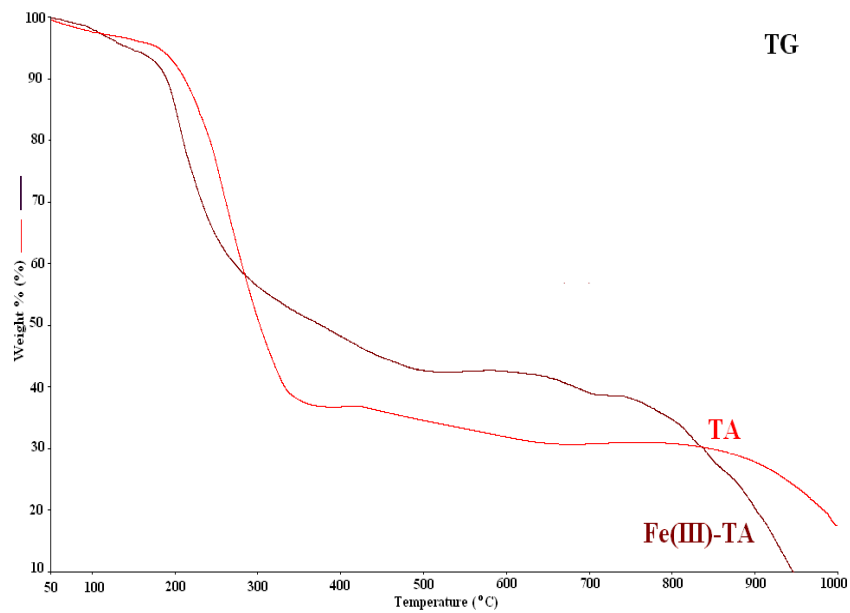
Figure 3.25 TG curves of TA and Fe(III)-TA
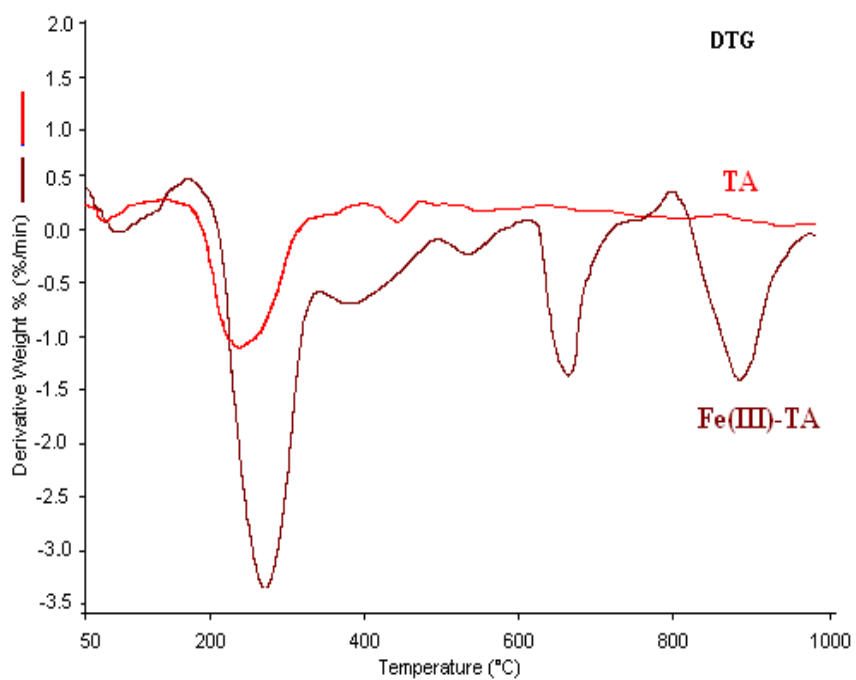
Figure 3.26 DTG curves of TA and Fe(III)-TA.

64

The TGA curves of Valex (Özacar, Soykan & Şengil, 2006) and TA showed three-step and Fe(III)-Valex, Fe(III)-TA complexes showed four-step thermal decomposition.

Table 3.3 Thermogravimetric (TG and DTG) data* of Valex, Fe(III)-Valex, TA and Fe(III)-TA.

Sample	1.step		2.step		3.step		4.step	
	DTG Maxima (°C)	% Mass loss	DTG Maxima (°C)	% Mass loss	DTG Maxima (°C)	% Mass loss	DTG Maxima (°C)	% Mass loss
Valex	82	5	278	31	799	23	-	-
Fe(III)-Valex	83	4	262	35	435	12	897	34
TA	79	1	266	49	456	21	-	-
Fe(III)-TA	80	5	283	44	670	13	898	16

*Data were obtained under dynamic nitrogen atmosphere at a heating rate of 10˚C/min

The first step of mass losses could be attributed to evaporation of adsorbed water and the other steps were due to thermal decompositions of the samples. Evaporation of adsorbed water was carried out approximately at 83°C with a mass losses of 5% and 4% for Valex and Fe(III)-Valex complex and 1% and 5 % for TA, Fe(III)-TA complex, respectively.

The second decomposition step of Valex, Fe(III)-Valex complex, TA and Fe(III)-TA complex occured at approximately 270°C with a mass loss of 31% for Valex, 35% for Fe(III)-Valex complex, 49% for TA and 44% for Fe(III)-TA complex. This was corresponded to decarboxylation or may be attributed to partial decomposition of samples (Garro-Galvez, 1997; Aelenei, 2009).

Within a temperature range of 400-800°C as the third step, Valex, Fe(III)-Valex complex, TA and Fe(III)-TA complex were decomposed with 23%, 12%, 21%, 13% mass losses, respectively. This was probably due to the further loss of hydroxyls

groups of samples or oxidation of high carbon residue (CO_2, H_2O and CO) (Garro-Galvez, et al., 1997).

The fourth step decomposition of the complexes was carried out at extremely high temperatures 897 ^{o}C for both Fe(III)-Valex complex and Fe(III)-TA complex with 34% and 16% mass losses respectively. At 897 ^{o}C, the residues of remaining groups could be metal or metal oxides. On the other hand this situation may be caused complexation of Fe(III)-Valex or Fe(III)-TA inhibits thermal stability of the Valex or TA against the degradation and these were provided the fourth step decomposition. As a result, total mass losses of Valex, Fe(III)-Valex complex, TA and Fe(III)-TA complex were obtained 59%, 85%, 71% and 78% respectively.

In an another experiment by using a melting point apparatus, melting points of Fe(III)-Valex and Fe(III)-TA complexes were found to be 261°C.

3.1.3.3 XRD Analysis

The X-ray diffraction patterns of Valex, Fe(III)-Valex complex and TA, Fe(III)-TA complex were shown in Figure 3.27 and 3.28 respectively.
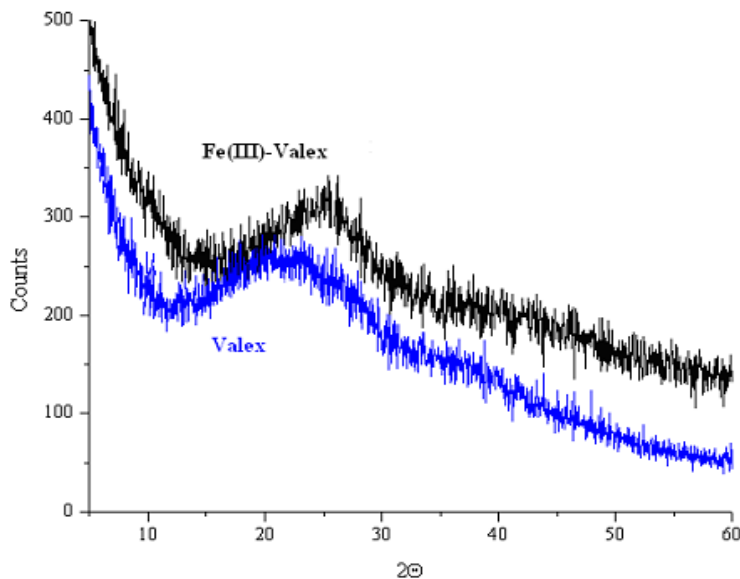
Figure 3.27 XRD patterns of Valex and Fe(III)-Valex.

A very broad and unresolved peak in the 2θ region of 20-30° was observed in the diffraction patterns. This may be due to their amorphous structures (Beltran, 2010; Iglesias, 2001). The peaks of complexes in the range of 2θ=20-30° were a little bit sharper with respect to valex and TA where broader peaks were observed. 2θ value of Valex shifted to higher 2θ value from 23.7^o to 26.2^o compared to the Fe(III)-Valex complex 2θ value.
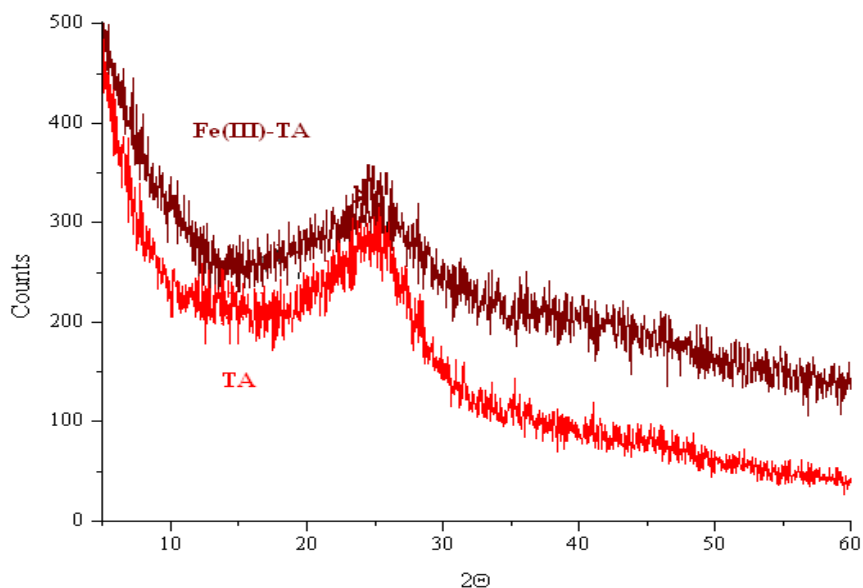
Figure 3.28 XRD patterns of TA and Fe(III)-TA.

2θ value of TA was observed at 25.9° and this value slightly shifted to higher 2θ value, from the 25.9^o to 26.2^o, at the Fe(III)-TA complex. The actual structures of the complexes were not shown due to the fact that single crystal form of the complexes were not achieved.

3.1.3.4 ESR and Magnetic Susceptibility Analyses

Chemical environment of unpaired electrons that localize to the molecule affects the spectroscopic splitting factor (g factor) which shows the magnetic features. The ESR spectrum of Fe(III) ions are given ESR spectrum at about g=4.3 (Bou-Abdallah & Chasteen, 2008).

Similar ESR spectra were observed for both the high spin Fe(III)-Valex and Fe(III)-TA complexes and the spectrum of Fe(III)-TA complex is given in Figure 3.29.

Magnetic susceptibility values of the Fe(III)-Valex and Fe(III)-TA complexes were measured at 293 K and evaluated in terms of the number of unpaired electrons and hybrid species.
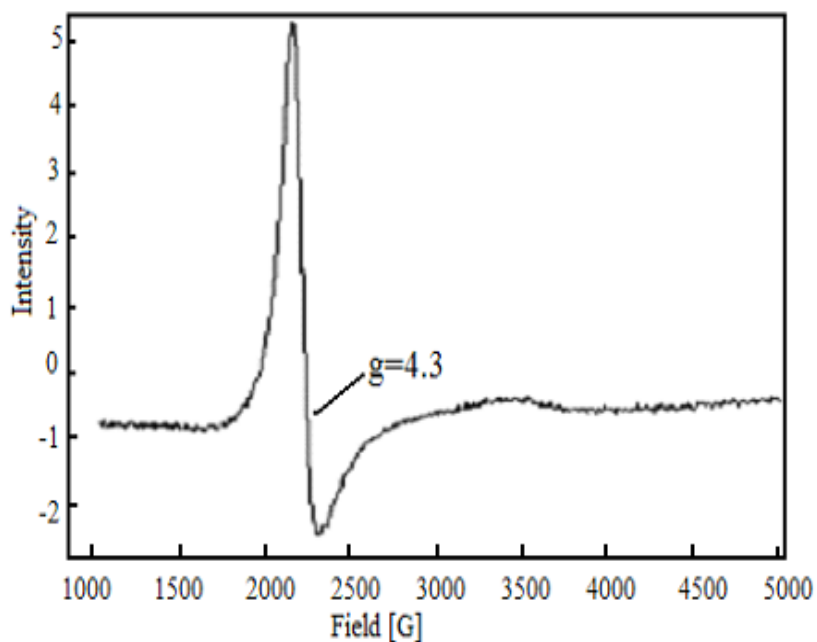
Figure 3.29 ESR spectra of Fe(III)-TA complex at room temperature

When the values were applied to equation (2.10) in section 2.2.3.4. X_g values were calculated as:

$$Xg = 1.086 \times 2.5 \times [410 - (-30)] \Big/ 10^9 \times (0.96 - 0.84)$$

$$Xg = 9.96 \times 10^{-6} \ erg.G^{-2}$$

When this X_g value of complexes placed in equation (2.11), the molar magnetic susceptibility of complexes was calculated as:

$$X_m = 9.96 \times 10^{-6} \times 1850$$

$$X_m = 0.018$$

The value of the effective magnetic moment, μ_{eff}, in Bohr magneton was calculated by equation (2.12) in section 2.2.3.4;

$$\mu_{eff} = 2.84\sqrt{X_m xT}$$

$$\mu_{eff} = 2.84\sqrt{0.018 x 293} = 6.52$$

The experimental magnetic susceptibility was calculated as μ_{eff} = 6.52 BM (Bohr Magneton). This result was consistent with the presence of the Fe^{3+}. It was indicated that both complexes have paramagnetic properties (Drokina, 2010; Chikate, 2005).

.

3.1.3.5 MALDI-TOF MS Analysis

Experimental and calculated mass groups of Valex, Fe(III)-Valex complex, TA and Fe(III)-TA complex are given in Figure 3.30-3.33 and Table 3.4-3.7 respectively. Samples characteristically lost multiple galloyl (G) moietie (*m/z* 152) during fragmentation. Also gallic acid (GA) 169 m/z and iron(III) (Fe^{3+}) 56m/z fragments were used for mass analysis. TA and Valex molecular weights was shown as M_1, in figures 3.30 and 3.32. Complexes molecular weights was shown as M_2, in figures 3.31 and 3.33.
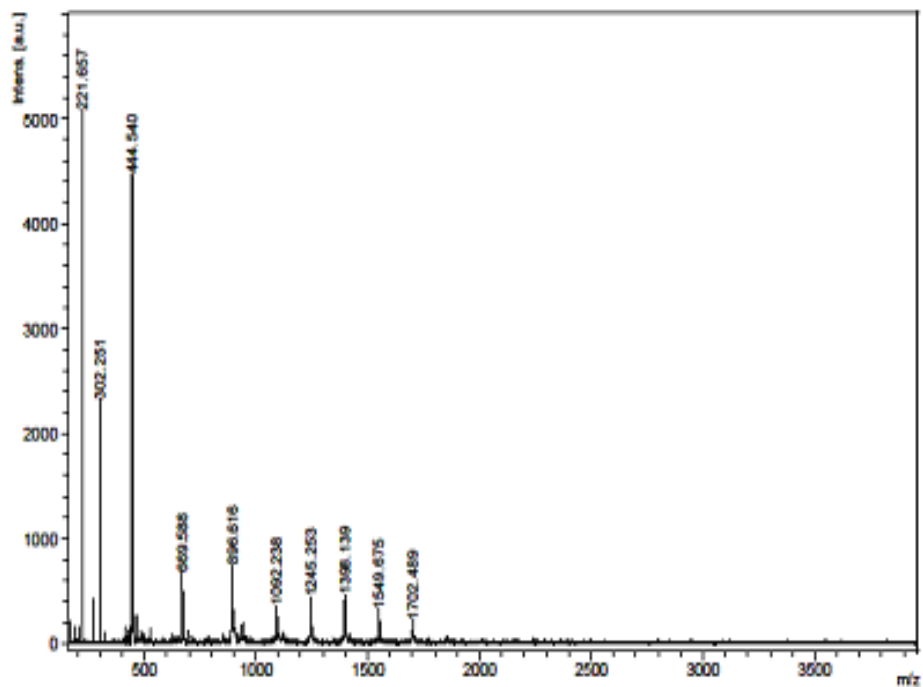
Figure 3.30 MALDI-TOF Mass spectrum of Valex

Table 3.4 MALDI-TOF Mass analysis data of Valex

Experimental Mass (m/z)	Calculated Mass (m/z)	
1702	1701	$[M_1]$
1550	1549	$[M_1–G]$
1398	1397	$[1550–G]$
1245	1245	$[1398–G]$
1092	1093	$[1245–G]$
941	941	$[1092–G]$
897	897	$[941–CO_2]$
669	668	$[897–C_{13}H_9O_4]$
444	442	$[669–C_8H_3O_8]$
302	302	$[444–C_6H_2O_4]$
222	222	$[302–C_6H_8]$
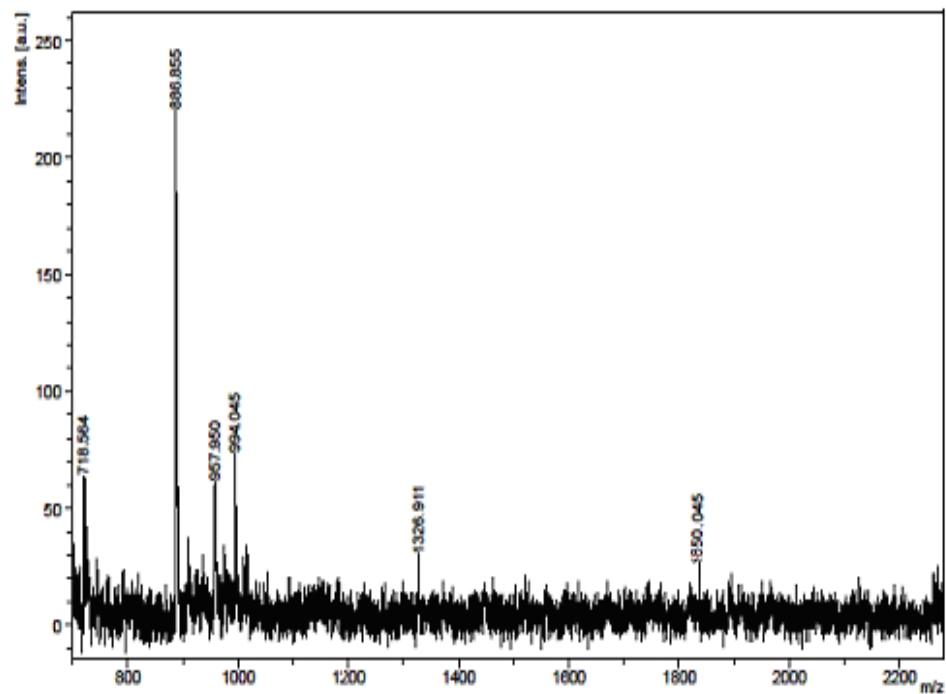
Figure 3.31 MALDI-TOF Mass spectrum of Fe(III)-Valex

Table 3.5 MALDI-TOF Mass analysis data of Fe(III)-Valex

Experimental Mass (m/z)	Calculated Mass (m/z)	
1850	1849	$[M_2]$
1327	1326	$[M_2–C_{22}H_{12}O_{12}Fe]$
994	995	$[1327–C_{13}H_{16}O_{10}]$
957	958	$[994–2H_2O]$
887	885	$[957–FeO]$
718	718	$[887–C_7H_5O_5]$
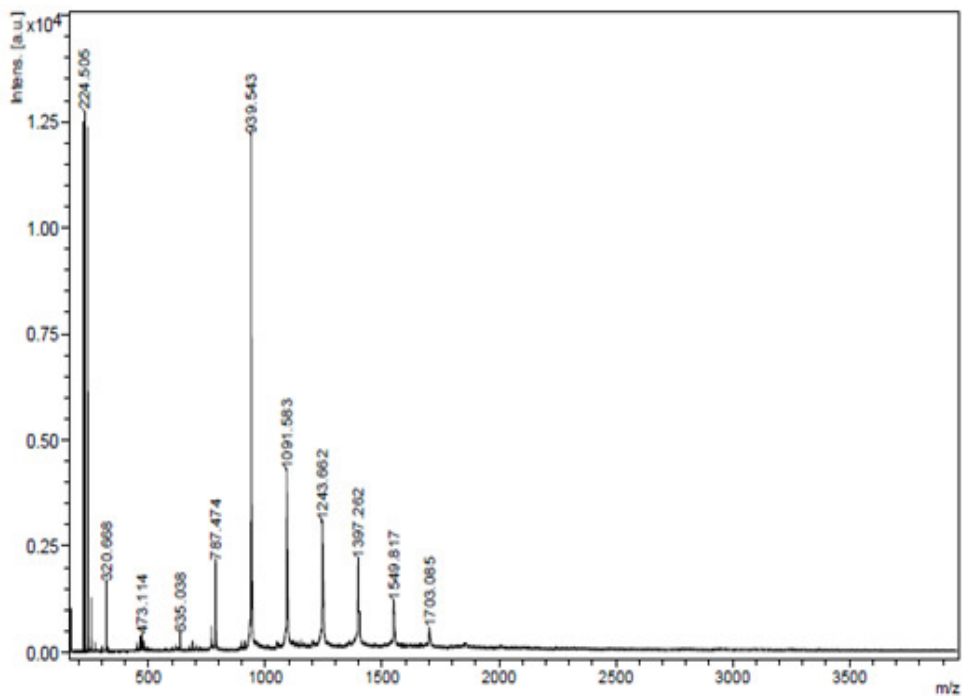
Figure 3.32 MALDI-TOF Mass Spectrum of TA

Table 3.6 MALDI-TOF Mass analysis data of TA

Experimental Mass (m/z)	Calculated Mass (m/z)	
1703	1701	$[M_1]$
1549	1549	$[M_1–G]$
1397	1397	$[1549–G]$
1243	1245	$[1397–G]$
1091	1093	$[1243–G]$
939	941	$[1091–G]$
787	789	$[939–G]$
635	637	$[787–G]$
473	471	$[635–C_8H_4O_4]$
320	320	$[473–C_7H_5O_4]$
224	222	$[320–C_5H_6O_2]$
168	170	GA
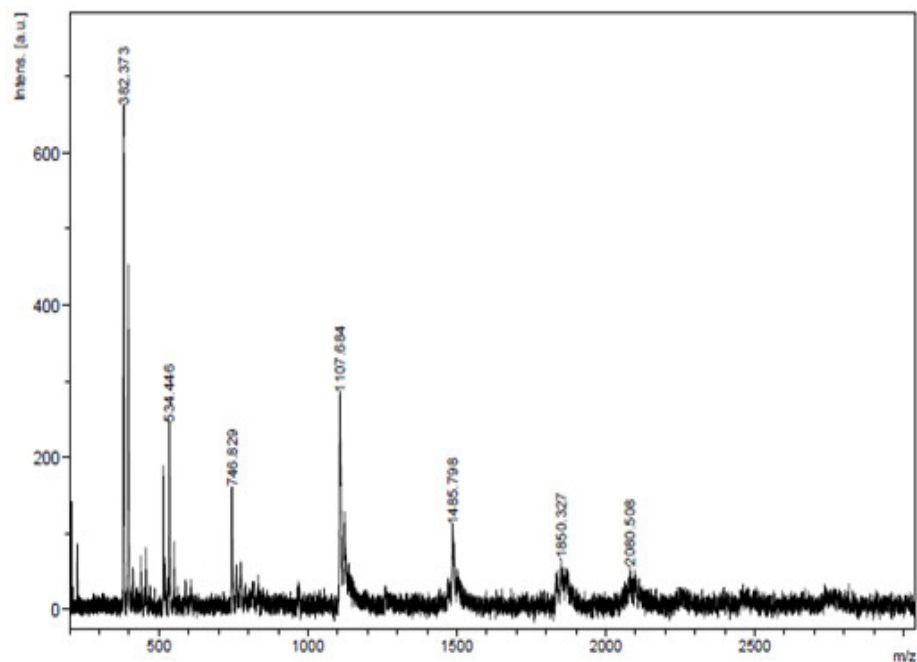
Figure 3.33 MALDI-TOF Mass Spectrum of Fe(III)-TA

Table 3.7 MALDI-TOF Mass analysis data of Fe(III)-TA

Experimental Mass (m/z)	Calculated Mass (m/z)	
1850	1849	$[M_2]$
1485	1485	$[M_2–C_{15}H_9O_{11}]$
1107	1105	$[1485–C_{16}H_{12}O_{11}]$
746	747	$[1107–C_{18}H_8O_5Fe]$
534	538	$[746–G–Fe]$
382	382	$[534–G]$

Molecular weights of Valex, Fe(III)-Valex complex, TA and Fe(III)-TA complex were determined from MALDI-TOF MASS spectrum as 1703, 1850 ($M_2L.2H_2O$), 1702 and 1850 m/z ($M_2L.2H_2O$) respectively. As a comparison, the molecular weight of the valex is approximately equal to molecular weight of the tannic acid (M=

1701.2 g mol^{-1} Riedel-de Haën 1401-55-4). Besides the molecular weights were the same in the both of the complexes.

3.1.3.6 X-Ray Photoelectron Spectroscopy (XPS) Analysis

XPS spectra of Fe(III)-Valex and Fe(III)-TA complexes were the same and Fe(III)-TA complex XPS spectra was shown in Figure 3.34.
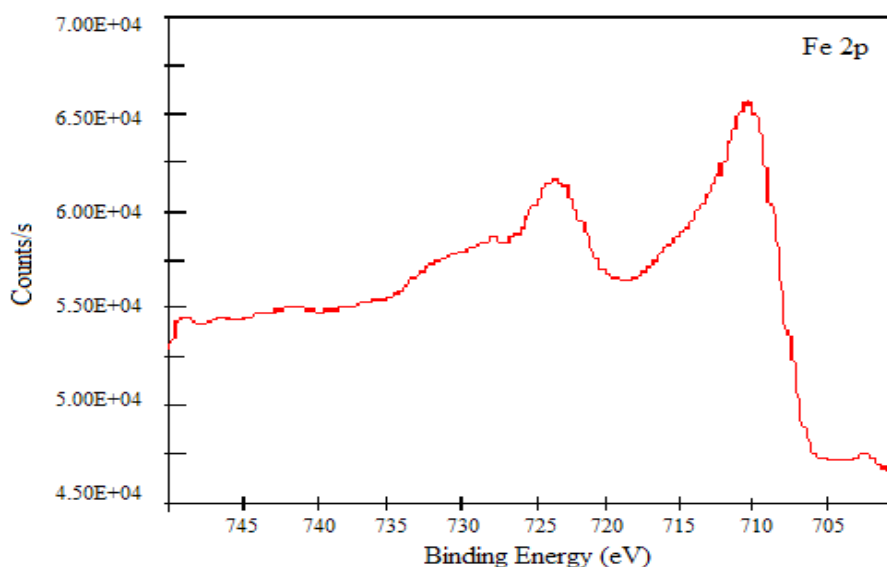
Figure 3.34 XPS spectra of Fe(III)-TA complex.

XPS characterization of the complexes was confirmed the existence of Fe^{3+} ions. In Figure 3.34, the core level spectrum of Fe $^{3+}$ has a 2p$_{3/2}$ binding energy of 710 eV and 2p$_{1/2}$ of binding energy 724 eV (Mekki, Holland, McConville & Salim, 1996; Panigrahy, Aslam & Bahadur, 2012).

3.1.3.7 ^{1}H-NMR Analysis

TA and its complexes spectra were recorded in mixture of DMSO/Methanol (3:1) as standard. In Figures 3.35 and 3.36 ^{1}H-NMR spectra of TA and Fe(III)-TA complex were given respectively.

According to the rates calculated from integration coefficients, there were 36 proton between chemical shift of δ= 3.5-5.0ppmand they belongs to aromatic C-H and gallol groups. Also there were 4 proton between chemical shift of δ= 5.0-6.5ppm and 12 proton between chemical shift of δ= 6.5-8.5ppm belongs to glucose protons and galloyl group's protons respectively. When the ^{1}H-NMR spectrum analysis of TA was examined, they observed in the low-field δ= 6.5-8.5ppm range because of multiplet peaks of galloyl group's protons (H$_b$) were slightly shielding. Due to shielding from the surrounding electronegative atoms in chemical environment, multiplet peaks of aromatic C-H and gallol group's protons (H$_a$), chemical shift values was observed in high-field range of 3.5-5.0ppm. Four hydrogen (Hc) belongs to the glucose ring in the center of tannic acid molecular structure were partially shielding. Hc protons multiplet peaks chemical shifts were observed in the range of δ= 5.0-6.5ppm. DMSO solvent signals were seen at δ=3.3ppm and δ=2.4ppm respectively.
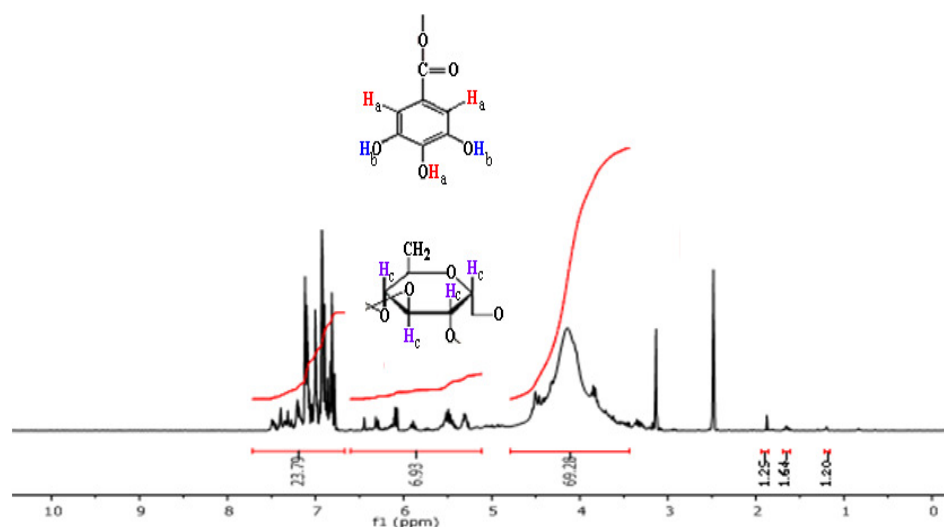
Figure 3.35 ^{1}H-NMR Spectra of TA

When the NMR spectra of TA and Fe(III)-TA complex were compared, obvious differences in peak intensities were showed. In both spectra the equal amount of solvent was used. Because the solubility of complex is less than TA. This has led to more intensive solvent peaks at the complex spectra.

In the complex NMR spectra, the relaxation times directly related to the width of signals. The less relaxation time indicates that resonance is in a wide frequency region and this indicates that signal's width is enlarged. Due to the a relaxation time decrease, signal splitting was not observed because the increased in the width of signal. So the signals at complex NMR of in the range of δ= 5.0 - 7.5ppm were seen more broad.
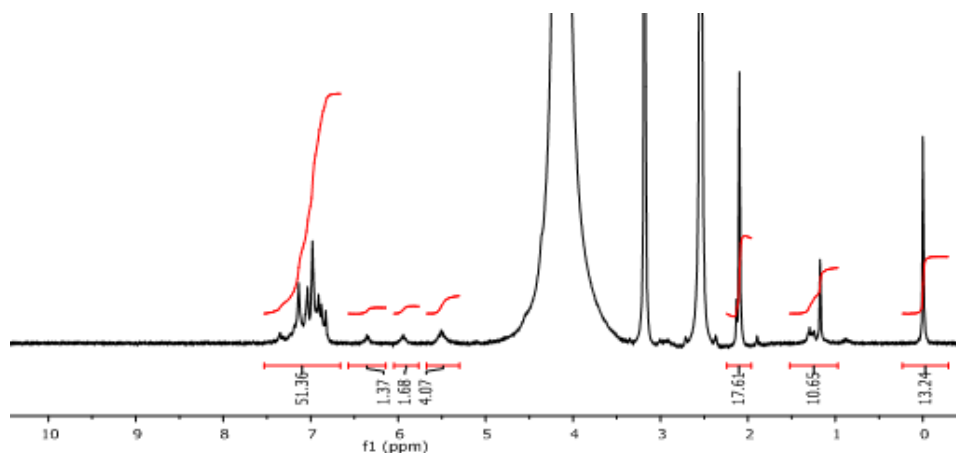
Figure 3.36 ^{1}H-NMR Spectra of Fe(III)-TA Complex

In the H-NMR spectra Fe(III)-TA complex lower field signals (in the range of 5-8ppm) intensities were decreased due to the complexation of TA with Fe(III). Higher field signals (in the range of 0-5ppm) intensity were increased depending on the increasing the amount of the solvent.

3.1.4 Complex Percent Yield Calculation

Actual yield of purification of the synthesized Fe(III)-TA complex was obtained 2.061g (m_2) for the calculation of efficiency. Theoretical mass of complex were calculated as 2.311g (m_1).

Percent yield calculation of complex was computed with these values in Equation (2.13) given in section 2.2.4:

$$Yield\% = [2.061 / 2.311] x100$$

$$Yield\% = 89.2$$

Complex percent yield was calculated as 89.2%.

3.1.5 Antioxidant Activities of Fe(III)-Valex and Fe(III)-TA Complexes

Comparison of DPPH radical scavenging activities of Valex, Fe(III)-Valex complex, TA, Fe(III)-TA complex, BHA and BHT at 50 µg/mL were shown in Figure 3.37 and Table 3.8.
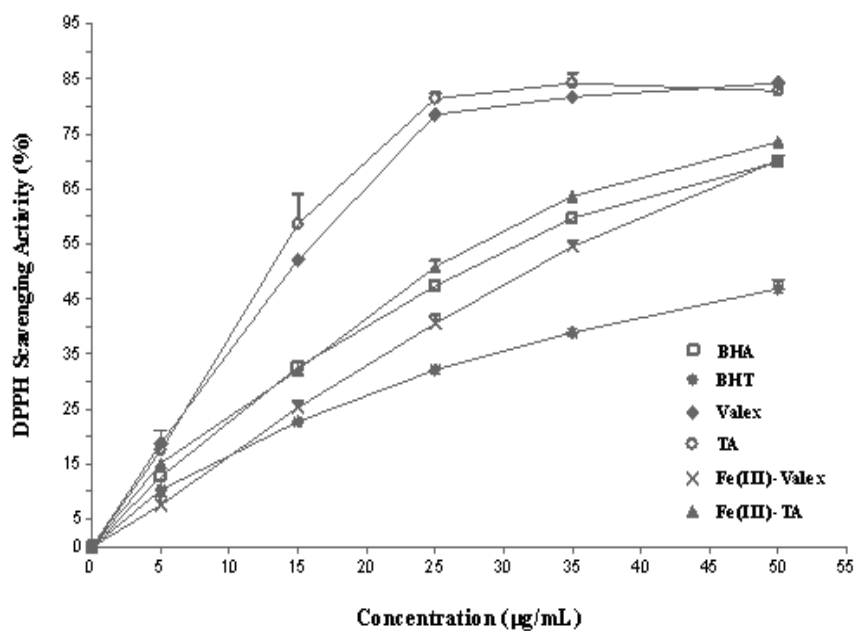
Figure 3.37 Antioxidant activity (%) of BHA, BHT, Valex, TA, Fe(III)-Valex and Fe(III)-TA. Each value means ± SD of three different experiments.

Valex showed the strongest scavenging activity at 50 µg/mL with 84.22 % on DPPH radicals. In addition, TA showed approximately the same activity with 82.82%. Fe(III)-TA, Fe(III)-Valex complex and BHA showed slightly lower radical scavenging activities as 73.53%, 70.18%, 69.94% respectively.

Table 3.8 Antioxidant activity (%) of BHA, BHT, Valex, TA, Fe(III)-Valex and Fe(III)-TA,. Each data means ± SD of three different experiments

Concentration (µg/mL)	BHA	BHT	Valex	TA	Fe(III)-Valex	Fe(III)-TA
0	0.00±0.00	0.00±0.00	0.00±0.00	0.00±0.00	0.00±0.00	0.00±0.00
5	12.77±0.17	10.33±0.98	18.77±2.44	17.49±0.52	7.57±1.60	15.19±0.46
15	32.66±0.05	22.74±0.31	52.12±1.23	58.65±5.51	25.31±1.10	32.14±0.55
25	47.38±0.06	32.16±0.38	78.50±0.24	81.43±0.99	40.57±1.61	50.86±1.17
35	59.72±0.04	38.91±0.81	81.74±1.22	84.20±1.82	54.53±1.02	63.71±0.05
50	69.94±0.61	46.92±1.58	84.22±0.66	82.82±0.57	70.18±0.23	73.53±0.30

In addition, the lowest activity was observed with BHT (46.92%) at 50 µg/mL. Statistically significant ($p < 0.05$) correlation was found among the complexes and the controls. On the other hand the antimicrobial and antifungal activities of Fe(III)-Valex and Fe(III)-TA complexes were investigated but they have neither antimicrobial nor antifungal activity as a result of Disk diffusion experiments. Although there are studies showing the antimicrobial or antifungal effects of tannic acid or valex, no such evidence was found for their complexes.

On the other hand, the superoxide anion-scavenging activity of complexes was determined, but in the present concentrations complexes did not show any significant activity. Also the inhibition activity of complex against hydroxyl radicals was determined by measuring the level of oxidation of 2-deoxy-D-ribose by ^-OH with subsequent measurement of the products by their reaction with thiobarbituric acid (TBA). But complexes did not show significant activity.

3.2 Synthesis, Characterization and Applications of Tannic Acid Resin

3.2.1 Characterization of Tannic Acid Resin

3.2.1.1 FTIR Analysis

The FTIR analysis of TA, TR and TR-B was shown in Figure 3.38.
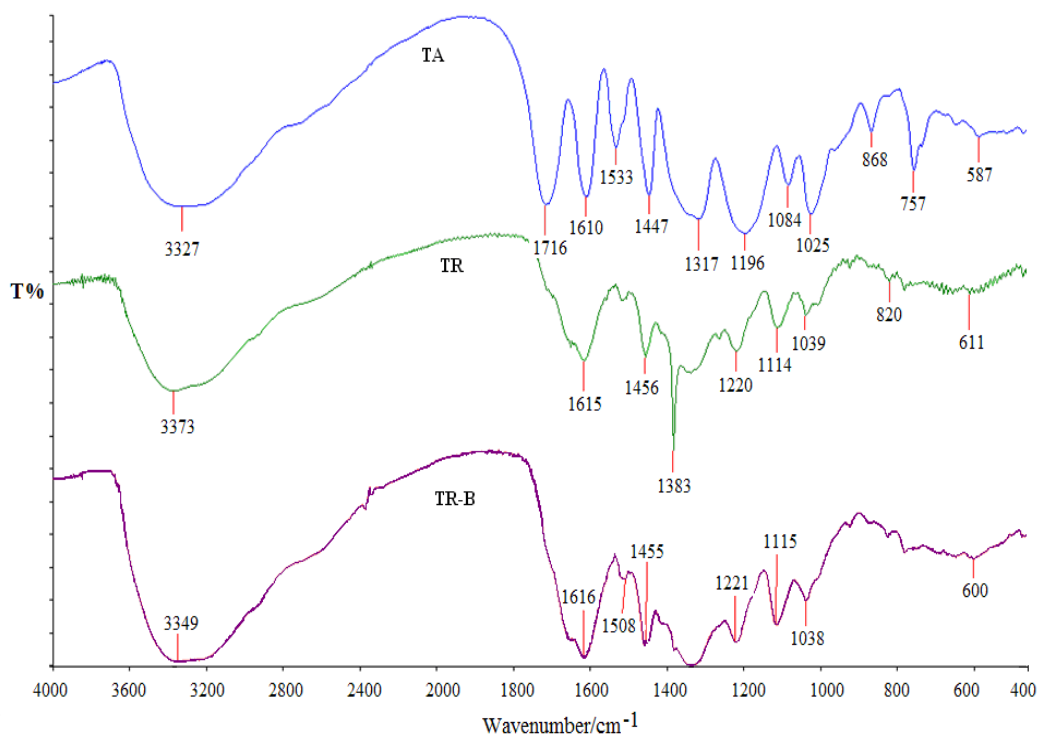
Figure 3.38 FTIR spectra of TA, TR and TR-B.

In all spectra, the wide bands in the region of 3600–3000 cm^{-1} were due to –OH stretchings. The characteristic phenolic –OH groups were intensively presented within the nature of TA.

The band at 1716 cm^{-1} in the spectrum of TA was related to carboxyl–carbonyl groups. The absorption bands at 1610 and 1533 cm^{-1} were due to aromatic –C=C– bonds and the band at 1447 cm^{-1} was due to –C–C– deformation vibrations in the

phenolic groups. The band at 1317 cm^{-1} in the spectrum of TA was attributed to phenol groups. The aromatic C–H deformation bands were observed at 1196 cm^{-1}.

The bands at 1100-1010 cm^{-1} were related to C–O stretching and C-H deformations. The deformation vibrations of the C–H bonds in the benzene rings also gave small absorption bands between the ranges of 900–550 cm^{-1}.

When the spectrum of TR was compared to the spectrum of TA, the broad band at 3327 cm^{-1} was shifted to 3373 cm^{-1} and the shape of this wide band was changed. The intensities of the bands at around 1716 cm^{-1} and 1610 cm^{-1} which were related to –C=O and –C=C– vibrations were reduced and the bands were combined with each other at around 1615 cm^{-1}. This change was occurred most probably due to the environmental change of C=O groups because of the interaction of formaldehyde with TA.

The intensity of the band at around 1533 cm^{-1} was reduced and its shape was a little bit changed in the resin. The band at 1447 cm^{-1} was shifted to 1456 cm^{-1} and the intensity of this band was slightly changed due to the formation of methylene bridges by the reaction with formaldehyde. Also after this reaction a sharp band was occurred at 1383 cm^{-1}. The bands between 1320 and 1020 cm^{-1} region were shifted and remarkable changes were observed in the shapes of these bands in the spectrum of TR which may be due to the formation of –C–O–C– linkages (Scheme 3.1). Intensities of the bands in the range of 900–550 cm^{-1} were completely reduced (Özacar, Soykan & Şengil, 2006).

Relative intensities of the bands of TR between 1700 and 1000 cm^{-1} region were changed in the spectrum of TR-B; because of the specific affinity and complex formation between boron and some phenolic groups grafted on the resin surface of TR. The wide band at 3349 cm^{-1} was due to free hydroxyl groups of TR and B-OH stretching vibrations. The intensity of the band at around 1615 cm^{-1} was increased after adsorption process. The B-O stretching vibrations were observed in the region of 1500-1100 cm^{-1} and significant changes were observed in these bands by the

adsorption of boron onto TR. The sharp band located at 1383 cm^{-1} which was probably due to -CH bending vibration was also, remarkably changed. The shapes of other bands in the fingerprint region were not changed but these bands were little bit shifted. In the spectrum of TR-B, by the formation of O-B-O bonds small changes were observed at the bands between 900-700 cm^{-1} regions after boron adsorption.
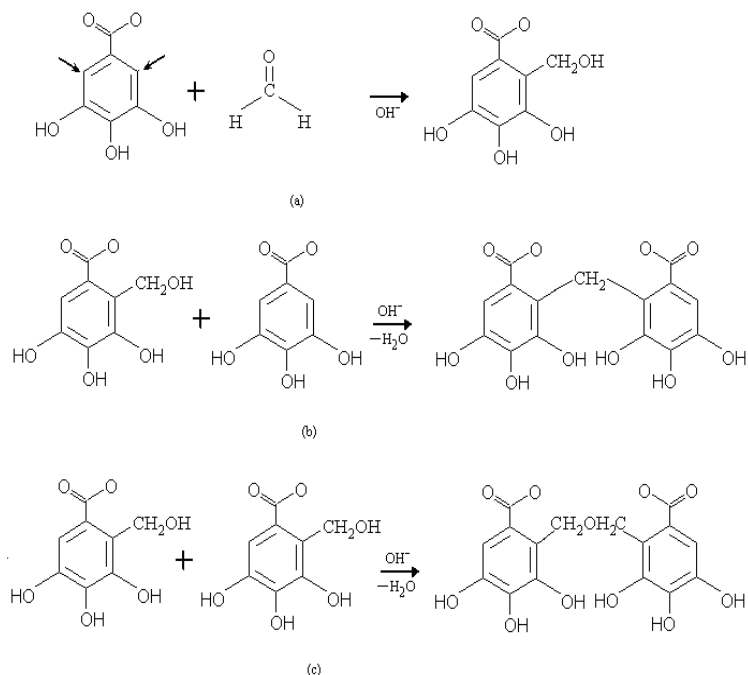
Scheme 3.1 Reaction of galloyl group in tannic acid with formaldehyde. (a) methylolation reaction of galloyl unit in TA, (b) condensation reaction of galloyl unit in TA (Garro-Galvez, Fechtal & Riedl, 1996).

TR formation reactions with formaldehyde are shown in Scheme 3.1. There are two possible condensation reaction paths for the reaction of Tannic acid and formaldehyde, leading to the formation of a methylene bridge. The first step of two mechanisms, methylolation, is an electrophilic aromatic substitution reaction [Scheme 3.1(a)]. The second step is a condensation reaction. The two mechanism involve a hydroxymethyl group with either a proton of the aromatic ring (ortho position), with the release of one molecule of water [Scheme 3.1(b)], or a hydroxymethyl group with the simultaneous release of one molecule of water and one molecule of formaldehyde [Scheme 4(c)]. In both cases, a methylene bridge is created. Thus, the formaldehyde reaction at the ortho position of a sufficiently large

number of galloylated rings of tannic acid, would open the door to the formation of a three dimensional structure (crosslinking) upon reaction conditions. This type of network is generally regarded as the best resin system (Özacar, Soykan & Şengil, 2006).

3.2.1.2 SEM Analysis

SEM images of TA, TR and TR-B at x2000 magnification were shown in Figure 3.39.
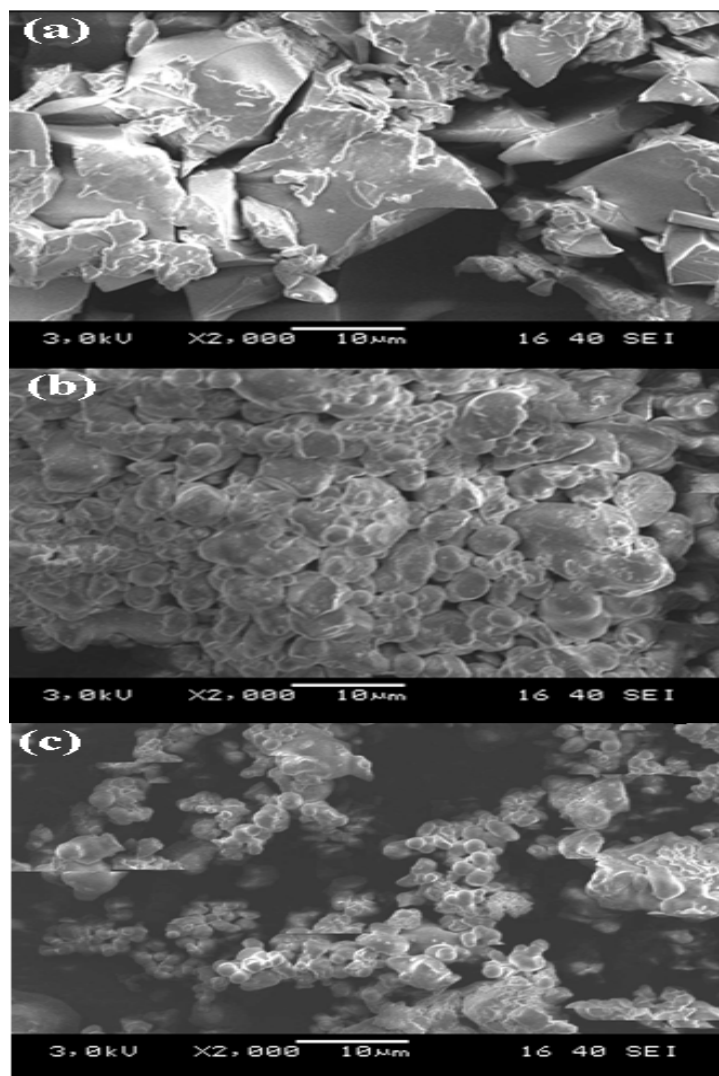
Figure 3.39 SEM images of the surfaces of (a) TA,(b) TR and (c) TR-B at x2000 magnification.

TA generally displayed a smooth surface with particles having different dimensions without a specific shape (Figure 3.39a), besides TR and TR-B exhibited oval shaped sphericity (Figure 3.39b and 3.39c).

The SEM analysis results showed that the morphology of TA was changed when it was cross-linked with formaldehyde. It could be claimed that a compact and condensed structure was formed in TR so big aggregates were observed. When boron was adsorbed (TR-B), the sizes of the spheres were decreased and the aggregates were dissociated into smaller particles, also wide holes and pores occurred among the aggregates. There were some deformed spheres at the surface of TR-B indicating the irregular structure of the sample compared to TR.

3.2.1.3 Thermal Analysis

The TG/DTG data of TR and TR-B were presented in Figure 3.40 and Table 3.9.
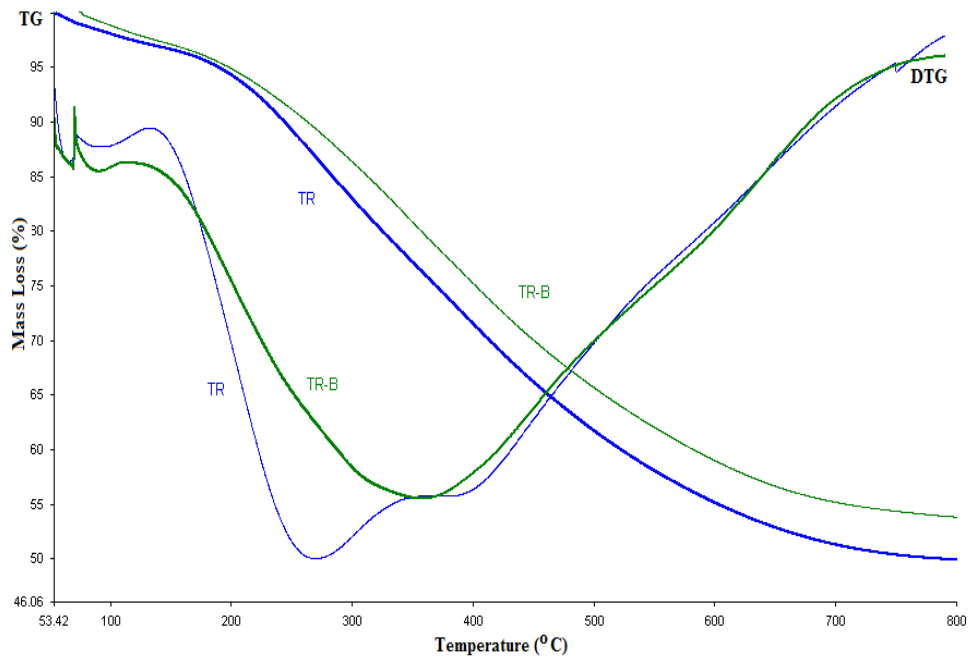
Figure 3.40 TG and DTG curves of TR and TR-B

The TGA curves of both samples showed three-step thermal decomposition. The first step of mass losses could be attributed to evaporation of adsorbed water and the other steps were due to thermal decompositions of the samples.

Table 3.9 Thermogravimetric data[*] of TR and TR-B

Samples	1.Stage		2.Stage		3.Stage	
	DTG Maxima (^{o}C)	% Mass loss	DTG Maxima (^{o}C)	% Mass loss	DTG Maxima (^{o}C)	% Mass loss
TR	79	3	242	19	392	29
TR-B	76	4	223	8	391	37

[*]Data were obtained under dynamic nitrogen atmosphere at a heating rate of 10˚C min^{-1}.

Evaporation of adsorbed water was carried out at 79 ^{o}C and 76 ^{o}C with 3% and 4% mass losses for TR and TR-B, respectively. The decomposition temperature range of 200–250 ^{o}C with a mass loss of 19% for TR and 8% for TR-B were observed in the second stage.

The third stage was occurred approximately at 390 ^{o}C for both samples which may be due to the fragmentation of the intramolecular forces. TR and TR-B were decomposed with 29% and 37% mass losses, respectively. It might be suggested that the adsorption of boron onto TR was realized due to the alteration observed in the DTG maxima of different decomposition stages.

3.2.2 Adsorption Studies

The effect of contact time on boron adsorption was primarily measured at certain time intervals between 0.5-36 hours at different temperatures (288, 298, 308 K), for further studies. Results indicated that boron adsorption attained equilibrium within 24 h; thereafter any significant increase was not observed. Therefore, all other adsorption experiments were performed at this contact time.

3.2.2.1 Effect of Boron Concentration

The effect of initial boron concentration on the boron adsorption onto TR at different temperatures was shown in Figure 3.41.
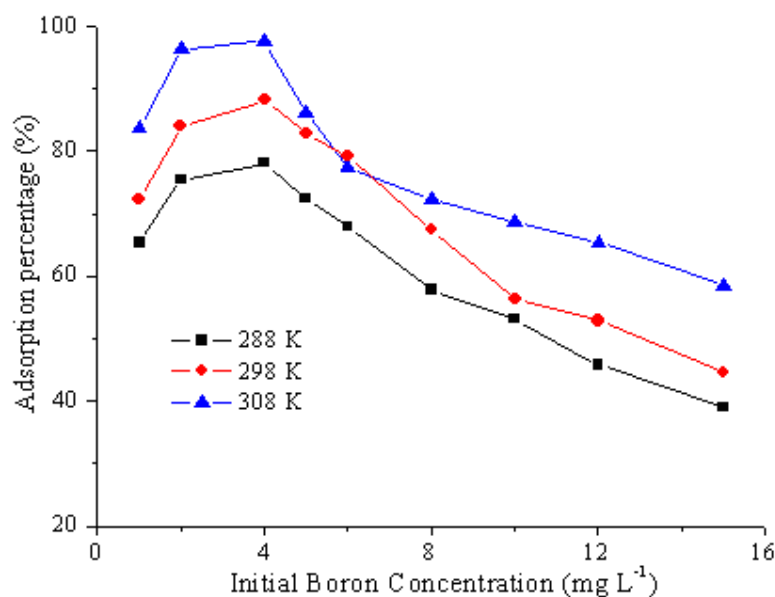
Figure 3.41 Effect of initial boron concentration at different temperatures (0.1g TR; pH=7.0; 24 h)

For all studied temperatures the adsorption of boron was increased up to 4 mgL^{-1} initial boron concentration, but then initial concentration of boron was furthermore increased, a significant decrease was observed at adsorption percentage.

This situation may have been caused by the blocking of the active sites of the adsorbent at high concentrations and the presence of limited adsorption regions. The results showed that maximum boron adsorption was observed at 4 mgL^{-1} boron concentration and at 308 K with a percentage of 88%.

3.2.2.2 Effect of pH

The pH of the solution is a considerably important parameter in the whole adsorption process and particularly on the amount of adsorbed boron. The pH of the solution influences the degree of ionization of the boric acid. At lower pH (<7) values the major species is H_3BO_3. At pH values around 9.0, the H_3BO_3 and $B(OH)_4^-$ concentrations are practically the same. But, at higher pH values (11.0), $B(OH)_4^-$ is the predominant species (pK_a: 9.2) (Lou, 1999; Magara, 1998).

However, zeta potentials of some tannic acid based adsorbents were determined and found around pH=2.2. These resins had negative surface above pH 2 and the negativity of surface increased with the increase in pH. This is related with the increase in the ionization of the phenolic (-OH) groups.

It was understood that the ionization was reached maximum at around pH=5-6. For these reason, due to the electrostatic nature of the sorption with metal cations onto the phenolic resins, it had been expected that the adsorption of the metal cations onto the resins was around pH=5-6 (Özacar, 2006; Dollimore, 1964; Yurtsever, 2009). The effect of initial pH on the boron adsorption of TR was given in Figure 3.42.
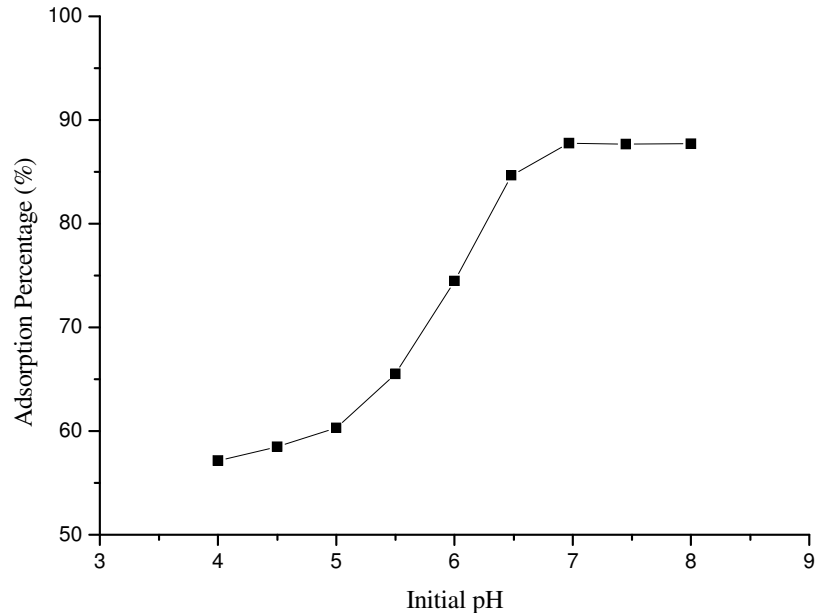
Figure 3.42 Effect of initial pH on boron adsorption (0.1g TR; 4 mgL^{-1} B; 308 K; 24 h).

When the pH was raised from 4.0 to 7.0 the amount of adsorbed boron was increased due to the access H_3BO_3 species. Adsorption of boron was more effective at pH=7.0 with a highest adsorption percentage of 88%. Above pH=7.0, the boron adsorption remained constant.

The adsorption at higher pH values (more than pH=9.0) was not encouraged due to the decomposition of TR (Şengil & Özacar, 2009). Desorption of boron from the TR-B was also studied. Firstly desorption studies were carried out in distilled water. Some practical desorption was occurred. Then, 0.01 M HNO_3 and 0.01 M H_2SO_4 solutions were used for desorption studies but the results were low (found as around 31%). Afterwards desorption studies were carried out by using the adsorbent (after adsorption at pH=7.0) with 0.01M HCl solution. At that time, 81 percentage of desorption efficiency was achieved. All the results showed that TR could be used as an appropriate adsorbent in the adsorption process of boron from aqueous solutions in terms of its relatively high sorption capacity.

3.2.2.3 Effect of Adsorbent Dosage

Adsorbent dosage was varied from 0.01 to 0.5g during the studies and the results were shown in Figure 3.43.
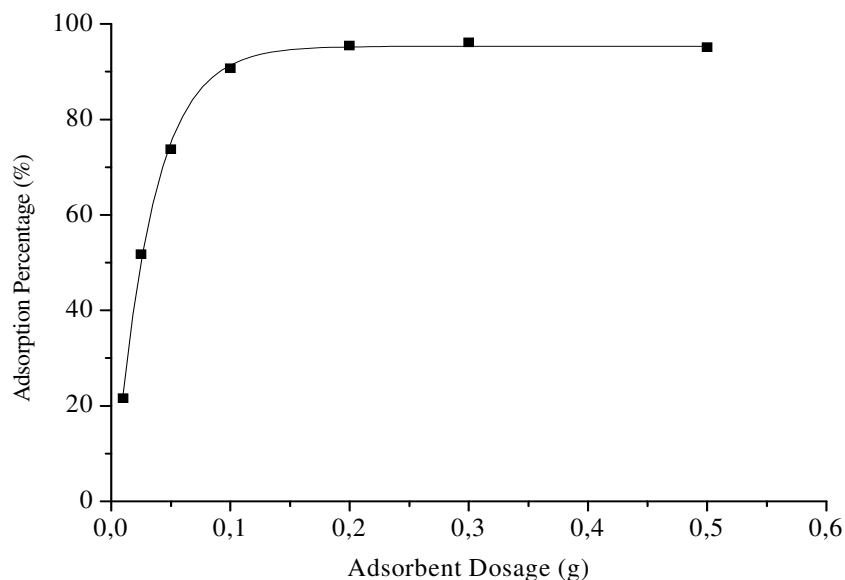
Figure 3.43 Effect of adsorbent dosage on boron adsorption(4mgL^{-1} B; pH=7.0; 308K; 24 h).

The adsorbed amount of boron was firstly increased within the adsorbent dosage of 0.01-0.1g. This is due to an increase in the sorption sites for boron species. Beyond an adsorbent dosage of 0.1g, adsorbed amount of boron remained constant. This may have been due to the fact that the equilibrium was reached in the solid-solution interface. Also, there was an equilibrium between the boron species H_3BO_3 and $B(OH)_4^-$. But due to the pH of the solution the conversion of H_3BO_3 to $B(OH)_4^-$ was not possible. These might be the reasons of no significant change in the adsorption capacity.

3.2.3 Kinetics Studies of Adsorption

The kinetic parameters for the adsorption of boron onto TR at various temperatures were given in Table 3.10. The correlation coefficients (R^2) of both models were compared and the results strongly suggested that the adsorption of boron onto TR was most appropriately represented by a pseudo-second-order rate process. The rate constant k_2 was increased with increasing temperature, while the value of q_2 was relatively temperature independent. Therefore, the pseudo second order equation was in agreement with a chemical sorption mechanism (Şengil & Özacar, 2009).

Table 3.10 Kinetic parameters for the adsorption of boron onto TR

Temperature (K)	288	298	308
Pseudo-first-order			
q_1 (mg g^{-1})	3.18	1.95	1.62
k_1 x 10^2 (min^{-1})	0.60	0.60	0.40
R^2	0.76	0.88	0.74
Pseudo-second-order			
q_2 (mg g^{-1})	1.66	1.68	1.78
k_2 x10^2 (g/mg min)	0.37	0.62	0.73
R^2	0.99	0.99	0.99

3.2.4 Results of Adsorption Isotherms

Adsorption isotherms are basic requirements for designing any adsorption system. Adsorption isotherms of the samples were presented in Figure 3.44.
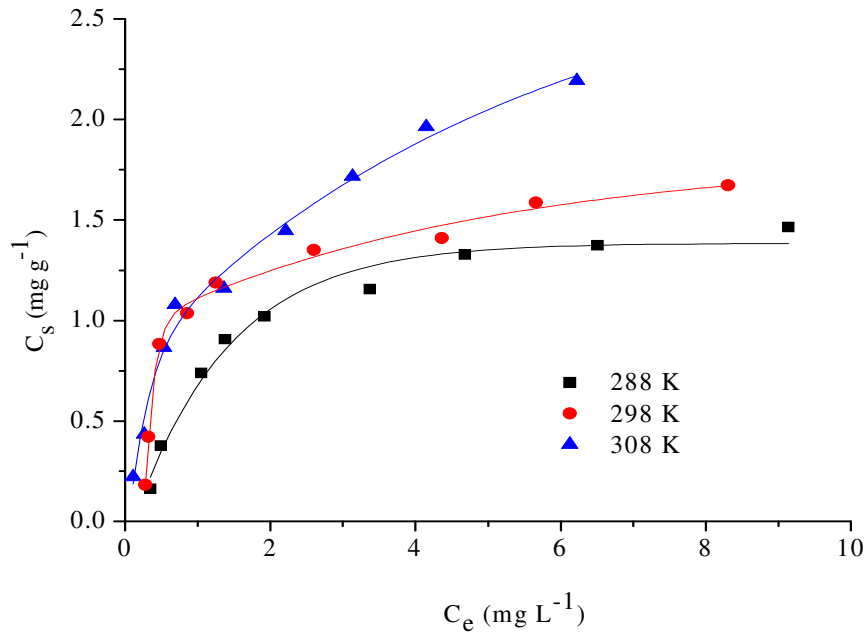
Figure 3.44 Isotherms for boron adsorption onto TR at different temperatures.

It can be seen from Figure 3.44, the adsorption of boron onto TR exhibited an "L–shaped" curve (Giles, McEwan, Nakhwa & Smith, 1960), suggesting that the adsorbent had a high affinity for the adsorbate at low concentrations, but as the concentration increases, the affinity for the adsorbate will decrease because empty adsorbent sites were preoccupied (Sparks, 2003).

The constants related to Langmuir and Freundlich isotherms were given in Table 3.11. The results suggested that the adsorption data were well suited with Langmuir equation ($R^2 = 0.99$ at 308 K).

Table 3.11 Langmuir and Freundlich isotherm constants for the adsorption of boron onto TR

Temperature (K)	288	298	308
Langmuir-Lineer form			
Q_o (mg g^{-1})	1.82	1.91	2.56
a_L (L mg^{-1})	0.50	0.84	0.78
K_L (Lg^{-1})	0.92	1.60	1.99
R^2	0.96	0.95	0.99
Freundlich-Lineer form			
K_f (mg g^{-1})	0.54	0.77	0.91
n_f	0.58	0.48	0.59
R^2	0.83	0.70	0.88

Therefore, the adsorption of boron onto TR was monolayer and the sorption process was realized with chemical adsorption. These results were compatible with L type isotherms having n_f values smaller than one ($n_f < 1$) (Freundlich, 1906), suggesting a strong affinity between the adsorbate and the adsorbent and chemisorption. Q_o was calculated as 2.56 mg g^{-1}. For example, the adsorption of boron reached 0.25 mg g^{-1} for Caulerpa racemosa var. cylindracea (CRC) (Bursali, Cavas, Seki, Bozkurt & Yurdakoc, 2009), 3.64 mg g^{-1} for clinoptilolite (Kavak, 2011), 2.53 and 0.12 mg g^{-1} for Camlıca Bentonite 1 and 2, respectively (Seyhan, Seki, Yurdakoc & Merdivan, 2007), 3.39 for calcined alunite (Kavak, 2009), 1.12, 0.98 and 0.94 mg g^{-1} for Siral 5, Siral 40 and Siral 80, respectively (Yurdakoç, Seki, Karahan & Yurdakoç, 2005).

However, adsorption capacities from Langmuir equation as 11.4 and 24.3 mg g^{-1} for tannin gel and amine-modified tannin gel were obtained under the conditions of pH=8.8 and at 303 K with the initial boron concentration of 200 mg L^{-1} (Morisada, Rin, Ogata, Kim & Nakano, 2011).

3.2.5 Thermodynamic Parameters of Adsorption

In order to evaluate the nature of the adsorption process, the standard free energy (ΔG^o), enthalpy change (ΔH^o) and entropy change (ΔS^o) have been estimated. The thermodynamic parameters of boron adsorption onto TR at 288, 298, and 308 K were determined and the results were given in Table 3.12.

Table 3.12 Thermodynamic parameters for the adsorption of boron onto TR[*]

Temperature (K)	K_d	ΔG^o (kJ mol^{-1})	ΔH^o (kJ mol^{-1})	ΔS^o (J mol^{-1}K^{-1})
288	1.518	-0.998		
298	1.695	-1.308	16.297	59.694
308	2.354	-2.192		

**(4mgL^{-1}B; pH=7.0; 0.1g TR and 24 h)

The negative values of $\Delta G°$ at all temperatures indicated the spontaneous nature and the positive value of $\Delta H°$ suggested the endothermic nature of boron adsorption onto TR. The $\Delta G°$ at 308 K was the highest negative value than the others, so more energetically favorable adsorption was occurred at this temperature. The positive value of $\Delta S°$ showed the increased randomness at the solid/solution interface during the adsorption process and increase in degree of freedom (Malkoc & Nuhoglu, 2010).

In the point of views of the adsorption data, adsorption kinetics and thermodynamics, the adsorption mechanism may be partly a result of ion exchange or complexation between boron and phenolic groups on the TR surface. Thus, a proposed reaction mechanism was represented in Scheme 3.1.

$$B(OH)_3 + H_2O \rightleftharpoons B(OH)_4^- + H^+$$
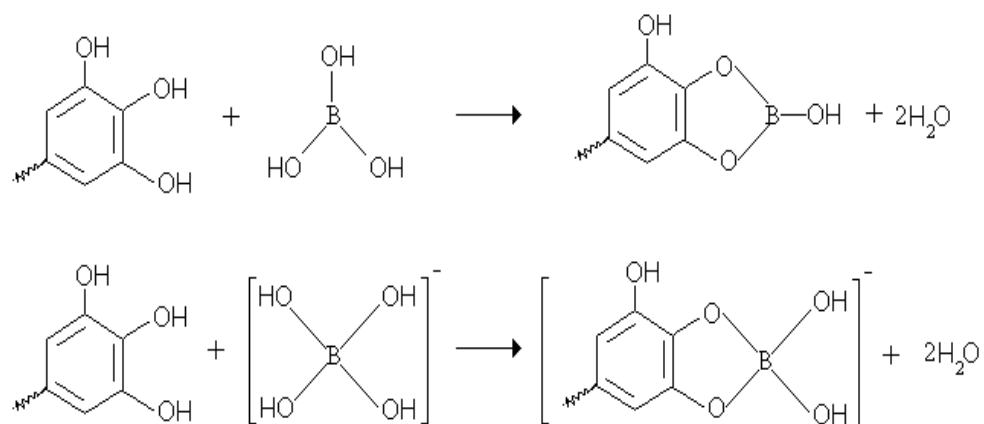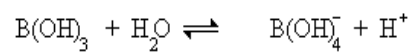
Scheme 3.2 Hypothetically proposed reaction between boron [H_3BO_3 or $B(OH)_4^-$] and TR

CHAPTER FOUR

CONCLUSION

4.1 Conclusion

   Tannins are naturally found in the chestnut, valonia oak, gall, acorn, sumac, etc. in different ratios and they have polyphenolic units in their structure. Plants that contain plentifully tannins are used in leatherworking (they are used as packed substances) and dyeing. The presence of hydroxyl group (-OH) and rings in their structure provide them to form complexes with metals.

   This thesis, two different studies have been conducted on tannin. The first part of the study presented the chelation of Fe(III) with TA and valonia extract which was called Valex (widely grown in the western Anatolian region in Turkey especially in Salihli). When Fe(III) and Valex or TA solutions were combined, complex was formed with an absorbance maximum of 575nm at pH=4.4. Complexes that are created in different buffers was decided to use a dark violet-colored complex (pH=4.4) in the paint industry because of the OH groups of Valex and TA were capable of forming dark violet coloured complex with Fe(III) with high reactivity.

   An interaction between Ligand (Valex or TA) and Fe(III) is important to understand the metal-ligand behavior. M/L ratio or pH could change significantly the coordinated species in solution. So the stoichiometric composition and stability constants values of the Fe(III)-TA and Fe(III)-Valex complexes at different pH values were determined and compared. The Slope ratio and Mole ratio method were used for the spectrophotometric determination of the complex stoichiometries in pH range from 2.4 to 8.4.

   Results obtained using mole ratio method were showed that the stoichiometry of both Fe(III)-Valex and Fe(III)-TA complexes were 1:1 at pH=2.4 and 2:1 at pH=6.4. Likewise results obtained using slope ratio method showed that the stoichiometry of both Fe(III)-Valex and Fe(III)-TA complexes were 2:1 at pH=4.4 and 4:1 at pH=8.4.

Valex and TA were found to be good iron chelators and form highly colored complexes with iron to chelator ratio of 2:1 at pH=4.4. And percent yield calculation of the their complexes was obtained as 89.2%.

The stability constant values of both Fe(III)-Valex and Fe(III)-TA complexes for each pH were calculated. The stability constants (K) were obtained as 0.8×10^3, 1.5×10^8, 1.1×10^9, 3.9×10^{17} for Fe(III)-Valex complexes and 1.1×10^3, 1.5×10^8, 2.0×10^9, 1.4×10^{17} for Fe(III)-TA complexes at pH=2.4, 4.4, 6.4 and 8.4 respectively. Although the stability constants of basic medium complexes are more stable, because of its dark violet color M_2L complex at pH=4.4 was chosen.

In the FTIR spectra of Valex and TA, some distinctive changes were observed in the complex spectrum. Due to the complex formation between Fe(III) ions and phenolic groups of the ligands, several bands were not only shifted slightly, but also reduced in intensity.

Thermal decomposition of Valex, TA, Fe(III)-TA and Fe(III)-Valex complexes were investigated in nitrogen atmosphere. Valex and TA exhibited three-step decompositions while Fe(III)-TA and Fe(III)-Valex complex exhibited four-step thermal decomposition. The first step of mass losses could be attributed to evaporation of adsorbed water for all samples. The other steps were due to thermal decomposition stages of the products. The TGA thermograms and derivative thermogravimetric (DTG) curves of synthesized complexes showed that total mass losses of Valex, Fe(III)-Valex complex, TA and Fe(III)-TA complex were 59%, 85%, 71% and 78% respectively.

XRD images of Valex, Fe(III)-Valex, TA and Fe(III)-TA complex showed that they were amorphous. A very broad and unresolved peak in the 2θ region of 20-30° was observed in the diffraction patterns. The peaks of complexes in the range of 2θ=20-30° were a little bit sharper with respect to valex and TA where broader peaks were observed. 2θ value of Valex shifted to higher 2θ value from 23.7° to 26.2° compared to the Fe(III)-Valex complex 2θ value.

2θ value of TA was observed at 25.9° and this value slightly shifted to higher 2θ value, from the 25.9° to 26.2°, at the Fe(III)-TA complex. The actual structures of the complexes were not shown due to the fact that single crystal form of the complexes were not achieved.

Similar ESR spectra were observed for both the high spin Fe(III)-Valex and Fe(III)-TA complexes. The g factor was determined as g = 4.3 in Fe(III)-TA ESR spectrum and this supported the fact that the complex was Fe^{3+} complex. According to the magnetic susceptibility analysis, the magnetic susceptibility of the Fe(III)-TA complex was μ= 6.52 BM. This result indicated that the Fe(III)-Valex and Fe(III)-TA complexes have paramagnetic properties

Molecular weights of Valex, Fe(III)-Valex complex, TA and Fe(III)-TA complex were determined from MALDI-TOF MS spectrum as 1703, 1850, 1702 and 1850 m/z respectively.

As a comparison, the molecular weight of the valex is approximately equal to the molecular weight of the tannic acid (M= 1701.2 g mol^{-1}). As well the molecular weights were the same in the both of the complexes.

XPS characterization of the complexes was confirmed the existence of Fe^{3+} ions. Spectra of Fe(III)-Valex and Fe(III)-TA complexes were the same. In the Fe(III)-TA complex XPS spectra, the core level spectrum of Fe $^{3+}$ has a $2p_{3/2}$ binding energy of 710 eV and $2p_{1/2}$ of binding energy 724 eV. So the XPS spectra of the Fe(III)-TA complex proved the existence of Fe^{3+}.

When the NMR spectra of TA and Fe(III)-TA complex was compared, obvious differences in peak intensities was showed. In both spectra the amount of solvent was used equal. Because the solubility of complex is less than TA. This has led to more intensive solvent peaks at the complex spectra. In the H-NMR spectra Fe(III)-TA complex lower field signals (in the range of 5-8ppm) intensities were decreased due

to the complexation of TA with Fe(III). Higher field signals (in the range of 0-5ppm) intensity were increased depending on the increasing the amount of the solvent.

Eventually results of characterization of Valex and TA showed very little differences, it can be stated that Valex presents structures and functional groups which tend to be similar to the tannic acid.

In recent years, antioxidants are the most popular supplements, which prolong general life, reduce the risk of developing diseases such as heart disease or cancer, and anti-aging effects and is known by people of all walks of life became available. Antioxidant properties of tannins can result from their free radical scavenging activity but their ability to chelate transition metal ions also plays an important role.

The probable applications of the synthesized complexes were investigated in terms of their antioxidant and antimicrobial activities. The antioxidant activity of complexes was determined and the complexes showed increased DPPH radical scavenging activity linearly with increasing concentrations such as controls BHA and BHD.

At 50 µg/ml, DPPH radical scavenging activity of the controls and the samples decreased in the following order: Valex (84.22%) ≈ TA (82.82%) > Fe(III)-TA complex (73.53%) ≈ Fe(III)-Valex complex (70.18%) ≈ BHA (69.94%) > 10%Fe-5%Valex complex (49.23%) ≈ BHT (46.92%). On the other hand the Fe(III)-Valex complex has neither antimicrobial nor antifungal activity as the result of Disk diffusion experiments. Valex is a very good antioxidant (84.22%) specific for natural extracts with its polyphenolic structure. In conclusion, Fe(III)-Valex, Fe(III)-TA, Valex, TA had effective DPPH scavenging activity.

Considering all the results obtained in this part of the study, it could be said that Valex and tannic acid are the effective natural antioxidant components and their complexes can be used as food preservative agents or nutraceuticals. But, complexes showed no antimicrobial, antifungal, superoxide anion radical scavenging and

hydrogen peroxide scavenging activities. On the other hand complexes may be used as a coloring agent because of its color in the paint industry.

Second part of the study, TR was synthesized and used for the boron adsorption from aqueous solutions. Tannins are water soluble compounds, so in order to use tannins as adsorbents; they need to be modified to insoluble tannin gels. This could be done either through the reaction between gallic acid units of gallotannins and formaldehyde due to the strong nucleophilicity of their rings or immobilization of the tannins onto various water-insoluble matrices.

A series of batch experiments were conducted to study the adsorption isotherm and adsorption kinetics. It was seen that the adsorption data were well suited with Langmuir equation. Thus, it was determined that the adsorption of boron onto TR was monolayer adsorption.

By applying the kinetic models to the experimental data, it was demonstrated that the kinetics of boron adsorption was followed by the pseudo-second-order rate equation which indicated chemical adsorption.

In addition, thermodynamic calculations showed that boron adsorption onto TR was endothermic and spontaneous in nature. The optimum adsorption (88%) was occurred at 24h and 308 K with 0.1g TR and 4 mgL^{-1} boron solution (pH=7.0).

The monolayer adsorption capacity was obtained as 2.56 mg g^{-1}. Desorption studies were first carried out in distilled water. Any practical desorption was occurred. And then in 0.01 M HNO$_3$ and 0.01 M H$_2$SO$_4$ solutions were used for desorption studies. But the results were not satisfactory (found as around 31%). Further desorption study was carried out by using the adsorbent (after adsorption at pH=7.0) with 0.01M HCl solution. At that time, 81 percentage of desorption efficiency was achieved. All the results showed that TR could be used as an appropriate adsorbent in the adsorption process of boron from aqueous solutions in terms of its relatively high sorption capacity.

REFERENCES

Abbasi, S., Daneshfar, A., Hamdghadareh, S. & Farmany, A. (2011). Quantification of sub-nanomolar levels of gallic acid by adsorptive stripping voltammetry. *International Journal of Electrochemical Science*, *6*, 4843 – 4852.

Abdel-Ghani, N.T., Hefny, M. & El-Chaghaby, G.A.F. (2007). Removal of lead from aqueous solution using low cost abundantly available adsorbents. *International Journal of Environmental Science Technology*, *4* (1), 67-73.

Aelenei, N., Popa, M.I., Novac, O., Lisa, G. & Balaita, L. (2009). Tannic acid incorporation in chitosan-based microparticles and in vitro controlled release. *Journal of Materials Science: Materials in Medicine*, 20 (5), 1095–1102.

Akiyama, H., Fujii, K., Yamasaki, O., Oono, T. & Iwatsuki, K. (2001). Antibacterial action of several tannins against Staphylococcus aureus. *Journal of Antimicrobial Chemotherapy, 48* (4): 487–491.

Anonymous, (1984). Sümer Holding Co-Türkiye, Reports on Valex, Turkey.

Arts, I.C. & Hollman, P.C. (2005). Polyphenols and disease risk in epidemiologic studies. *American Journal of Clinical Nutrition, 81* (1), 317-325.

Bagchi, D., & Preuss, H.G. (2007). Obesity: epidemiology, pathophysiology, and prevention. *Oxon*: CRC Press.

Bai, Y., Song, F., Chen, M., Xing, J., Liu, Z. & Liu, S. (2004). Characterization of the Rutin-metal complexes by electrospray ionization Tandem mass spectrometry. *Analytical Sciences, 20* (8) 1147-1151.

Balaban, A.T., Banciu, M. & Pogany, I. (1983). Application of physical Methods in Organic chemistry. Encyclopaedic and scientific Pb., Bucharest.

Bele, A.A., Jadhav, V.M. & Kadam, V.J. (2010). Potential of Tannins: A Review. *Asian Journal of Plant Sciences, 9*(4), 209-214.

Bektas, N., Oncel, S., Akbulut, H.Y. & Dimoglo, A. (2004). Removal of boron by electrocoagulation. *Environmental Chemistry Letters*, *2* (2), 51-54.

Beltrán, J.J., Novegil, F.J., García, K.E. & Barrero, C.A. (2010). On the reaction of iron oxides and oxyhydroxides with tannic and phosphoric acid and their mixtures. *Hyperfine Interactions*, *195* (1-3), 133–140.

Bermejo-Barrera, P. & Cocho de Juan, J.A. (2006). Analytical procedures for the lead determination in biological and environmental samples. Lead: *Chemistry, Analytical Aspects, Environmental Impact and Health Effects*, 229-337.

Bicak, N., Gazi, M. & Bulutcu, N. (2003). N,N-bis(2,3-dihydroxypropyl) octadecylamine for liquid-liquid extraction of boric acid. *Separation Science and Technology, 38* (1), 165-177.

Bicak, N. & Senkal, B.F. (1998). Sorbitol-modified poly (N-glycidyl styrene sulphonamide) for removal of boron. *Journal of Applied Polymer Science*, *68*, 2113-2119.

Binbuga, N., Chambers, K., Henry, W.P. & Schultz, T.P. (2005). Metal chelation studies relevant to wood preservation. 1.Complexation of propyl gallate with Fe^{2+}. *Holzforschung*, *59* (2), 205–209.

Blois, M.S. (1958). Antioxidant determinations by the use of a stable free radical. *Nature*, *181*, 1199–1200.

Bou-Abdallah, F. & Chasteen, N.D. (2008). Spin concentration measurements of high-spin (g = 4.3) rhombic iron(III) ions in biological samples: theory and application. *Journal of Biological Inorganic Chemistry*, *13* (1), 15–24.

Bouguerra, W., Mnif, A., Hamrouni, B. & Dhahbi, M. (2008). Boron removal by adsorption onto activated alumina and by reverse osmosis. *Desalination*, *223*, 31-37.

Brown, J.E., Khodr, H., Hider, R.C. & Rice-Evans, C.A. (1998). Structural dependence of flavonoid interactions with Cu^{2+} ions: implications for their antioxidant properties. *Journal of Biochemistry, 330* (3), 1173-1178.

Brune, M., Hallberg, L. & Skanberg, A.B. (1991). Determination of iron-binding phenolic groups in foods. *Journal of Food Science, 56* (1), 128-131.

Bulgariu, L., Rătoi, M., Bulgari, D. & Macoveanu, M. (2008). Equilibrium study of Pb(II) and Hg(II) sorption from aqueous solutions by moss peat. *Environmental Engineering and Management Journal*, *7*(5), 511-516.

Burkinshaw, S.M. & Allafan B.B. (2003). The development of a metal-free, tannic acid-based aftertreatment for nylon 6,6 dyed with acid dyes-part 1: initial studies. *Dyes and Pigments*, *58*(3), 205-218.

Bursali, E.A., Cavas, L., Seki, Y., Bozkurt, S.S. & Yurdakoc, M. (2009). Sorption of boron by invasive marine seaweed: Caulerpa Racemosa var. Cylindracea. *Chemical Engineering Journal*, *150* (2-3), 385-390.

Bursali, E.A, Coskun, S., Kizil, M. & Yurdakoc, M. (2011). Synthesis, characterization and in vitro antimicrobial activities of boron/starch/polyvinyl alcohol hydrogels. *Carbohydrate Polymers*, *83*(3), 1377-1383.

Cammack, R., Attwood, T.K., Campbell, P.N., Parish, J.H., Smith, A.D., Stirling, J.L. & Vella, Eds F. (2006). Oxford dictionary of biochemistry and molecular biology. (second edition) Oxford University Press.

Chen, G., Zhang, L.-K. & Pramanik, B. N. (2006). LC/MS: Theory, Instrumentation, and Applications to Small Molecules, in HPLC for Pharmaceutical Scientists (eds Y. Kazakevich and R. LoBrutto), John Wiley & Sons, Inc., Hoboken, NJ, USA. doi: 10.1002/9780470087954.ch7

Chen, H-Y., & Yen, G-C. (2007). Antioxidant activity and free radical-scavenging capacity of extracts from guava (*Psidium guajava* L.) leaves. *Food Chemistry, 101* (2), 686–694.

Chen, J., Gu, B., LeBoeuf, E.J, Pan, H. & Dai, S. (2002). Spectroscopic characterization of the structural and functional properties of natural organic matter fractions. *Chemosphere*, *48*, 59–68.

Cheng, G.W. & Crisosto, C.H. (1997). Iron-polyphenol complex formation and skin discoloration in peaches and nectarines. *Journal of the American Society Horticultural Science, 122*(1), 95-99.

Cheynier, V. (2005). Polyphenols in foods are more complex than often thought. *The American Journal of Clinical Nutrition, 81*(l), 223–229.

Chikate, R.C. & Padhye, S.B. (2005). Transition metal quinone-thiosemicarbazone complexes 2: magnetism, ESR and redox behavior of iron(II), iron(III), cobalt(II) and copper(II) complexes of 2-thiosemicarbazido-1-4-naphthoquinone. *Polyhedron*, *24* (13), 1689-1700.

Chu, W.L., Lim, Y.W., Radhakrishnan, A.K. & Lim, P.E. (2010). Protective effect of aqueous extract from Spirulina platensis against cell death induced by free radicals. *BMC Complementary & Alternative Medicine*, *10*, 53-60.

Clark, C.L., Jacobs, M.R.J. & Appelbaum, P.C. (1998). Antipneumococcal activities of levofloxacin and clarithromycin as determined by agar dilution, microdilution, E-test, and disk diffusion methodologies. *Journal of Clinical Microbiology*, *36* (12), 3579–3584.

Cruz, B.H., Diaz-Cruz, J.M., Arino, C. & Estaban, M., (2000). Heavy metal binding by tannic acid: a voltammetric study. *Electroanalysis, 12* (14), 1130-1137.

Darbouret D., & Kano I. (2000). Ultrapure water blank for boron trace analysis. *Journal of Analytical Atomic Spectrometry, 15*, 1395-1399.

Data, S.P. & Bahadoria, P.B.S. (1999). Boron adsorption and desorption in some acid soils of West Bengal, India. *Journal of Plant Nutrition and Soil Science*, *162*, 183–191.

Deng, Z., Coudray, C., Gouzoux, L., Mazur, A., Rayssiguier, Y. & Pepin, D. (2000). Effects of acute and chronic coingestion of $AlCl_3$ with citrate or polyphenolic acids on tissue retention and distribution of aluminum in rats. *Biological Trace Element Research,* 2000, *76* (3), 245-256

De Souza, R.F.V. & De Giovani, W.F. (2005). Synthesis, spectral and electrochemical properties of Al(III) and Zn(II) complexes with flavonoids. *Spectrochimica Acta Part A*, *61*(9), 1985-1990.

Dıgrak, M., Ilçım, A., Alma, M.H. & Sen, S. (1999). Antimicrobial activites of the extracts of various plants (valex, mimosa bark, gallnut powders, Salvia sp. and Phlomis sp.). *Turkish Journal of Biology*, *23*, 241-248.

Di Carlo, G., Mascolo, N., Izzo, A.A. & Capasso, F. (1999). Flavonoids: old and new aspects of a class of natural therapeutic drugs, *Life Sciences*, *65*(4), 337-353.

Dilek, Ç., Özbelge, H.Ö., Bıçak, N. & Yılmaz, L. (2002). Removal of boron from aqueous solutions by continuous polymer-enhanced ultrafiltration with polyvinyl alcohol. *Separation Science and Technology, 37*(6), 1257-1271.

Dollimore, D. & Heal, G.R. (1964). An improved method for the calculation of pore size distribution from adsorption data. *Journal of Applied Chemistry*, *14* (3), 109-114.

Drokina, T., Petrakovskii G., Keller, L. & Schefer J. (2010). Investigation of the magnetic structure in $NaFeGe_2O_6$ using neutron powder diffraction. *Journal of Physics: Conference Series,* 251, 012016.

Elhabiri, M., Carrer, C., Marmolle, F. & Traboulsi, H., (2007). Complexation of iron(III) by catecholate-type polyphenols. *Inorganica Chimica Acta, 360* (1), 353–359.

Esmaeili, M.A. & Sonboli, A. (2010). Antioxidant, free radical scavenging activities of Salvia brachyantha and its protective effect against oxidative cardiac cell injury. *Food and Chemical Toxicology*, *48* (3), 846–853.

Fatima, N. & Maqsood., Z.T. (2005). Study of formation constants of vanadium (III)-catecholate complexes. *Journal of Saudi Chemical Society*, *9*(3), 519-528.

Fernandez, M.T., Mira, M.L., Florencio, M.H. & Jennings, K.R. (2002). Iron and copper chelation by flavonoids: an electrospray mass spectrometry study. *Journal of Inorganic Biochemistry, 92* (2) 105-111.

Freundlich, H. (1906). Über die adsorption in lösungen, Zeitschrift Fur Physikalische Chemie, *57*, 384-410.

Garro-Galvez, J.M., Fechtal, M. & Riedl, B. (1996). Gallic Acid as a model of tannins in condensation with formaldehyde. *Thermochimica Acta*, *274*, 149-163.

Garro-Galvez, J.M., Riedl, B. & Conner, A.H. (1997). Analytical studies on Tara tannins. *Holzforschung*, *51*, 235-243.

Ghaedi, M., Biyareh, M.N., Kokhdan, S.N., Shamsaldini, S., Sahraei, R., Daneshfar, A. & Shahriyar, S., (2012). Comparison of the efficiency of palladium and silver nanoparticles loaded on activated carbon and zinc oxide nanorods loaded on activated carbon as new adsorbents for removal of Congo red from aqueous solution: Kinetic and isotherm study. *Materials Science and Engineering: C*, *32*(4), 725-734.

Ghaedia, M., Hekmati Jah, A., Khodadoust, S., Sahraei, R., Daneshfar, A., Mihandoost, A. & Purkait, M.K., (2012). Cadmium telluride nanoparticles loaded on activated carbon as adsorbent for removal of sunset yellow. *Spectrochimica Acta Part A, 90*, 22– 27.

Ghaedia M., Khajesharifi, H., Hemati Yadkuri, A., Roosta, M., Sahraei, R. & Daneshfar, A., (2012). Cadmium hydroxide nanowire loaded on activated carbon as efficient adsorbent for removal of Bromocresol Gren. *Spectrochimica Acta Part A*, *86*, 62– 68.

Giles, C.H., McEwan T.H., Nakhwa, S.N. & Smith, D. (1960). Studies in adsorption Part XI. A system of classification of solution adsorption isotherms, and its use in diagnosis of adsorption mechanisms and in measurement of specific surface areas of solids. *Journal of the Chemical Society*, *4*, 3973-3993.

Goldberg, S., Forster, H.S., Lesch, S.M. & Heick, E.L. (1996). Influence of anion competition on boron adsorption by clays and soils. *Soil Science*, 161 *(2)*, 99-103.

Gupta, G., Mazumdar, U. K., Gomathi, P., & Kumar, R. S. (2004). Antioxidant and Free Radical Scavenging Activities of *Ervatamia coronaria* Stapf. Leaves. *Iranian Journal of Pharmaceutical Research, 3* (2), 119-126.

Gutteridge, J. M. & Halliwell, B. (1988). The deoxyribose assay: an assay both for free hydroxyl radical and for site specific hydroxyl radical production. *Biochemical Journal, 253*(3), 932–933.

Hagerman, A.E. (2002). Tannin Handbook. Miami University, Oxford OH 45056.

Halliwell, B., Gutteridge, J. M. C., & Aruoma O. I. (1987). The deoxyribose method: a simple "test tube" assay for determination of rate constants for reactions of hydroxyl radicals. *Analytical Biochemistry, 165* (1), 215-219.

Hanay, A., Boncukcuoglu, R., Kocakerim, M.M. & Yilmaz, A.E. (2003). Boron removal from geothermal waters by ion exchange in a batch reactor. Fresenius *Environmental Bulletin, 12* (10), 1190-1194.

Haslam, E. (1989). Plant polyphenols: vegetable tannins revisited. *Cambridge University Press*, Cambridge.

Haslam, E., Lilley, T.H., Warminski, E., Liao, H., Cai, Y., Martin, R., Gaffney, S.H., Goulding, P.N. & Luck, G. (1992). In phenolic compounds in food and their effects on health II. ACS Symposium Series, ACS, Washington, ch. 2.

Ho, Y.S. & McKay, G. (1998). Sorption of dye from aqueous solution by peat. *Chemical Engineering Journal*, *70* (2), 115-124.

Igbinosa, O.O., Igbinosa, E.O. & Aiyegoro, O.A. (2009). Antimicrobial activity and phytochemical screening of stem bark extracts from Jatropha curcas (Linn). *African Journal of Pharmacy and Pharmacology, 3*(2), 58-62.

Iglesias, J., García de Saldaña, E. & Jaen, J.A. (2001). On the tannic acid interaction with metalic iron. *Hyperfine Interactions*, *134*(1), 109-114.

Jaén, J.A., González, L., Vargas, A. & Olave, G. (2003). Gallic acid, ellagic acid and pyrogallol reaction with metallic iron. *Hyperfine Interactions 148*(14), 227–235.

Jaén, J.A. & Navarro, C. (2009). Mössbauer and infrared spectroscopy as a diagnostic tool for the characterization of ferric tannates. *Hyperfine Interactions*, *192* (1-3), 61-67.

Jiang, J.Q., Xu, Y., Quill, K., Simon, J. & Shettle, K. (2006). Mechanisms of boron removal with electrocoagulation. *Environmental Chemistry*, *3* (5), 350-354.

Kabay, N., Yilmaz, I., Yamac, S., Samatya, S., Yüksel, M., Yüksel, Ü., Arda, M., Saglam, M., Iwanaga, T. & Hirowatari, K. (2004). Removal and recovery of boron from geothermal wastewater by selective ion exchange resins. I. Laboratory tests. *Reactive & Functional Polymers*, *60*, 163-170.

Kabay, N., Yılmaz, I., Bryjak, M. & Yuksel, M. (2006). Removal of boron from aqueous solutions by a hybrid ion exchange-membrane process. *Desalination*, *198*, 158-165.

Karahan, S., Yurdakoc, M., Seki, Y. & Yurdakoc, K. (2006). Removal of boron from aqueous solution by clays and modified clays. *Journal of Colloid and Interface Science*, *293* (1), 36-42.

Karamać, M. (2009). Chelation of Cu(II), Zn(II), and Fe(II) by tannin constituents of selected edible nuts. *International Journal of Molecular Sciences*, *10* (12), 5485-5497.

Kavak, D. (2011). Boron adsorption by clinoptilolite using factorial design. *Environmental Progress & Sustainable Energy*, *30* (4), 527-532.

Kavak, D. (2009). Removal of boron from aqueous solutions by batch adsorption on calcined alunite using experimental design. *Journal of Hazardous Materials*, *163* (1), 308-314.

Keren, R., Groosl, P.R. & Sparks, D.L. (1994). Equilibrium and kinetics of borate adsorption-desorption on pyrophyllite in aqueous suspensions. *Soil Science Society of America Journal*, *58*, 1116–1122.

Khanbabaee, K. & van Ree, T. (2001). Tannins: classification and definition. *National Product Reports*, *18*(6), 641–649.

Kiel, J.S., Thomas, H.G. & Mani, N. (2004). Diphenhydramine tannate composition and method of use, US Patent – 40234593.

Kim, S. & Kim, H.J. (2003). Curing behaviors and viscoelastic properties of pine & wattle tannin-based adhesives by dynamic mechanical thermal analysis & FTIR–ATR microscopy study. *Journal of Adhesion Science and Technology*, *17* (10), 1369-1383.

Kim, Y.H., Alam, M.N., Marutani, Y., Ogata, T., Morisada, S. & Nakano, Y., (2009). Improvement of Pd(II) adsorption performance of condensed-tannin gel by amine modification. *Chemistry Letters*, *38* (10), 956-957.

Kim, Y. H. & Nakano, Y. (2005). Adsorption mechanism of palladium by redox within condensed-tannin gel. *Water Research*, *39* (7), 1324–1330.

Kim, Y.H. & Nakano, Y., (2008). Effect of Br$^-$ on the adsorption rate of palladium(II) ions onto condensed-tanningel in chloride media. *Separation Science and Technology*, *43* (9-10), 2386-2395.

Kim, Y.-H., Ogata, T. & Nakano, Y., (2007b). Kinetic analysis of palladium(II) adsorption process on condensed-tannin gel based on redox reaction models. *Water Research, 41* (14), 3043-3050.

Kim, Y.H., Ogawara, Y., Ogata, T. & Nakano, Y., (2007a). Adsorption mechanism of selenite (Se^{4+}) by redox within condensed tannin gel under concentrated hydrochloric acid solution. *Chemistry Letters, 36* (11), 1316-1317.

Kizil, M., Kizil, G., Yavuz, M. & Aytekin, C. (2002). Antimicrobial activity of the Tar obtained from the roots and stems of Pinus brutia", *Pharmaceutical Biology (Formerly International Journal of Pharmacognosy), 40* (2), 135-138.

Kolodziej, H. & Kiderlen, A.F. (2005). Antileishmanial activity and immune modulatory effects of tannins and related compounds on Leishmania parasitised RAW 264.7 cells. *Phytochemistry, 66* (17), 2056–2071.

Korkmaz, M., Şaylı, U., Şaylı, B.S., Bakırdere, S., Titretir, S., Yavuz Ataman, O. & Keskin, S. (2007). Estimation of human daily boron exposure in a boron-rich area. *British Journal of Nutrition, 98* (3), 571–575.

Koseoglu, H., Kabay, N., Yüksel, M. & Kitis, M. (2008). The removal of boron from model solutions and seawater using reverse osmosis membranes. *Desalination*, *223*, 126-133.

Kostyuk, V.A., Potapovich, A.I., Strigunova, E.N., Kostyuk, T.V. & Afanas'ev, I.B. (2004). Experimental evidence that flavonoid metal complexes may act as mimics of superoxide dismutase. *Archives of Biochemistry and Biophysics, 428* (2), 204-208.

Kraal, P., Jansen, B., Nierop, K.G.J. & Verstraten, J.M., (2006). Copper complexation by tannic acid in aqueous solution. *Chemosphere, 65* (11), 2193–2198.

Langmuir, I. (1918). Adsorption of gases on plane surfaces of glass, mica and platinum. *Journal of the American Chemical Society*, *40* (9), 1361-1403.

Leflein, R.J. & D'Addio, A.D. (2003). Antitussive/antihistaminic compositions. US Patent- 6566396

Li, X., Liu, R., Wu, S., Liu, J., Cai, S. & Chen, D. (2011). Efficient removal of boron acid by N-methyl-D-glucamine functionalized silica–polyallylamine composites and its adsorption mechanism. *Journal of Colloid and Interface Science, 361* (1), 232-237.

Liao, X., Li, L. & Shi, B. (2004). Adsorption recovery of thorium(IV) by Myrica rubra tannin and larch tanin immobilized onto collagen fibres. *Journal of Radioanalytical and Nuclear Chemistry*, *260*(3), 619-625.

Liao, X., Lu, Z., Zhang, M., Liu, X. & Shi, B. (2004). Adsorption of Cu(II) from aqueous solutions by tannins immobilized on collagen. *Journal of Chemical Technology & Biotechnology*, *79*(4), 335–342.

Liao, X., Ma, H., Wang, R. & Shi, B. (2004). Adsorption of UO_2^{2+} on tannins immobilized collagen fiber membrane. *Journal of Membrane Science*, *243*(1-2), 235–241.

Lim, Y.Y. & Murtijaya, J. (2007). Antioxidant properties of *Phyllanthus amarus* extracts as affected by different drying methods. *LWT-Food Science and Technology*, *40* (9), 1664-1669.

Lopes, G.K.B., Schulman, H.M. & Hermes-Lima M. (1999). Polyphenol tannic acid inhibits hydroxyl radical formation from Fenton reaction by complexing ferrous ions. *Biochimica et Biophysica Acta. 1472*, 142-152.

Lou, J., Foutch, G.L. & Jung, W.N. (1999). The sorption capacity of boron on anionic exchange resin. *Separation Science and Technology*, *34* (15), 2923-2941.

Lü, L., Liu, S.W., Jiang, S.B. & Wu, S.G. (2004). Tannin inhibits HIV-1 entry by targeting gp41". *Acta Pharmacologica Sinica, 25* (2), 213–218.

Magara, Y., Tabata, A., Kohki, M., Kawasaki, M. & Hirose, M. (1998). Development of boron reduction system for sea water desalination. *Desalination*, *118* (1-3), 25-33.

Malkoc, E. & Nuhoglu, Y. (2010). Nickel(II) adsorption mechanism from aqueous solution by a new adsorbent-Waste Acorn of Quercus Ithaburensis. *Environmental Progress & Sustainable Energy, 29*(3), 297-306.

Mammela, P., Savolainen, H., Lindroosa, L., Kangas, J. & Vartiainen, T. (2000). Analysis of oak tannins by liquid chromatography-electrospray ionisation mass spectrometry. *Journal of Chromatography A, 891* (1), 75–83.

Manach, C., Scalbert, A., Morand, C., Rémésy, C. & Jiménez, L. (2004). Polyphenols: food sources and bioavailability. *American Journal of Clinical Nutrition*, *79*(5), 727-747.

Matsumoto, M., Matsui, T. & Kondo, K.J. (1999). Adsorption mechanism of boric acid on chitosan resin modified by saccharides. *Journal of Chemical Engineering of Japan*, *32* (2), 190-196.

McDonald, M., Mila, I. & Scalbert, A. (1996). Precipitation of metal ions by plant polyphenols: Optimal conditions and origin of precipitation. *Journal of Agricultural and Food Chemistry*, *44*(2), 599-606.

McDougall, G., Martinussenb, I. & Stewart, D. (2008). Towards fruitful metabolomics: High throughput analyses of polyphenol composition in berries using direct infusion mass spectrometry. *Journal of Chromatography B*, *871*, 362–369.

Mekki, A., Holland, D., McConville, C.F. & Salim, M. (1996). An XPS study of iron sodium silicate glass surfaces. *Journal of Non-Crystalline Solids*, *208* (3), 267-276.

Mira, L., Fernandez, M.T., Santos, M., Rocha, R., Florencio, M.H. & Jennings, K.R. (2002). Interactions of flavonoids with iron and copper ions: a mechanism for their antioxidant activity. *Free Radical Research, 36* (11) 1199-1208.

Montaudo, G., Montaudo, M.S. & Samperi, F. (2002). Martix-assisted laser desorption /ionization mass spectrometry of polymers (MALDI-MS). In: Montaudo, G., Lattimer, R.P. (Eds.), *Mass Spectrometry of Polymers*. CRC Press, Boca Raton, FL, 419–521.

Moore, J.A. (1997). An assessment of boric acid and borax using the IEHR evaluative process for assessing human development and reproductive toxicity of agents. Expert scientific committee. *Reproductive Toxicology*, *11* (1), 123–160.

Morisada, S., Kim, Y.-H., Ogata, T., Marutani, Y. & Nakano, Y., (2011). Improved adsorption behaviors of amine-modified tannin gel for palladium and platinum ions in acidic chloride solutions. *Industrial and Engineering Chemistry Research 50* (4), 1875-1880.

Morisada, S., Rin, T., Ogata, T., Kim, Y.H. & Nakano, Y. (2011) Adsorption removal of boron in aqueous solutions by amine-modified tannin gel. *Water Research, 45* (13), 4028-4034.

113

Mussche, R. (1989). Isolering, struktuurbepaling en industriële toepassingen van hydrolyseerbare plantaardige looistoffen. *Farm Tijdschr België 66*(1):2-6.

Nakamura, Y., Tsuji, S., & Tonogai, Y. (2003). Method for analysis of tannic acid and its metabolites in biological samples: application to tannic acid metabolism in the rat. *Journal of Agricultural and Food Chemistry, 51*(1), 331-339.

Nakano, Y., Takeshita, K. & Tsutsumi, T., (2001). Adsorption mechanism of hexavalent chromium by redox within condensed-tannin gel. *Water Research, 35* (2), 496-500.

Niemetz, R. & Gross G.G. (2005). Enzymology of gallotannin and ellagitannin biosynthesis. *Phytochemistry*, *66*(17), 2001–2011.

Nohynek, L.J., Alakomi, H-L., Kähkönen, M.P., Heinonen, M., Helander, I.M., Oksman-Caldentey, K.M. & Puupponen-Pimiä, R.H. (2006). Berry phenolics: antimicrobial properties and mechanisms of action against severe human pathogens. *Nutrition and Cancer, 54*(1), 18–32.

Nonaka, G. (1989). Isolation and structure elucidation of tannins. *Pure & Applied Chemistry*, *61* (3), 357-360.

Okuda, T. (2005). Systematics and health effects of chemically distinct tannins in medicinal plants. *Phytochemistry*, *66*, 2012-2031.

Ozen, T., Demirtaş, I., & Akşit, H. (2011). Determination of antioxidant activities of various extracts and essential oil compositions of Thymus praecox subsp. skorpilii var. Skorpilii. *Food Chemistry, 124* (1), 58–64.

Özacar, M., Soykan, C. & Şengil, İ.A. (2006). Studies on synthesis, characterization, and metal adsorption of mimosa and valonia tannin resins. *Journal of Applied Polymer Science*, *102* (1), 786-797.

Özacar, M. & Şengil, İ.A. (2003). Effect of tannins on phosphate removal using alum. *Turkish Journal of Engineering and Environmental Science*, *27*, 227-236.

Özacar, M., Şengil, I.A. & Türkmenler, H. (2008). Equilibrium and kinetic data, and adsorption mechanism for adsorption of lead onto valonia tannin resin. *Chemical Engineering Journal, 143* (1-3), 32–42.

Özay, P., Yurdakoç, M., Karakaplan, M. & Hoşgören, H. (2006). Extraction of boron with diols in petroleum benzine and n-amyl alcohol. *Asian Journal of Chemistry*, *18* (2), 1277-1284.

Özcan, A.S. & Özcan, A. (2004). Adsorption of acid dyes from aqueos solutions onto acid-activated bentonite. *Journal of Colloid and Interface Science*, *276* (1), 39-46.

Öztürk, N. & Kavak, D. (2004). Boron removal from aqueous solutions by adsorption on waste sepiolite and activated waste sepiolite using full factorial design. *Adsorption*, *10* (3), 245-257.

Panigrahy, B., Aslam, M. & Bahadur, D. (2012). Effect of Fe doping concentration on optical and magnetic properties of ZnO nanorods. *Nanotechnology*, *23* (11), 115601.

Parajuli, D., Kawakita, H., Inoue, K., Ohto, K. & Kajiyama, K. (2007). Persimmon peel gel for the selective recovery of gold. *Hydrometallurgy*, *87* (3-4), 133-139.

Parks, J.L., & Edwards, M. (2005). Boron in the Environment. *Critical Reviews in Environmental Science and Technology*, *35*, 81-114.

Pasumarthi, S., Chimata, M.K., Chetty, C.S. & Challa, S. (2011). Screening of phytochemical compounds in selected medicinal plants of Deccan Plateau and their viability effects on Caco-2 cells. *Journal of Medicinal Plants Research*, *5*(32), 6955-6962.

Peak, D., Luther, G.W. & Sparks, L. (2003). ATR-FTIR spectroscopic studies of boric acid adsorption on hydrous ferric oxide. *Geochimica et Cosmochimica Acta*, *67* (14), 2551-2560.

Perron, N.R. & Brumaghim, J.L., (2009). A review of the antioxidant mechanisms of polyphenol compounds related to iron binding. *Cell Biochemistry Biophysics, 53*(2), 75–100.

Perron, N.R., Hodges, J.N., Jenkins, M. & Brumaghim, J.L. (2008). Predicting how polyphenol antioxidants prevent DNA damage by binding to iron. *Inorganic Chemistry*, *47* (14), 6153–6161.

Pizzi, A. (1983). Wood Adhesives: Chemistry and Technology, New York & Basel: Marcel Dekkar.

Pizzi, A., (1982). Condensed tannins for adhesive. *Industrial and Engineering Chemistry Product Research and Development*, *21* (3), 359-369.

Pizzi, A., (2009). Polyflavonoid tannins self-condensation adhesives for wood particleboard. *Journal of Adhesion, 85* (2-3), 57-68.

Predoi, D. (2007). A study on iron oxide nanoparticles coated with dextrin obtained by coprecipitation. *Digest Journal of Nanomaterials and Biostructures, 2*(1), 169-173.

Quideau, S. (2009). Chemistry and biology of ellagitannins: An underestimated class of bioactive plant polyphenol. World Scientific Publishing Co. Pte. Ltd., Singapore.

Rahim, A.A., Kassim, J. (2008). Recent development of vegetal tannins in corrosion protection of iron and steel. *Recent Patents on Materials Science*, *1*(3), 223-231.

Ristic M.Dj. & Rajakovik Lj.V. (1996). Boron removal by anion exchangers impregnated with citric and tartaric acids. *Separation Science and Technology*, *31* (20), 2805-2814.

Ross, A.R.S., Ikonomou, M.G. & Orians, K.J. (2000). Characterization of dissolved tannins and their metal-ion complexes by electrospray ionization mass spectrometry. *Analytica Chimica Acta, 411* (1-2), 91–102.

Ross, J.A. & Kasum, C.M. (2002). Dietary flavonoids: Bioavailability, metabolic effects, and safety. *Annual Review of Nutrition*, *22*, 19-34.

Rowe, D.R. & Abdel-Magid, I.M. (1995). *Handbook of Wastewater Reclamation and Reuse*, Florida: Springer.

Rump, H.H. & Krist, H. (1999). Laboratory manual for the examination of water, waste water and soil, 3rd completely revised edition. Weinheim: Wiley-VCH.

Ryan, P. & Hynes M.J. (2007). The kinetics and mechanisms of the complex formation and antioxidant behaviour of the polyphenols EGCg and ECG with iron(III). *Journal of Inorganic Biochemistry, 101* (4), 585–593.

Sabarudin A., Oshita K., Oshima M., & Motomizu S. (2005). Synthesis of cross-linked chitosan possessing *N*-methyl-D-glucamine moiety for adsorption/ concentration of boron in water samples and its accurate measurement by ICP-MS and ICP-AES. *Talanta*, *66*, 136–144.

Salah, N., Miller, N.J., Paganga, G., Tijburg, L., Bolwell, G.P. & Rice-Evans, C. (1995). Polyphenolic flavanols as scavengers of aqueous phase radicals and as chain-breaking antioxidants. *Archives of Biochemistry and Biophysics*, *322*(2), 339-346.

Salminen, J.P., Ossipov, V., Loponen, J., Haukioja, E. & Pihlaja, K. (1999). Characterization of hydrolyzable tannins from leaves of betula pubescens by high-performance liquid chromatography-mass spectrometry. *Journal of Chromatography A, 864*(2), 283-291.

Sánchez-Martín, J., González-Velasco, M., Beltrán-Heredia, J., Gragera-Carvajal, J. & Salguero-Fernández, J., (2010). Novel tannin-based adsorbent in removing cationic dye (Methylene Blue) from aqueous solution. Kinetics and equilibrium studies. *Journal of Hazardous Materials, 174* (1-3), 9-16.

Santos-Buelga, C. & Scalbert, A. (2000). Proanthocyanidins and tannin-like compounds-nature, occurrence, dietary intake, and effects on nutrition and health. *Journal of the Science of Food and Agriculture*, *80* (7), 1094-1117.

Schofield, P., Mbugua, D.M. & Pell, A.N. (2001). Analysis of condensed tannins: a review. *Animal Feed Science and Technology*, *91* (1-2), 21-40.

Self, R., Eagles, J., Galletti, G.C., Mueller-Harvey, I., Hartley, R.D., Lea, A.G.H., Magnolato, D., Richli, U., Gujer, R. & Haslam, E. (1986). Fast atom bombardment mass spectrometry of polyphenols (syn. vegetable tannins). *Biological Mass Spectrometry, 13* (9), 449-468.

Senkal, B.F. & Bicak, N. (2003). Polymer supported iminodipropylene glycol functions for removal of boron. *Reactive & Functional Polymers*, *55*, 27-33.

Sepulveda, L., Ascacio, A., Rodriguez-Herrera, R., Aguilera-Carbo, A. & Aguilar, C.N. (2011). Ellagic acid: Biological properties and biotechnological development for production processes. *African Journal of Biotechnology, 10* (22), 4518–4523.

118

Seyhan, S., Seki, Y., Yurdakoc, M. & Merdivan, M. (2007). Application of iron-rich natural clays in Çamlica, Turkey for boron sorption from water and its determination by fluorimetric-azomethine-H method. *Journal of Hazardous Materials*, *146* (1-2), 180-185.

Shi, B. & Di, Y. (2000). Plant polyphenols. Science Press. Beijing, P.R. China.

Silverstein, R.M., Bassler, G.C. & Morrill T.C. (1991). Spectrometric identification of organic compounds, (5th Ed.), Wiley, New York.

Simonnot, M.O., Castel, C., Nicolai, M., Rosin, C., Sardin, M. & Jauffret, H. (2000). Boron removal from drinking water with a boron selective resin: is the treatment really selective?. *Water Research*, *34* (1), 109-116.

Sinha, N.K., Mukhopadhyay, R., Dhupia, D., Das Gupta, S. & Baldev, R. (2011). Development of fluorocarbon rubber for backup seals of sodium cooled fast breeder reactor, *Materials and Design*, *32*(10), 5141-5153.

Sisti, M., De Santi, M., Fraternale, D., Ninfali, P., Scoccianti, V. & Brandi, G. (2008). Antifungal activity of *Rubus ulmifolius* Schott standardized in vitro culture. *LWT - Food Science and Technology, 41* (5), 946-950.

Skoog, D.A., Holler, F.J. & Nieman, T.A. (1998). Principles of instrumental analysis. (5th ed.), Harcourt Brace & Company, Philadelphia, 1998.

Skoog, D.A. & Leary, J.L. (1992). Principles of Instrumental Analysis. Harcourt Brace Jovanovich College Publishing, Philadelphia, PA, 4th edn, 123-173.

Smith, B.M., Todd, P. & Bowman, C.N. (1995). Boron removal by polymer-assisted ultrafiltration. *Separation Science and Technology*, *30* (20), 3849-3859.

South, P.K. & Miller, D.D. (1998). Iron binding by tannic acid: Effects of selected ligands. *Food Chemistry, 63* (2), 167-172.

Sparks, D.L. (2003). Environmental soil chemistry. (2nd ed.) Elsevier-Academic Press, New York.

Stoner, G.D. & Morse, M.A. (1997). Isothiocyanates and plant polyphenols as inhibitors of lung and esophageal cancer. *Cancer Letters*, *114*(1-2), 113-119.

Su, C. & Suarez, D. (1995). Coordination of adsorbed boron: A FTIR spectroscopic study. *Environmental Science and Technology*, *29*, 302–311.

Sudrajat, H., Bang, N.D. & Trung, P.X. (2008). Removal of Cd (II) from aqueous solution by Bruguiera sexangula poir tannin-based adsorbent. *Journal of Applied Sciences in Environmental Sanitation, 3* (2), 91-100.

Sungur, Ş. & Uzar, A., (2008). Investigation of complexes tannic acid and myricetin with Fe(III). *Spectrochimica Acta Part A, 69*, 225–229.

Sütçü, L. (2005). Removal of boron from waters using fly ash. http/www.library.iyte.edu.tr/tezler/.../T000329.pdf.

Şengil, İ.A. & Özacar, M. (2009). Competitive biosorption of Pb^{2+}, Cu^{2+} and Zn^{2+} ions from aqueous solutions onto valonia tanin resin. *Journal of Hazardous Materials, 166* (2-3), 1488-1494.

Şengil, I.A., Özacar, M. & Türkmenler, H. (2009). Kinetic and isotherm studies of Cu (II) biosorption onto valonia tannin resin. *Journal of Hazardous Materials*, *162* (2-3), 1046–1052.

Takeda, K., Yamashita, T., Takahashi, A. & Timberlake, C.F. (1990). Stable blue complexes of anthocyanin-aluminium-3-*p*-coumaroyl- or 3-caffeoyl-quinic acid involved in the blueing of Hydrangea flower. *Phytochemistry*, *29* (4), 1089-1091.

Thevenon, M.-F., Tondi, G. & Pizzi, A., (2009). High performance tannin resin-boron wood preservatives for outdoor end-uses. *European Journal of Wood and Wood Products, 67* (1), 89-93.

Toderaş, M., Filip, S. & Ardelean I. (2006). Structural study of the Fe_2O_3-B_2O_3-BaO glass system by FTIR spectroscopy. *Journal of Optoelectronics and Advanced Materials*, *8*(3), 1121-1123.

Üçer, A., Uyanik, A. & Aygün, Ş.F. (2006). Adsorption of Cu(II), Cd(II), Zn(II), Mn(II) and Fe(III) ions by tannic acid immobilised activated carbon. *Separation and Purification Technology, 47* (3), 113–118.

Vazquez, G., Gonzalez-Alvarez, J., Freire, S., Lopez-Lorenzo, M. & Antorrena, G. (2002). Removal of cadmium and mercury ions from aqueous solution by sorption on treated Pinus pinaster bark: kinetics and isotherms. *Bioresource Technology, 82*(3), 247–251.

Xiao, Y.K., Liao, B.Y., Liu, W.G., Xiao, Y. & Swihart, G.H. (2003). Ion exchange extraction of boron from aqueous fluids by Amber-lite IRA 743 resin. *Chinese Journal of Chemistry*, *21* (8), 1073-1079.

Xie, C. & Cui, H. (2003). Detection of tannic acid at trace level in industrial wastewaters using a highly sensitive chemiluminescence method. *Water Research*, *37*(1), 233–237.

Yahya, S., Mohamad Shah, A.M. & Rahim, A.A. (2008). Phase Transformation of Rust in the Presence of Various Tannins. *Journal of Physical Science, 19*(1), 31–41.

Yang, Z., Lu, J. & Wang, L., (2005). Synthesis and fluorescent properties of Zn(II) complex with functionalized polystyrene containing salicylaldehyde end group. *Polymer Bulletin, 53*, 249–257.

Yilmaz, A.E., Boncukcuoglu, R. & Kocakerim, M.M. (2007). A quantitative comparison between electrocoagulation and chemical coagulation for boron removal from boron-containing solution. *Journal of Hazardous Materials, 149*, 475-481.

Yılmaz, E., Boncukcuoglu, R., Yılmaz, M.T. & Kocakerim, M.M. (2005). Adsorption of boron from boron-containing wastewaters by ion-exchange in a continuous reactor. *Journal of Hazardous Materials* B,*117*, 221–226.

Yonglan, X. & Jiang, J.Q. (2008). Technologies for boron removal. *Industrial & Engineering Chemistry Research, 47* (1), 16-24.

Yoshida, T., Hatano, Ts., Ito, H., Okuda, T. & Quideau S.(Ed.). (2009). Structural diversity and antimicrobial activities of ellagitannins chemistry and biology of ellagitannins, *World Scientific Publishing*, Singapore, 55–93.

Yoshino, M., Ito, M., Haneda, M., Tsubouchi, R. & Murakami, K. (1999). Prooxidant action of aluminum ion – Stimulation of iron-mediated lipid peroxidation by aluminum. *Biometals, 12* (3), 237-240.

Yurdakoc, M., Karakaplan, M. & Hosgören, H. (1999). Effect of long-chain amines on the extraction of boron from $CaCl_2$ brine with CTMP in petroleum benzine. *Separation Science and Technology, 34* (13), 2615-2625.

Yurdakoç, M., Seki, Y., Karahan, S. & Yurdakoç, K. (2005). Kinetic and thermodynamic studies of boron removal by Siral 5, Siral 40, Siral 80. *Journal of Colloid and Interface Science, 286* (2), 440-446.

Yurtsever, M. & Sengil, I. A. (2009). Biosorption of Pb(II) ions by modified quebracho tannin resin. *Journal of Hazardous Materials*, *163* (1), 58-64.

Zhan, X.M., Miyazaki, A. & Nakano, Y., (2001). Mechanisms of lead removal from aqueous solutions using a novel tannin gel adsorbent synthesized from natural condensed tanin. *Journal of Chemical Engineering of Japan*, *34* (10), 1204-1210.

Zhan, X.M. & Zhao, X. (2003). Mechanism of lead adsorption from aqueous solutions using an adsorbent synthesized from natural condensed tannin. *Water Research*, *37* (16), 3905-3912.

Zeng, Y., Liao, X., He, Q. & Shi, B. (2009). Recovery of Th(IV) from aqueous solution by reassembled collagen-tannin fiber adsorbent. *Journal of Radioanalytical and Nuclear Chemistry*, *280* (1), 91–98.